

The Leading Journal of Engineering, Applied Science and Technology

Industrial

Electronics

Biomedical

Civil

Aerospace

Computer

Electrical

Chemical

Mechanical



**ENGINEERING**



## TIME TO CHANGE THE WAY ACADEMICS WORKS? TRY ACAMEDICS!

If you are not using the Internet, please skip this ad and enjoy the rest of the journal. The average burden of reading this ad is two minutes, which may add two months of productivity to your academic life. Seriously!

Whether you organize a conference, publish a journal, or serve on a committee to collect and review applications, you can use the Internet to make your life easier. We are not talking about emails. We are talking about state-of-the-art online systems to collect submissions, assign them to reviewers, and finally make a decision about each submission. We are talking about value-added services, such as payment and registration systems to collect registration fees online. We are talking about digital document services, such as proceedings CD/DVD development and duplication, or creating professional-looking digital documents.

Finally, we are talking about AFFORDABLE PRICE, QUALITY, and CUSTOMIZATION. And we are talking about each of them at the same time.

By the way, you don't have to be a computer geek to use our systems. We have a couple of them, and they will do all the technical mumbo jumbo for you. We also have a few select people from academics like you, and they know what you do. You just relax and enjoy our systems.

If you are still reading this ad, chances are you are interested in our systems or services. So, visit us at [www.acamedics.com](http://www.acamedics.com). While you are there, check the names of our clients as well. Most of them are quite familiar, but the list is too long to include here.



---

# INTERNATIONAL JOURNAL OF MODERN ENGINEERING

The INTERNATIONAL JOURNAL OF MODERN ENGINEERING (IJME) is an independent, not-for-profit publication, which aims to provide the engineering community with a resource and forum for scholarly expression and reflection.

IJME is published twice annually (Fall and Spring issues) and includes peer-reviewed articles, book and software reviews, editorials, and commentary that contribute to our understanding of the issues, problems, and research associated with engineering and related fields. The journal encourages the submission of manuscripts from private, public, and academic sectors. The views expressed are those of the authors and do not necessarily reflect the opinions of IJME or its editors.

## EDITORIAL OFFICE:

Mark Rajai, Ph.D.  
Editor-in-Chief  
Office: (818) 677-2167  
Email: [ijmeeditor@iajc.org](mailto:ijmeeditor@iajc.org)  
Dept. of Manufacturing Systems  
Engineering & Management  
California State University  
Northridge  
18111 Nordhoff Street  
Northridge, CA 91330-8332

## THE INTERNATIONAL JOURNAL OF MODERN ENGINEERING EDITORS

*Editor-in-Chief:*

**Mark Rajai**

California State University-Northridge

*Associate Editors:*

**Alok Verma**

Old Dominion University

**Li Tan**

Purdue University North Central

*Production Editor:*

**Philip Weinsier**

Bowling Green State University-Firelands

*Subscription Editor:*

**Morteza Sadat-Hossieny**

Northern Kentucky University

*Financial Editor:*

**Li Tan**

Purdue University North Central

*Executive Editor:*

**Sohail Anwar**

Penn State University

*Manuscript Editor:*

**Philip Weinsier**

Bowling Green State University -Firelands

*Copy Editors:*

**Victor J. Gallardo**

University of Houston

**Li Tan**

Purdue University North Central

*Publishers:*

**Jerry Waite**

University of Houston

**Hisham Alnajjar**

University of Hartford

*Web Administrator:*

**Saeed Namyar**

Namyar Computer Solutions

---

# TABLE OF CONTENTS

<i>Editor's Note: IJME Celebrates Ten Years of Service.....</i>	<i>3</i>
<i>Philip Weinsier, IJME Manuscript Editor</i>	
<i>Design Prototyping for Manufacturability .....</i>	<i>5</i>
<i>Molu Olumolade, Central Michigan University; Daniel M. Chen, Central Michigan University;</i>	
<i>Hing Chen, Central Michigan University</i>	
<i>An Effective Control Algorithm for a Grid-Connected Multifunctional Power Converter.....</i>	<i>10</i>
<i>Eung-Sang Kim, Korea Electrotechnology Research Institute; Byeong-Mun Song, Baylor University;</i>	
<i>Shiyoung Lee, The Pennsylvania State University Berks Campus</i>	
<i>Using Inertial Measurement to Sense Crash-Test Dummy Kinematics .....</i>	<i>17</i>
<i>Sangram Redkar, Arizona State University; Tom Sugar, Arizona State University;</i>	
<i>Anshuman Razdan, Arizona State University;</i>	
<i>Ujwal Koneru, Arizona State University; Bill Dillard, Archangel Systems; Karthik Narayanan, Archangel Systems</i>	
<i>Pre-amp EDFA ASE Noise Characterization for Optical Receiver Transmission Performance Optimization.....</i>	<i>26</i>
<i>Akram Abu-aisheh, University of Hartford; Hisham Alnajjar, University of Hartford</i>	
<i>Low Power Self Sufficient Wireless Camera System.....</i>	<i>31</i>
<i>Faruk Yildiz, Sam Houston State University</i>	
<i>Preserving Historical artifacts through Digitization and Indirect Rapid Tooling.....</i>	<i>42</i>
<i>Arif Sirinterlikci, Robert Morris University; Ozden Uslu, Microsonic Inc.; Nicole Behanna, Robert Morris University;</i>	
<i>Murat Tiryakioglu, Robert Morris University</i>	
<i>Fully-Reversed Cyclic Fatigue of a Woven Ceramic Matrix Composite at Elevated Temperatures .....</i>	<i>49</i>
<i>Mehran Elahi, Elizabeth City State University</i>	
<i>Simulation of a Tennis Player's Swing-Arm Motion.....</i>	<i>56</i>
<i>Hyounkyun Oh, Savannah State University; Onaje Lewis, Georgia Institute of Technology;</i>	
<i>Asad Yousuf, Savannah State University; Sujin Kim, Savannah State University</i>	
<i>An Innovative Implementation Technique of a Real-Time Soft-Core Processor .....</i>	<i>64</i>
<i>Reza Raeisi, California State University, Fresno; Mr Sudhanshu Singh, California State University, Fresno</i>	
<i>Application of QFD into the Design Process of a Small Job Shop.....</i>	<i>69</i>
<i>M. Affan Badar, Indiana State University; Ming Zhou, Indiana State University; Benjamin A. Thomson, Reynolds &amp; Co.</i>	
<i>Usage of Axiomatic Design Methodology in the U.S. Industries .....</i>	<i>76</i>
<i>Ali Alavizadeh, George Washington University; Sudershan Jetley, Bowling Green State University</i>	
<i>Feasibility Study for Replacing Asynchronous Generators with Synchronous Generators in Wind-Farm Power Stations.....</i>	<i>84</i>
<i>Mohammad Taghi Ameli, Power and Water University of Technology (PWUT);</i>	
<i>Amin Mirzaie, Power and Water University of Technology (PWUT); Saeid Moslehpoour, University of Hartford</i>	
<i>A Survey on Admission-Control Schemes and Scheduling Algorithms.....</i>	<i>91</i>
<i>Masaru Okuda, Murray State University</i>	
<i>Instructions for Authors .....</i>	<i>102</i>

---

# EDITOR'S NOTE: IJME CELEBRATES TEN YEARS OF SERVICE



---

Philip Weinsier, IJME Manuscript Editor

## IJME: 10-Year Anniversary

IJME is proud to offer this anniversary issue, celebrating ten years of service to the engineering community. The editors and staff of IJME would like to take this opportunity to sincerely thank all of the authors who have contributed to this journal over the years. Embarking now on a second decade, we would also like to welcome both returning authors and authors new to the publishing scene.

## IAJC Journals

IAJC, the parent organization of IJME and IJERI, is a first-of-its-kind, pioneering organization acting as a global, multilayered umbrella consortium of academic journals, conferences, organizations, and individuals committed to advancing excellence in all aspects of education related to engineering and technology. IAJC is fast becoming the association of choice for many researchers and faculty, due to its high standards, personal attention, fast-track publishing, biennial IAJC conferences, and its diversity of journals—IJME, IJERI and about 10 other partner journals.

Only weeks before we went to print, IAJC took over the editorship of a third journal: the Technology Interface Journal, stewarded since 1996 by its founding editor, Dr. Jeff Beasley. Everyone at IAJC would like to thank Dr. Beasley for all that he has done for the field of engineering technology. In spite of its expansion to the international market, the newly named Technology Interface International Journal (TIIJ) will continue its dedication to the field of engineering technology and adhere to the same publishing standards set forth by the IAJC Board of Directors.

## Current Issue

The acceptance rate for this issue was roughly 30%. And, due to the hard work of the IJME editorial review board, I am confident that you will appreciate the articles published here. IJME, along with IJERI and TIIJ, are available online ([www.tiij.org](http://www.tiij.org) , [www.ijme.us](http://www.ijme.us) & [www.ijeri.org](http://www.ijeri.org)) and in print.

## IAJC-ASEE 2011 Joint International Conference

The editors and staff at IAJC would like to thank you, our readers, for your continued support and look forward to seeing you at the next IAJC conference. Look for details on any of the IAJC, IJME or IJERI web sites as well as upcoming email updates. Please also look through our extensive web site ([www.iajc.org](http://www.iajc.org)) for information on chapters, membership and benefits, and journals.

This third biennial IAJC conference will be a partnership with the American Society for Engineering Education (ASEE) and will be held at the University of Hartford, CT, April 15-16, 2011. The IAJC-ASEE Conference Committee is pleased to invite faculty, students, researchers, engineers, and practitioners to present their latest accomplishments and innovations in all areas of engineering, engineering technology, math, science and related technologies.

Presentation papers selected from the conference will be considered for publication in one of the three IAJC journals or other member journals. Oftentimes, these papers, along with manuscripts submitted at-large, are reviewed and published in less than half the time of other journals. Please refer to the publishing details at the back of this journal, or visit any of our web sites.

## International Review Board

IJME is steered by IAJC's distinguished Board of Directors and is supported by an international review board consisting of prominent individuals representing many well-known universities, colleges, and corporations in the United States and abroad. To maintain this high-quality journal, manuscripts that appear in the *Articles* section have been subjected to a rigorous review process. This includes blind reviews by three or more members of the international editorial review board—with expertise in a directly related field—followed by a detailed review by the journal editors.

---

## Acknowledgment

Listed here are the members of the editorial board, who devoted countless hours to the review of the many manuscripts that were submitted for publication. Manuscript reviews require insight into the content, technical expertise related to the subject matter, and a professional background in statistical tools and measures. Furthermore, revised manuscripts typically are returned to the same reviewers for a second review, as they already have an intimate knowledge of the work. So I would like to take this opportunity to thank all of the members of the review board.

## Editorial Review Board Members

If you are interested in becoming a member of the IJME editorial review board, go to the IJME web site (Submissions page) and send me—Philip Weinsier, Manuscript Editor—an email. Please also contact me also if you are interested in joining the conference committee.

Mohammad Badar	Indiana State University (IN)
Kevin Berisso	Ohio University (OH)
Kaninika Bhatnagar	Eastern Illinois University (IL)
Elinor Blackwell	North Carolina Ag&Tech State (NC)
Boris Blyukher	Indiana State University (IN)
Jessica Buck	Jackson State University (MS)
John Birmingham	Clayton State University (GA)
Vigyan Chandra	Eastern Kentucky University (KY)
Isaac Chang	Cal Poly State University SLO (CA)
Hans Chapman	Morehead State University (KY)
Rigoberto Chinchilla	Eastern Illinois University (IL)
Raj Chowdhury	Kent State University (OH)
Michael Coffman	Southern Illinois University (IL)
Kanchan Das	East Carolina University (NC)
Paul Deering	Ohio University (OH)
Z.T. Deng	Alabama A&M University (AL)
Raj Desai	Univ of Texas Permian Basin (TX)
Marilyn Dyrud	Oregon Institute of Technology (OR)
David Edward	Ivy tech C.C. of S. Indiana (IN)
Joseph Ekstrom	Brigham Young University (ID)
Mehran Elahi	Elizabeth City State University (NC)
Ahmed Elsawy	Tennessee Tech University (TN)
Bob English	Indiana State University (IN)
Rasoul Esfahani	DeVry University, USA
Clara Fang	University of Hartford (CT)
Fereshteh Fatehi	North Carolina A&T State U. (NC)
Vladimir Genis	Drexel University (PA)
Liping Guo	Northern Illinois University (IL)
Earl Hansen	Northern Illinois University (IL)
Bernd Haupt	Penn State University (PA)
Rita Hawkins	Missouri State University (MO)
Shelton Houston	Univ of Louisiana at Lafayette (LA)
Luke Huang	University of North Dakota (ND)
Charles Hunt	Norfolk State University (VA)
Dave Hunter	Western Illinois University (IL)
Ghassan Ibrahim	Bloomsburg University (PA)

John Irwin	Michigan Tech University (MI)
Sudershan Jetley	Bowling Green State University (OH)
Rex Kanu	Ball State University (IN)
Petros Katsioloudis	Berea College (KY)
Khurram Kazi	Acadiaoptronics (MD)
Satish Ketkar	Wayne State University (MI)
Ognjen Kuljaca	Alcorn State University (MS)
Jane LeClair	Excelsior College (NY)
Shiyoung Lee	Penn State University Berks (PA)
Soo-Yen Lee	Central Michigan University (MI)
Stanley Lightner	Western Kentucky University (KY)
Jimmy Linn	Eastern Carolina University (NC)
Daniel Lybrook	Purdue University (IN)
G.H. Massiha	University of Louisiana (LA)
Jim Mayrose	Buffalo State College (NY)
Thomas McDonald	Eastern Illinois University (IL)
David Melton	Eastern Illinois University (IL)
Richard Meznarich	University of Nebraska-Kearney (NE)
Sam Mryyan	Excelsior College (NY)
Arun Nambiar	California State U.—Fresno (CA)
Ramesh Narang	Indiana Univ - Purdue U. (IN)
Argie Nichols	Univ Arkansas Fort Smith (AR)
Troy Ollison	University of Central Missouri (MO)
Basile Panoutsopoulous	United States Navy
Jose Pena	Purdue University Calumet (MI)
Karl Perusich	Purdue University (IN)
Patty Polastri	Indiana State University (IN)
Mike Powers	III Technical Institute (OH)
Huyu Qu	Honeywell International, Inc.
John Rajadas	Arizona State University (AZ)
Desire Rasolomampionona	Warsaw U. of Technology (POLAND)
Mulchand Rathod	Wayne State University (MI)
Sangram Redkar	Arizona State University-Poly (AZ)
Michael Reynolds	Univ Arkansas Fort Smith (AR)
Marla Rogers	Wireless Systems Engineer
Anca Sala	Baker College (MI)
Balaji Sethuramasamyraja	Cal State U.—Fresno (CA)
Ajay K Sharma	Ambedkar Institute of Technology (INDIA)
J.Y. Shen	North Carolina Ag&Tech State (NC)
Ehsan Sheybani	Virginia State University (VA)
Carl Spezia	Southern Illinois University (IL)
Randy Stein	Ferris State University (MI)
Li Tan	Purdue University North Central (IN)
Ravindra Thamma	Central Connecticut State U. (CT)
Li-Shiang Tsay	North Carolina Ag&Tech State (NC)
Jeffrey Ulmer	University of Central Missouri (MO)
Philip Waldrop	Georgia Southern University (GA)
Haoyu Wang	Central Connecticut State U. (CT)
Jyhwen Wang	Texas A&M University (TX)
Baijian (Justin) Yang	Ball State University (IN)
Faruk Yildiz	Sam Houston State University (TX)
Emin Yilmaz	U. of Maryland Eastern Shore (MD)
Yuqiu You	Morehead State University (KY)
Pao-Chiang Yuan	Jackson State University (MS)
Biao Zhang	US Corp. Research Center ABB Inc.
Chongming Zhang	Shanghai Normal U., P.R. (CHINA)
Jinwen Zhu	Missouri Western State U. (MO)

# DESIGN PROTOTYPING FOR MANUFACTURABILITY

Molu Olumolade, Central Michigan University; Daniel M. Chen, Central Michigan University; Hing Chen, Central Michigan University

## Abstract

Prototyping is one of the best ways to ensure Design for Manufacturability (DFM), and to bring all areas of a company involved in getting a product to market to come together and work for a common goal. Decisions made during this design stage will ultimately determine the cost of producing the product. In this study, the authors evaluated the concept of concurrently designing a part, modifying it, and further evaluating the design through prototyping to ensure that the part can be efficiently and effectively manufactured. Presented here is the examination of the interrelationship between Computer-Aided Design and Computer-Aided Manufacturing (CAD/CAM) for designing a part and the ability to make modifications (at no expense to functionality) for preparing the part for manufacturability.

## Introduction

Among others elements, manufacturing competitiveness requires sustained growth and earnings by building customer loyalty through the creation of high-value products in a very dynamic global market. Not only are most companies under pressure to develop products within rapidly shrinking time periods, companies must also build products, which can be manufactured, produced, serviced and maintained. In accomplishing this task, it is evident that one must strive for functional design, while keeping in mind that a functional design must be manufacturable and reliable. Product designers, therefore, have the responsibility for a product that meets all the characteristics of functionality, reliability, appearance, and cost effectiveness.

Prior to the concept of design for manufacturability (DFM), designers had worked alone or in the company of other designers in isolated areas dedicated to such operations. Typically, completion of the design would be sent to manufacturing without much interaction, leaving manufacturing with the option of struggling with a part that is not designed for manufacturability or rejecting it only when it is too late to change the design. Hence, successful product development requires tools like DFM [1].

The most efficient fashion by which manufacturability can be secured is to develop the part in multi-functional teams with early and active participation of all involved, as shown in Figure 1. That is, the concept of design for manufacturability must include some elements of concurrent engineer-

ing, where each of the modifications of a designed part represent a transformational relationship between specifications, outputs and the concept the manufacturing represents [2]. Prasad [2] also asserts that "At the beginning of the transformation, the modifications of the design are gradually in abstract forms. As more and more of the specifications are satisfied, the product begins to take shape." Existing approaches to evaluating product manufacturability can be classified as: 1) direct or rule-based approaches [3] or 2) indirect or plan-based approaches [4]. The direct approaches have been considered to be more useful in domains such as near-net-shape manufacturing and less suitable for machined or electronics components, where interactions among manufacturing operations make it difficult to determine manufacturability of a design directly from the design description [5].

A product begins with a need, which is identified based on customer and market demands. The product goes through two major processes from conceptualization of the idea to the finished product: the design process and the manufacturing process. These two functions are the main areas in any production setting and, therefore, the interrelationship between them must always be of paramount importance to any product designer. Crow [6] asserts that design effectiveness is improved and integration facilitated when:

- Fewer active parts are utilized through standardization, simplification and group technology retrieval of information related to existing or preferred products and processes.
- Producibility is improved through incorporation of DFM practices.
- Design alternatives are evaluated and design tools are used to develop a more mature and producible design before release for production.
- Product and process design includes a framework to balance product quality with design effort and product robustness.

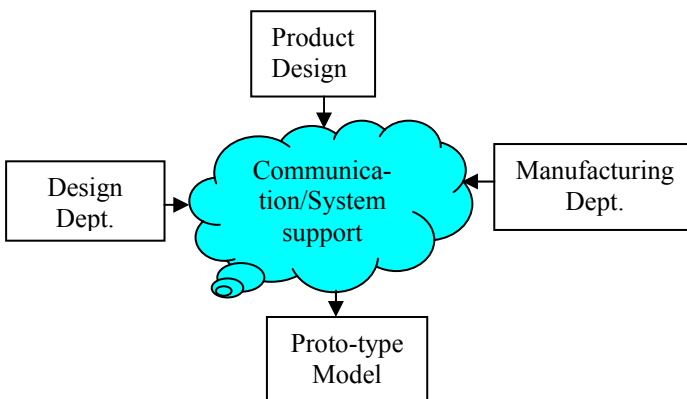


**Figure 1. Partial Concurrent Product Design Phase**

Prototyping is a simplification of a product concept. It is tested under a certain range of conditions to approximate the performances constructed to control possible variability in the tests, and is ultimately used to communicate empirical data about the part so that development decisions may be made with high confidence at reduced risk [7]. Prototyping evolves from computer-aided engineering (CAE). The question again is who should decide on prototyping the design.

## Computer-Aided Design/ Manufacturing (CAD/CAM)

Creating a CAD file interface increases the productivity of a designer, improves the quality of design and establishes a manufacturing database. Initially, CAD systems were conceived as automated drafting stations in which computer-controlled plotters produced engineering drawings. CAM, on the other hand, was developed to effectively plan, manage, and control manufacturing functions. According to Rehg and Kraebber [8], the evolution of CAD/CAM technology has made it possible to integrate many technical device areas that have for so long developed separately. CAD/CAM is the integration of design and manufacturing activities by means of computer systems. Methods used to manufacture a product are a direct function of its design and, therefore, the integrations of the two systems must always be considered when designing a product for manufacturability. CAD/CAM establishes a direct link between product-design and manufacturing departments. The goal of CAD/CAM is not only to automate certain phases of design and certain phases of manufacturing, but also to automate the transition from design to manufacturing.

In this study, the interrelationship between Computer-Aided Design and Computer-Aided Manufacturing (CAD/CAM) was explored to concurrently design a product

and produce a prototype of the design to ensure manufacturability that is efficient in terms of cost and appearance. For simplicity, the design was based on operations performed on general-purpose equipment such as Computer Numerically Controlled (CNC) machines. This was selected in order to enhance the progressive design of the product and because of such advantages as reduced lead-time, process optimization, and reduced setup and change-over times.

In a concurrent design environment, all departments involved work together by providing information pertinent to each department to the designer in order to solve the design problem. Through this cooperation, the designer has access to information from these departments at any time so that an evaluation of the design can be performed. In order to effectively do this, necessary information includes a manufacturability assessment, total amount of materials to be removed, desired tolerance and surface finish, cutting parameters and the machining time. By concurrently including both the manufacturing and production departments, the designer will be conversant on the machine floor, that is, capabilities of available machines, cutting tools and also the materials, dimensions, tolerances and surface finish. The information in serial engineering flows in succession from phase to phase [9]. This information will be compared to enhance the manufacturability of design feature.

## Problem Definition and Approach

The fundamental reason for designing a part is so that it can eventually be manufactured. In a traditional design cycle, manufacturing is often considered just a step that comes only after the design is complete (Figure 2).

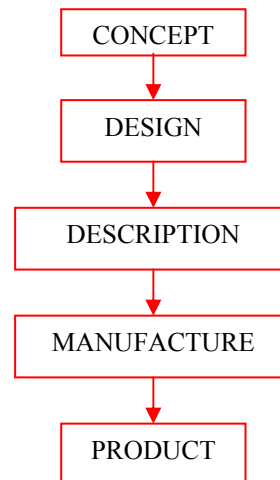


**Figure 2. CAD/CAM Current State**

With this approach, it becomes very difficult to coordinate the activities of those individuals involved in getting a product to the marketplace, and measure manufacturability to achieve overall system objectives. It cannot be denied, then, that the best way to achieve manufacturability is when both parties work together from the inception to the end of the design, as shown in Figure 3. Even though the designer works to bring the part into a position to be manufactured, he/she must maintain constant communication with manufacturing.

Manufacturing can be a major factor in design thinking and also provide such information as the state of manufacturing resources that might not otherwise be known to the designer. This cooperation helps identify manufacturing problems at the design stage, thereby minimizing the total cost of the part, improving the quality, and accelerating the introduction of the product into the marketplace. Certain

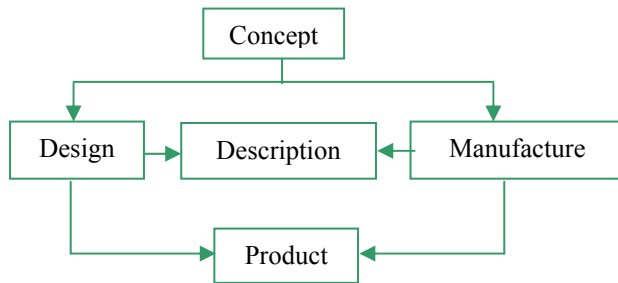


**Figure 3. CAD/CAM Proposed State**

design decisions greatly influence design for manufacturability and associated costs, and it is imperative that a designer understands the impact of these decisions early in the design process.

It is evident that the easier a part is to manufacture, the easier it will be for the part to respond to elements of interchangeability. That is, putting one part together with other parts that have been designed to the same criteria ensures easy assembly. A typical design process for manufacturing systems is often grouped into three stages. The first stage determines and characterizes three key components of the system: products produced, machines used, and the material-handling system used. For each component, designers usually have many alternatives, each alternative with different features and costs. Once the alternatives of the three components have been decided upon and characterized, the second stage is to integrate them and generate design alternatives. The third stage is to evaluate these design alternatives to see if they are economically justified in terms of manufacturability.

Efforts have been made to replace the human expert designer with artificial intelligence, neural networks and genetic algorithms [10]. These approaches have shown some potential in some areas but are limited in application. After a thorough analysis of all possible alternatives, the authors feel that design prototyping will bring the two most important departments (design and manufacturing) together as a team. The process considers the modification of the part design, as shown in Figure 4, and evaluates it for manufacturing feasibility [11]. This takes into consideration part design and production requirements that make it easier, more efficient and effective for manufacturability. The prototype considers the selection of a suitable material such that the part is producible in large quantities, and maintainable.

## Design Procedure and Discussion

The most elusive part of the term CAD/CAM is that deceptively simple oblique stroke, which links the two halves. Design (CAD) and manufacture (CAM) are best thought of as totally distinct and separate operations (figure 2) performed by different people, in different places, and at different times, using different tools and different skills. Based on this concept, once a design is complete, the designer's work is done. The designer simply hands the finished description of the object over to manufacturing, which uses the information as a guide to manufacture the part and, consequently, transform the concept into a product.

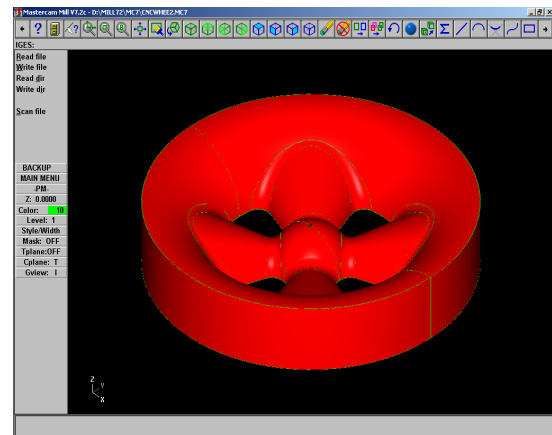


**Figure 4. Solid Part Model Design**

The process involves two groups, design and manufacturing, that must work together to ensure effective and economic manufacturability of the part. The design process begins with the redesigning of the part translated from the solid model in Figure 4 into the simulated design of Figure 5(a), using I-DEAS (Integrated Design Engineering Analysis Software). I-DEAS is solids-based, simulation-driven soft-

ware that provides full-function design analysis, drafting, testing and Numerical Control (NC) programming in support of mechanical design automation. It is a complete Mechanical Computer-Aided Engineering (MCAE) system. However, in order to enhance flexibility and adaptation to other systems, and manufacture a prototype of the part, the NC codes for this design were developed using the Mastercam (CAM) software. Mastercam was used in order to enhance the integration of two different software packages in order to increase flexibility and still maintain the level of concurrency needed to keep both design and manufacturing fully involved. Had this process been completely carried out in I-DEAS, the level of involvement of manufacturing would still have been reduced to a minimum. The use of Mastercam provided the concurrency and the interaction needed between design and manufacturing. In providing the most efficient design, the design meets all geometric specifications to within the parameters of resources available.

The initial part was designed following all geometric dimensioning and specifications. The part drawing was saved in I-DEAS, while the process moved to Mastercam software, where the part design was exported from I-DEAS as an IGES (Initial Graphics Exchange System) file to Mastercam. Mastercam gives programmers the power to capture their knowledge and build on their experiences. Using this software, the programmer has available the tools to modify any element of the part and immediately get updated tool paths without starting over.

In Figure 5a, which is the original part presented in Figure 4, the tool path was developed and simulated, and the result was saved and the part modified. The two designs were functionally identical. However, by simply reworking from two components to one, manufacturability was enhanced and manufacturing costs were reduced by more than 42 percent, as determined from code and time savings. The reduction of individual components made the final part easier to manufacture. After the original part was completed, the part was imported to Mastercam and NC codes were generated. Initially, the program resulted in 52,000 blocks of NC code being generated, and took 9.38 minutes of simulation time. After several iterations, the codes were reduced to 30,000 blocks and simulation time reduced to 4¾ minutes.

In the actual prototyping of the part, the CNC milling center was used. The manufacturing times for both designs—initial and modified—were measured during processing. For the initial stage of milling, the time observed was 4.0 hours, while a time of 2.37 hours was recorded for the modified version.

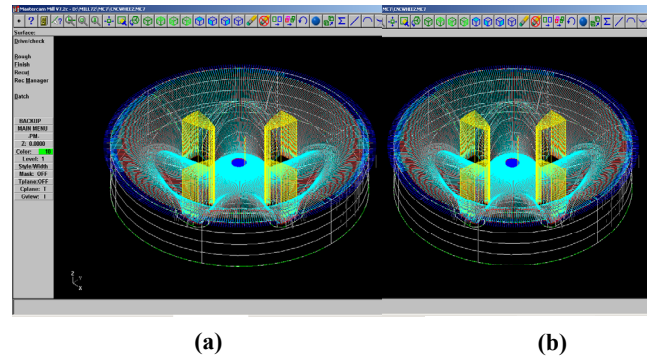


**Figure 5. Part Design with Toolpaths Simulation**

The design process can be viewed as a sequence of decisions performed iteratively based on uncertain information. Beginning from the earliest phases of the process, decisions were made that define the overall design strategies and their impact on manufacturing feasibility. In order to further enhance concurrency, flow between design and manufacturing, and to improve the design and manufacturing efficiency, the evaluation of tooling, material, clamping methods and machine setup were being performed, while the design was still being concluded. The resulting prototype, which was made out of wax, is shown in Figure 6.



**Figure 6. Actual Prototype**

## Conclusion

Design for manufacturability (DFM) is the process of proactively designing products to optimize all of the manufacturing functions, and to assure the best cost, quality, reliability, regulatory compliance, safety, time-to-market, and customer satisfaction. Early consideration of manufacturing

---

issues shortens product development time, minimizes development cost, and ensures a smooth transition into production for quicker time-to-market.

The process described here about design and prototyping for manufacturability, looks at the intersection of CAD and CAM and develops a process in which a part is designed and all necessary codes to manufacture it are generated and evaluated for easy manufacturability. Subsequent geometry changes are made until the part can be manufactured efficiently and economically, employing the integration of two software packages that respectively capture part design and production.

In order to avoid pitfalls, design and manufacturing engineers must work together, understand and use many tools of modern product development and design for manufacturability. It is no longer acceptable in the modern manufacturing environment for any of these individuals to work in isolation.

## References

- [1] Schilling, M. A., and Hill, C. W. L. (1998), "Managing the new product development process: Strategic Imperatives." *IEEE Engineering. Mgmt. Review.* Pp 55-68.
- [2] Prasad, B., Concurrent Engineering Fundamentals: Integrated Product and Process Organization. Prentice Hall, New Jersey, 1996.
- [3] Ishii, K. (1993), "Modeling of concurrent engineering design." In concurrent engineering Automation Tools and Techniques. Kusiak (Editor), John Wiley & Sons, New York, NY.
- [4] Minis, L., Herrmann, J. W., Lam, G. and Lin, E. (1999), "A generative approach for concurrent manufacturability evaluation and subcontractor selection." *Journal of Manufacturing Systems.* Vol18, No6. pp 383 – 395.
- [5] Herrmann, J. W. and Chinchokar, M. M., (2001), "Reducing Throughput Time During Product Design." *Journal of Manufacturing Systems.* V20, N.6, pp 416 – 428.
- [6] Crow K. A. (2001), "Design for Manufacturability," (DRM. Associates) [www.npd-solutions.com/dfm](http://www.npd-solutions.com/dfm).
- [7] Otto, K., and K. Wood, Product Design Technologies in Reverse Engineering and New Product Development, Prentice Hall, New Jersey, 2001.
- [8] Rehg, J. A., and H. W. Kraebber, Computer-Integrated Manufacturing 2/e, Prentice Hall, New Jersey, 2001.
- [9] A. portioli-Staudacher, H. Van Lnadeghem, M. Mapelli and C.E. Redaelli (2003) "Implementation of Concurrent engineering: A survey in Italy and Belgium" *Robotics and Computer Integrated Manufacturing.* V19, pp.225 – 238.
- [10] Senthil, K. A., Subramanian, V. and K. C. Seow (1998) "Conceptual Design Using GA," *International Journal of Advanced Manufacturing Technology.* V18, N.3, pp.72 - 81.
- [11] Structural Dynamics Research Corporation, I-DEAS Workshop: The Part Design Course IMW112-5, SDRC, Milford, Ohio, 1997.

## Biographies

**MOLU OLUMOLADE** is an Associate Professor of engineering and engineering technology in the school of Engineering and Technology at Central Michigan University. He teaches undergraduate courses in Engineering and manufacturing technology and graduate courses in engineering technology. He directs and performs research involving human factors approach to productivity improvement, scheduling and facility design and layout. Dr. Olumolade may be reached at [olumo1mo@cmich.edu](mailto:olumo1mo@cmich.edu)

**DANIEL M. CHEN** received his Ph.D. degree in Mechanical Engineering from Kansas State University in 1984. He is currently a Professor and teaches a variety of courses in both mechanical engineering and mechanical engineering technology programs. He served as a department chairperson 2001-2007, and led the departmental efforts in establishing undergraduate electrical and mechanical engineering programs. He is a registered Professional Engineer in the State of Michigan since 1986 , and his current research interests include computer-aided design (CAD) and computer-aided engineering (CAE), with a focus on their applications in engineering mechanics and machine design. Dr. may be reached at [chen1m@cmich.edu](mailto:chen1m@cmich.edu)

**HING CHEN** received his Masters in Industrial management in the Department of industrial and engineering technology at Central Michigan University. He currently works as a turbo engineer with Shun Tak-China Travel Ship Management Limited. Mr. Chen can be reached at [michael-chan@turboject.com.hk](mailto:michael-chan@turboject.com.hk)

# AN EFFECTIVE CONTROL ALGORITHM FOR A GRID-CONNECTED MULTIFUNCTIONAL POWER CONVERTER

Eung-Sang Kim, Korea Electrotechnology Research Institute; Byeong-Mun Song, Baylor University;  
Shiyoung Lee, The Pennsylvania State University Berks Campus

## Abstract

An effective control algorithm for a grid-connected multifunctional power converter is proposed and verified through computer simulation using MATLAB software. The proposed control algorithm performs suppression of harmonics and reactive power and compensation of an unbalanced phase current with the conventional function of active and reactive power control of the energy storage system. This multifunctional control utilizes a grid-connected power converter to convert it into an uninterruptible power supply (UPS). In this paper, the proposed control algorithm using instantaneous power control theory is verified through simulation using MATLAB. The results are discussed in detail along with mathematical models.

## Introduction

Power electronics technology has been widely applied to many major industrial systems. In these applications, a great deal of harmonic power is generated from the nonlinear loads of power equipment. The generated harmonics cause serious power-system interference and degrade power quality and system security as well [1] - [3]. Recent increases in power demand require more power plant construction; however, environmental problems and cost factors make it difficult to build as many new facilities as needed. Today, the battery energy storage system is considered an alternative for solving these short-term power-demand problems [4] - [8].

Battery energy storage in use with a second battery has the effect of daily peak load shedding by storing power at night and supplying power to the load during the daytime, thus improving the power factor (PF) by supplying reactive power. This system controls the active power by voltage phase difference and the reactive power by voltage magnitude using conventional power-control theory. However, with this system it is also necessary to establish additional compensation devices without compensation function for different orders of the harmonics and phase unbalance problems that frequently occur.

This paper proposes an operation control algorithm for a multifunctional battery energy storage system that adds an active filter function to eliminate harmonics to the active/reactive control function and phase unbalance compensation. The proposed control algorithm is based on instantaneous power-control theory and has the function of active power control, harmonics and reactive power suppression as well as unbalanced phase current compensation. In order to verify the effectiveness of the proposed algorithm, simulation using MATLAB was performed and the results are discussed in detail.

## Multifunctional Power Converter Basic Structure

The multifunctional power converter is a unit that can perform the role of active power control, suppression of harmonics and reactive power, and phase unbalance compensation. The proposed multifunctional power converter system consists of a three-phase inverter, a battery for charging and discharging of power, and an output controller as shown in Figure 1. The main source of voltage is a three-phase 380V, 60Hz supply, which supplies 8kW to the load. The multifunctional power converter is designed to supply 10kW of power to the load. The voltage of the battery is between 300V and 400V dc. The turns ratio of the isolation transformer is 1:1.

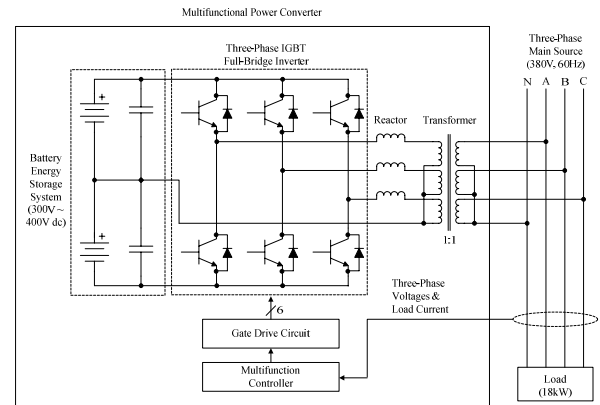


Figure 1. Basic structure of the proposed multifunctional power converter

The voltage-source inverter and the sinusoidal pulse-width modulator (SPWM) were adopted as the method of switching power devices utilizing insulated-gate bipolar transistors (IGBTs). The controller performs the on and off switching function of the IGBT device, according to the control algorithm presented below, by measuring the three-phase voltages and the load current. In general, the battery as an energy storage system is unnecessary for the active power filter itself; however, it is installed to control the active power in the proposed system.

## Conventional Control Algorithm

Instantaneous power is divided into active and reactive power. Instantaneous reactive power includes the power component from all kinds of disturbances exclusive of active power, as well as reactive power as a quantity newly defined as instantaneous power.

The conventional control algorithm performs the function of harmonics and reactive power suppression by setting the calculated reactive power component as the reference value that needs to be compensated for by the device. For a general three-phase power system, the instantaneous voltage,  $v_a$ ,  $v_b$ ,  $v_c$ , and the current,  $i_a$ ,  $i_b$ ,  $i_c$ , are expressed as instantaneous space vectors as in equation (1).

$$\begin{aligned}\bar{v} &= [v_a \quad v_b \quad v_c]^t \\ \bar{i} &= [i_a \quad i_b \quad i_c]^t\end{aligned}\quad (1)$$

The instantaneous active power of a three-phase circuit,  $p$ , which is expressed as the dot product of the instantaneous voltage and the current space vectors, can then be given by

$$p = \bar{v} \cdot \bar{i} = v_a i_a + v_b i_b + v_c i_c \quad (2)$$

For the instantaneous reactive power, the vector product of the instantaneous voltage and the current space vectors can also be defined as a new instantaneous reactive power vector,  $q$ .

$$\bar{q} = \bar{v} \times \bar{i} \quad (3)$$

From equations (1) and (3), equation (4) is obtained.

$$\begin{aligned}\bar{q} &= [q_a \quad q_b \quad q_c]^t \\ &= \begin{bmatrix} v_b & v_c \\ i_b & i_c \end{bmatrix} \begin{bmatrix} v_c & v_a \\ i_c & i_a \end{bmatrix} \begin{bmatrix} v_a & v_b \\ i_a & i_b \end{bmatrix}^t\end{aligned}\quad (4)$$

The instantaneous reactive power vector defined in equation (3) is a non-active power component, that is, the com-

ponent of extracting instantaneous active power from a three-phase circuit, which is defined as the instantaneous reactive power vector. The instantaneous active ( $\bar{i}_p$ ) and reactive ( $\bar{i}_q$ ) current vectors are defined using equations (2) and (3) as follows:

$$\bar{i}_p = [i_{ap} \quad i_{bp} \quad i_{cp}]^T = \frac{p}{\bar{v} \cdot \bar{v}} \bar{v} \quad (5)$$

$$\bar{i}_q = [i_{aq} \quad i_{bq} \quad i_{cq}]^T = \frac{q \times \bar{v}}{\bar{v} \cdot \bar{v}} \bar{v} \quad (6)$$

In order to prove the propriety of the instantaneous active and reactive current vectors, the following properties for  $\bar{i}_p$  and  $\bar{i}_q$  are considered.

$$\bar{i}_p + \bar{i}_q = \frac{p}{\bar{v} \cdot \bar{v}} \bar{v} + \frac{q \times \bar{v}}{\bar{v} \cdot \bar{v}} \bar{v} = \frac{(\bar{v} \cdot \bar{i}) \bar{v} + (\bar{v} \times \bar{i}) \times \bar{v}}{\bar{v} \cdot \bar{v}} \quad (7)$$

Using the vector product formula,  $-(a \times b) \times c = -(b \cdot c)a + (a \cdot c)b$ , equation (8) is obtained from equation (7).

$$\bar{i}_p + \bar{i}_q = \frac{(\bar{v} \cdot \bar{i}) \bar{v} + \{-(\bar{i} \cdot \bar{v}) \bar{v} + (\bar{v} \cdot \bar{v}) \bar{i}\}}{\bar{v} \cdot \bar{v}} = \bar{i} \quad (8)$$

This shows that any three-phase current vector,  $\bar{i}$ , can be reduced to two components,  $\bar{i}_p$  and  $\bar{i}_q$ . The reactive current,  $\bar{i}_q$ , is orthogonal to the voltage vector,  $\bar{v}$ , and the active current,  $\bar{i}_p$ , is parallel to the voltage vector,  $\bar{v}$ . Only the instantaneous active current vector,  $\bar{i}_p$ , is related to the instantaneous active power because the instantaneous active power is the dot product of vectors. This theory is proved by showing that  $\bar{v} \cdot \bar{i}_q = 0$  and  $\bar{v} \times \bar{i}_p = 0$ .

$$\bar{v} \cdot \bar{i}_q = \bar{v} \cdot \frac{(\bar{v} \times \bar{i}) \times \bar{v}}{\bar{v} \cdot \bar{v}} = \bar{v} \cdot \frac{-(\bar{i} \cdot \bar{v}) \bar{v} + (\bar{v} \cdot \bar{v}) \bar{i}}{\bar{v} \cdot \bar{v}} = 0 \quad (9)$$

$$\bar{v} \times \bar{i}_p = \bar{v} \times \left( \frac{p}{\bar{v} \cdot \bar{v}} \bar{v} \right) = 0 \quad (10)$$

Therefore,  $\bar{i}_p$  is the active current component parallel to the voltage vector,  $\bar{v}$ , and  $\bar{i}_q$  is the reactive current component orthogonal to  $\bar{v}$ . It is also shown that  $\bar{i}_p$  and  $\bar{i}_q$  are mutually orthogonal [9] - [12]. More detailed descriptions were derived from this work.

## Proposed New Control Algorithm

A multifunctional control algorithm for active power, harmonics and reactive power suppression, and unbalanced phase-current compensation is proposed in this paper. The major goal of the algorithm is to maintain the three-phase, sinusoidal voltage and current relationships regardless of load conditions. This means that the source provides the only constant active power in parallel with the multifunctional power converter. The proposed control algorithm sets the instantaneous active power as the reference for the compensator.

As described above, with the instantaneous source voltage and the load current that are given in equation (1), the instantaneous active power provided from the source to the load is given as equation (2) and the instantaneous active current component can be presented as mentioned above. If the instantaneous active power given in equation (2) is a constant, the desired three-phase current component,  $\bar{i}_{sd}$ , which is required in order to provide the active power from the source, can be obtained by equation (5). Then, the multifunctional power supply is controlled to provide the sum of the components to subtract the source current from the load current,  $\bar{i}_L$ , and previously-determined active-current command,  $\bar{i}_{cp}^*$ , for the reactive power control. The current command,  $\bar{i}_c^*$ , which must be provided by the multifunctional power supply, is given in equation (11).

$$\bar{i}_c^* = \bar{i}_L - \bar{i}_{sd} + \bar{i}_{cp}^* \quad (11)$$

For a load such as the rectifier in which the oscillation occurs in three-phase active power, the dc component of active power can be extracted using a low-pass filter (LPF). The low-pass filter is designed with a cut-off frequency of 10Hz and -40dB/decade of roll-off. Equation (12) shows the transfer function of the designed filter, and Figure 2 depicts the frequency response of the filter, which is represented using a Bode plot.

$$LPF(s) = \frac{769.2}{s^2 + 50.8s + 769.2} \quad (12)$$

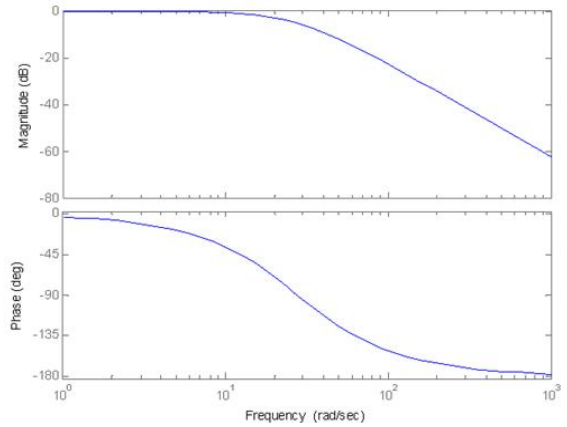


Figure 2. Frequency response of the low-pass filter

The dc component of the extracted active power is defined as  $p_{dc}$ , and the desired source current for providing  $P_{dc}$  is calculated using equation (5) as

$$\bar{i}_{sd} = \frac{p_{dc}}{\bar{v} \cdot \bar{v}} \bar{v} \quad (13)$$

The desired current command that must be provided by the multifunctional power supply is then expressed as follows:

$$\bar{i}_{cd}^* = \bar{i}_L - \bar{i}_{sd} \quad (14)$$

If the desired active power from the multifunctional power supply is defined as  $p_n$ , the active current command to provide  $p_n$  from the multifunctional power supply is represented as

$$\bar{i}_{cpn}^* = \frac{p_n}{\bar{v} \cdot \bar{v}} \bar{v} \quad (15)$$

Therefore, the final current command of the multifunctional power supply is expressed as

$$\bar{i}_c^* = \bar{i}_{cd}^* - \bar{i}_{cpn}^* \quad (16)$$

The block diagram of the control algorithm proposed in this paper is shown in Figure 3, and the controller performs functions such as active power control, reactive power and phase unbalance compensation, and harmonic suppression [13].

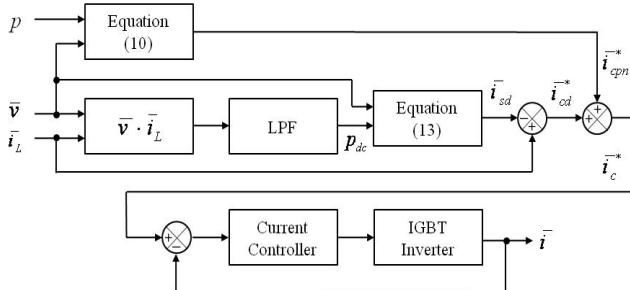


Figure 3. Block diagram of the proposed controller

## Simulation Results

In order to show the effectiveness of the proposed control algorithm, simulation was performed using MATLAB software with the assumption of the parallel operation of the multifunction power supply. The simulation was performed for the following functions: active power control, harmonics and reactive power suppression, unbalanced phase current compensation, and the connection with a rectifier load. The simulation results on the horizontal axis are the time in seconds.

## Real Power Control

An 18kW active-power load was connected to the power system. The simulation of a case where the source only supplies 8kW of active power was performed, setting the output command of active power of the multifunctional power supply at 10kW. The simulation results are illustrated in Figure 4. It shows that the multifunctional power supply provides 10kW of active power after about a 0.15s transient period. The transient is caused by the second-order response properties of the LPF.

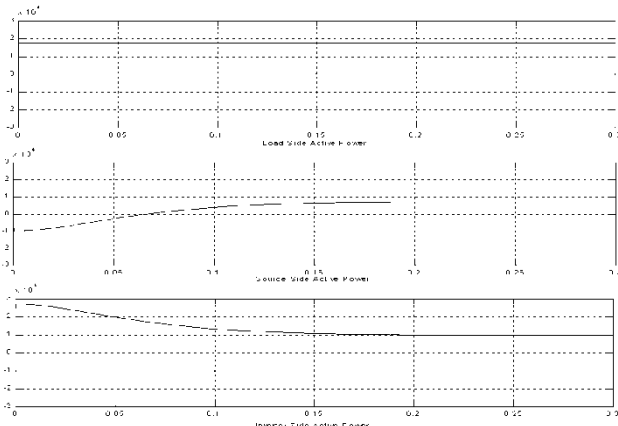


Figure 4. Real active power of the load, source, and inverter in W

## Harmonics and Reactive Power Control

A simulation for including 20% of the third harmonics and 10% of the fifth harmonics in the current provided to the load was performed. Results for 20% of the third harmonics and 10% of the fifth harmonics of phase-A system voltage and phase-A load current are shown in Figure 5, which indicates that the load current includes a lot of harmonics.

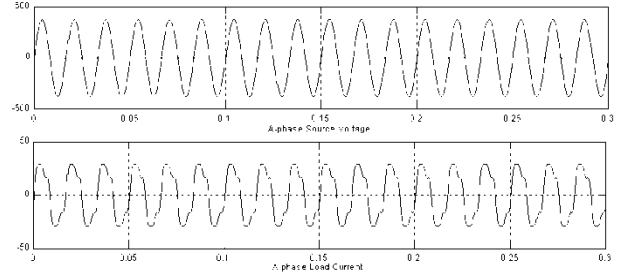


Figure 5. Waveforms of voltage in V and current in A including harmonics

In case the multifunctional power supply does not operate, the current shown in Figure 5 will be provided by the source. However, if the equipment does operate, then the sinusoidal current without any ripples will be supplied by the power supply after a transient phenomenon period of 0.15s as shown in Figure 6. The current waveform provided from the proposed equipment is shown in Figure 7.

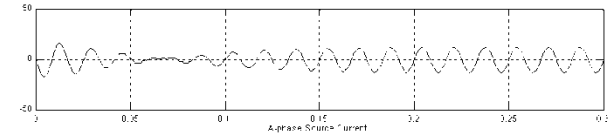


Figure 6. Current waveform in A after applying the proposed algorithm

For the current outputs in Figure 5 and Figure 7, the changes of active and reactive power are shown in Figure 8 and Figure 9, respectively. As indicated in Figure 8 and Figure 9, the source only supplies the DC voltage and the oscillation component of active power by the proposed algorithm, and the reactive power is provided from the multifunctional power supply.

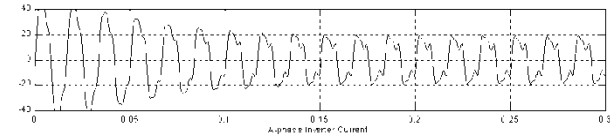
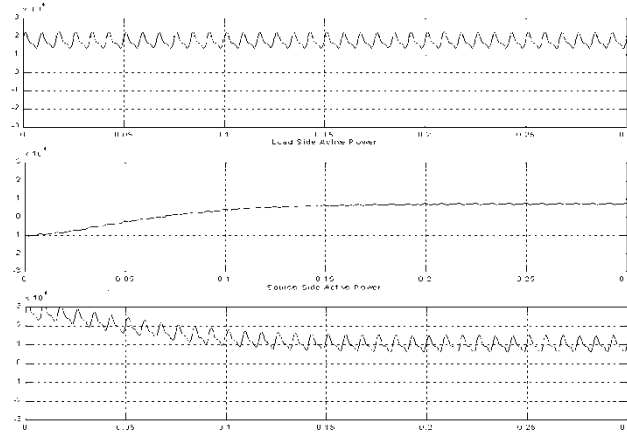
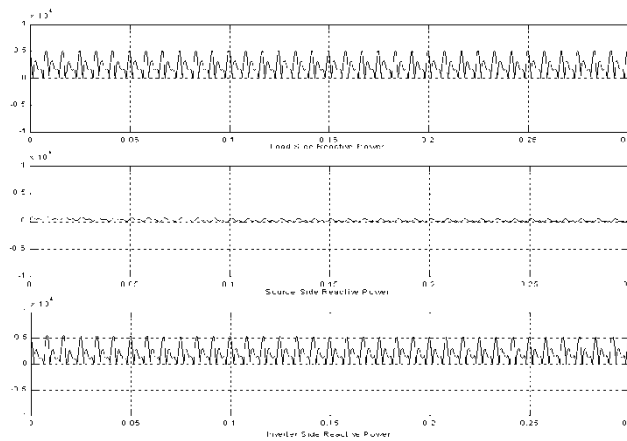


Figure 7. Current waveform in A of the multifunctional power supply



**Figure 8. Active power of load, source and multifunctional power supply in W**



**Figure 9. Reactive power of load, source and multifunctional power supply in W**

## Unbalanced Phase Current Compensation

In the three-phase system, the worst situation of unbalanced phase current occurs when only a phase current is supplied, and the other two phases have no current supply. The simulation results for this case are described in the following figures. The load-current waveform of the unbalanced phase is shown in Figure 10, and the current waveform supplied from the source is given in Figure 11. The current waveform supplied from the multifunctional power converter is illustrated in Figure 12. It is clearly shown, from Figure 10 to Figure 12, that the proposed control algorithm was successfully applied to the compensation of the unbalanced phase-current problem.

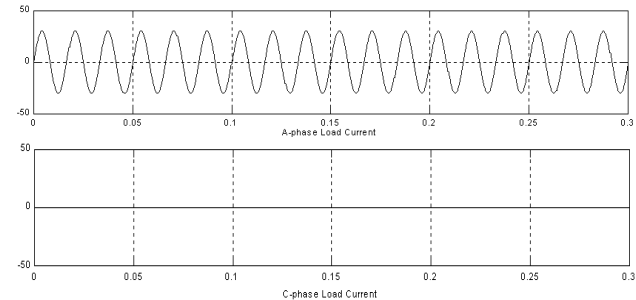


**Figure 10. Waveforms of the phases A and B load currents in A for the unbalanced system**

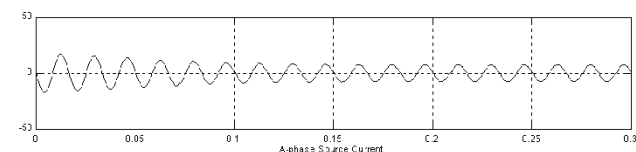


**Figure 11. Waveform of phase-A current in A for unbalanced phase**

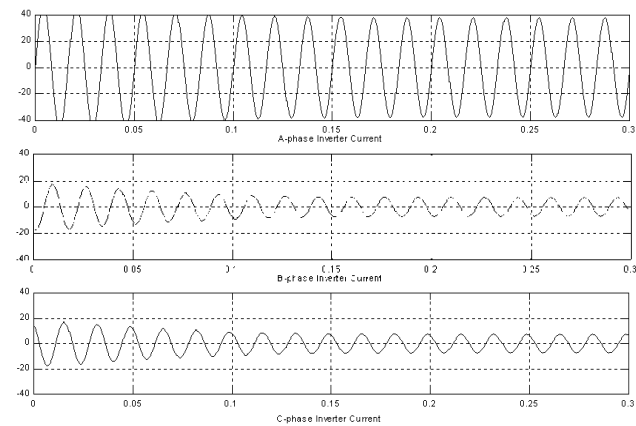


**Figure 12. Waveforms of the three-phase current in A of the multifunctional power supply**

## Connection with the Rectifier Load

A simulation was also performed for the case of a rectifier connected as a load. The waveforms of the three-phase load currents are given in Figure 13.

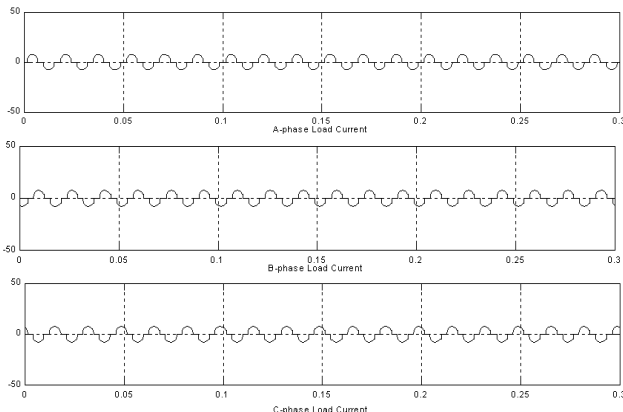


Figure 13. Waveforms of the rectifier load currents in A

The source voltage waveforms are shown in Figure 14 and indicate that the proposed algorithm functions successfully in this case also. Through several simulations, as mentioned above, it was proved that the proposed algorithm effectively performs real-power control, harmonics and reactive power suppression, and unbalanced phase current compensation as expected.

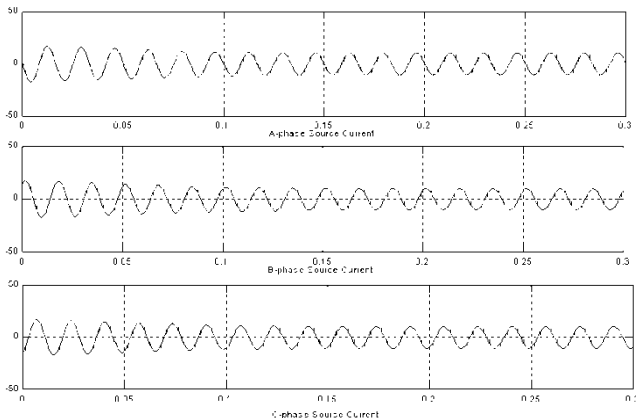


Figure 14. Waveforms of the source currents in A

## Conclusions

The operation control algorithm of a multifunctional power supply was proposed by adding functions such as active filters, harmonics and reactive power suppression, and unbalanced phase compensation to a conventional energy storage system for peak load shedding and load equalization. The major goal of the algorithm is to maintain the three-phase, sinusoidal voltage and current relationships regardless of load conditions, which means that the source provides the only constant active power in parallel with the proposed multifunctional power converter. The proposed control algorithm was based on instantaneous power theory and setting

the instantaneous active power as the reference for the compensator.

Through computer simulation using MATLAB, the effectiveness of the proposed control algorithm was demonstrated.

## References

- [1] C. Lascu, L. Asiminoaei, I. Boldea, and F. Blaabjerg, "Frequency response analysis of current controllers for selective harmonic compensation in active power filters," *IEEE Trans. on Industry Electronics*, vol. 56, no. 2, February 2009, pp. 337-347.
- [2] Y. Haiwen, G. Xin, and M. Hanguang, "Research on harmonic compensation effects for a kind of isolated power system," *The Ninth International Conference on electronic Measurement and Instruments, ICEMI*, 2009, pp. 4-681-4-686.
- [3] S.J. Chiang, S.C. Huang, and C.M. Liaw, "Three-phase multifunctional battery energy storage system," *IEE Proc.-Electr. Power Appl.*, vol. 142, no. 4, July 1995, pp. 275-284.
- [4] L. Asiminoaei, C. Lascu, F. Blaabjerg, and I. Boldea, "Performance improvement of shunt active power filter with dual parallel topology," *IEEE Trans. on Power Electronics*, vol. 22, no. 1, January 2007, pp. 247-259.
- [5] L. Marconi, F. Ronchi, and A. Tilli, "Robust perfect compensation of load harmonics in shunt active filters," *43<sup>rd</sup> IEEE Conference on Decision and Control*, December 2004, pp. 2978-2983.
- [6] D. Casini, M. Ceraolo, G. S. Furga, and D. Zaninelli, "A multifunction power supply center for experimental electric traction tests and certification," *IEEE Bologna PowerTech Conference*, June 2003, pp. 1-8.
- [7] C.M. Liaw, et al., "Small battery energy storage system," *IEE Proceeding-B*, vol. 140, no. 1, Jan. 1993, pp. 7-17.
- [8] M. Aredes and E.H. Watanabe, "New control algorithms for series and shunt three-phase four-wire active power filters," *IEEE Trans. on PWRD*, vol. 10, no. 3, July 1995, pp. 1649-1656.
- [9] Y. K. Akagi, and A. Nabae, "Instantaneous reactive compensators comprising switching devices without energy storage components," *IEEE Trans. on Industry App.*, vol. IA-20, no. 3, May/June 1984, pp. 625-630.
- [10] Y. S. Shiao, C. E. Lin, M. T. Tsai, and C. L. Huang, "Harmonic and reactive current compensation using a voltage source inverter in a battery energy storage system," *EPSR*, 1992, pp.25-33.
- [11] F.Z. Peng and J.H. Lai, "Generalized instantaneous reactive power theory for three-phase power system,"

---

*IEEE Trans. on Instrumentation and Measurement*, vol. 45, no. 1, Feb. 1996, pp. 293-297.

[12] M. Aredes, J. Hafner, and K. Heumann, "Three-phase four-wire shunt active filter control strategies," *IEEE Trans. on Power Electronics*, vol. 12, no. 2, March 1997, pp. 311-318.

[13] B. M. Song, J. S. Lai, C. Y. Jeong, and D. W. Yoo, "A soft-switching high-voltage active power filter with flying capacitor for urban maglev system applications," *Conf. Rec. of IEEE-IAS*, October 2001, pp.1461-1468.

## Biographies

**EUNG-SANG KIM** received his B.S. degree from Seoul Industrial University, Korea, in 1988 and his M.S. and Ph.D. degrees in Electrical Engineering from Soongsil University, Korea, in 1991 and 1997, respectively. Since 1991, he has been with the Department of Power Distribution System at the Korea Electrotechnology Research Institute (KERI), Korea, where he is currently a Principal Researcher and serves as a member of the Smart Grid Project Planning committee in Korea. His interests are new and renewable energy system designs and development of wind power, photovoltaic and fuel cell energy conversion systems.

**BYEONG-MUN SONG** received his B.S. and M.S. degrees in Electrical Engineering from Chungnam National University, Korea, in 1986 and 1988, respectively, and his Ph.D. degree in Electrical Engineering from Virginia Polytechnic Institute and State University, Blacksburg, VA in 2001. He was with the Korea Electrotechnology Research Institute and General Atomics. In 2004, he established his own venture company, ActsPower Technologies, San Diego, CA and served as the CEO/President and CTO. In August 2009, Dr. Song joined the Department of Electrical and Computer Engineering, Baylor University, Waco, Texas. His interests are in the design, analysis, simulation and implementation of high performance power converters, motor drives, and power electronics systems. Dr. Song is a Senior Member of IEEE.

**SHIYOUNG LEE** is currently an Assistant Professor of Electrical Engineering Technology at The Pennsylvania State University Berks Campus, Reading, PA. He received his B.S. and M.S. degrees in Electrical Engineering from Inha University, Korea, his M.E.E. in Electrical Engineering from Stevens Tech., Hoboken, NJ, and his Ph.D. degree in Electrical and Computer Engineering from Virginia Tech., Blacksburg, VA. He teaches courses in Programmable Logic Controls, Electro-Mechanical Project Design, Linear Electronics, and Electric Circuits. His research interest is digital

control of motor drives and power converters. He is a senior member of IEEE, as well as a member of ASEE, ATMAE, and IJAC.

# USING INERTIAL MEASUREMENT TO SENSE CRASH-TEST DUMMY KINEMATICS

Sangram Redkar, Arizona State University; Tom Sugar, Arizona State University; Anshuman Razdan, Arizona State University;  
Ujwal Koneru, Arizona State University; Bill Dillard, Archangel Systems; Karthik Narayanan, Archangel Systems

## Abstract

In this study, the authors present a novel fuzzy-logic signal-processing and sensor-fusion algorithm with quaternion implementation to compute dummy kinematic parameters in a vehicle crash event using inertial sensing. This algorithm is called Quaternion Fuzzy Logic Adaptive Signal Processing for Biomechanics (QFLASP-B). This algorithm is efficient and uses 3 rates obtained using gyroscopes and 3 accelerations obtained using accelerometers (one gyro and accelerometer pair per axis) to compute kinematic parameters in a crash event. In this study, this QFLASP-B algorithm was validated using MSC-ADAMS and Life-Mod simulation software. In virtual simulations of crash testing, the problem of forward kinematics was solved using MSC-ADAMS and Life-Mod to obtain body accelerations and body angular velocities. The inverse kinematic problem of computing inertial solution using body rates and accelerations was solved using QFLASP-B.

The results of these two analyses were then compared. The results revealed close similarities. In the experimental validation, the solution obtained from the Nine Accelerometer Package (NAP) was compared with the solution obtained from the three gyros and three accelerometers, or Inertial Measurement Unit (IMU), using the QFLASP-B algorithm for head orientation computation. These results were also closely aligned. The QFLASP-B algorithm is computationally efficient and versatile. It is capable of very high data rates enabling real-time solution computation and kinematic parameters determination. The adaptive filtering in QFLASP-B enables engineers to use low-cost MEMS gyroscopes and accelerometers, about \$30 each, which are typically noisy and show significant temperature dependence and bias drift—both short-term and long-term—to obtain meaningful and accurate results with the superior signal-processing and sensor-fusion algorithm. It is anticipated that this inertial tracking/sensing approach will provide an inexpensive alternative for engineers interested in measuring kinematic parameters in a crash event.

## Introduction

Motor vehicle accidents result in more than 40,000 fatalities and three million injuries each year in the United States. To increase occupant safety, it is important to study vehicle

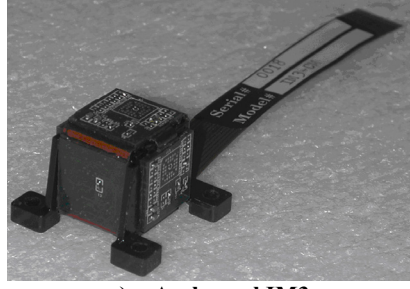
occupant kinematics and the mechanisms that generate the forces that injure vehicle occupants during crashes. Researchers have studied this problem from theoretical and practical aspects [1], [2]. Crash testing is routinely carried out to evaluate crashworthiness. Crash testing of dummies (Hybrid-II or III) and their kinematics plays a significant role in understanding occupant/pedestrian motion in crashes. There are various techniques currently used to record and understand vehicle–occupant or vehicle–pedestrian interaction. It is critical to know the positions and orientations of various body segments of a crash-test dummy in a typical crash event. This data is utilized to understand injury mechanism, severity of injury, effectiveness of seatbelts or airbags in order to determine the overall safety rating of the vehicle. There are various sensing techniques used to track the motion of a dummy in the crash scenario. Some of the widely used techniques for motion capture and sensing are high-speed video, accelerometry Nine Accelerometer Package (NAP) and inertial sensors [1]-[4]. Similar techniques are also used in Augmented Reality (AR) and Virtual Reality (VR) applications [5]-[6] for motion sensing.

The objective of this study was to present a novel software signal-processing algorithm and its applications to compute dummy kinematic parameters using inertial sensing. Currently, the sensors used for crash testing (like ATA rate-sensors gyroscopes and Endevco accelerometers) are very expensive, bulky and have strict power-conditioning and mounting requirements. In other words, using a sensor suit made up of currently-available hardware is not only expensive but also time consuming. Fortunately, recent advances in Micro Electro-Mechanical Systems (MEMS) technology have brought solid-state, integrated low-cost MEMS accelerometers and gyroscopes to market, which can theoretically be used for sensing applications.

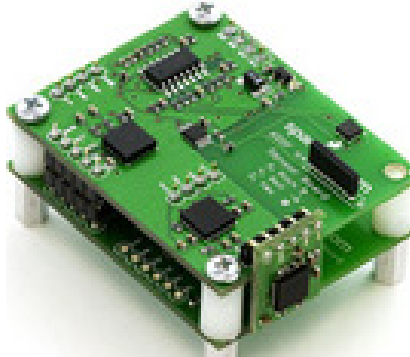
These MEMS sensors, despite their low cost, suffer from drift, scale-factor nonlinearity, noise and cross-axis errors [7]. It is almost impossible to use these sensors directly for crash testing applications. In this study, the authors present a smart Fuzzy Logic Adaptive Signal Processing (FLASP) algorithm that would enable engineers to use these low-cost MEMS sensors for accurate inertial sensing of kinematic parameters.

Some of the commercially-available IMUs are shown in Figure 1 [8]-[10]. In this study, Archangel's IMU, known as

IM3 (Inertial Measurement Cube), was used to implement the QFLASP-B algorithm. IM3 is a six-axis Inertial Measurement Unit (IMU) system in a single  $\frac{3}{4}$ " cube. This cube measures and thermally compensates accelerations in 3 orthogonal axes (local X, Y and Z) and rotational velocities in three orthogonal axes (about local X, Y and Z) and computes orientations, positions and velocities via an onboard DSP.



a) Archangel IM3



b) Sparkfun IMU



c) Analog Devices IMU

**Figure 1. Inertial Measurement Units**

The algorithm for inertial sensing (QFLASP-B) presented here runs on a low-cost DSP such as a DsPIC used by IM3, uses noisy measurements from MEMS sensors and produces equally accurate solutions obtained by high-cost precision sensors. This algorithm implements sensor-error models that

minimize systemic errors. Typically, for IMUs, signal-processing algorithms based on Kalman filtering are used [11]-[13] for sensor fusion. Unfortunately, sensor-fusion algorithms using Kalman filtering involve numerous matrix inversions and cannot be implemented on a low-cost DSP platform when high-update rates (100 Hz or more) are needed. The QFLASP-B algorithm proposed here does not involve any matrix inversions and can be implemented on a low-cost DSP with computing solutions at frequencies of 100Hz or more. This algorithm is presented in section 2, followed by its embedded implementation, simulation, and testing results in section 3. Finally, section 4 summarizes the work.

## An Algorithm for Inertial Sensing

The motivation for QFLASP can be explained by considering attitude-estimation problems with strap-down sensors, usually cast as a two-vector Wahba problem [15]. Given measurements of two non-co-linear vectors in a fixed-body frame, and with knowledge of the vectors in a reference frame, Wahba proposed an estimate of attitude by reducing the error between the reference vector set and the rotated vector set from the fixed-body frame. The use of quaternion representation eliminates the singularity issues associated with Euler-angle representations [16], [17]. The algorithm uses measurements from a fixed-body triad of gyros and accelerometers.

The estimation problem requires two frames – a fixed-body frame and a non-rotating inertial-reference frame. Let  $a$  and  $b$  represent the reference frame and the fixed-body frame, respectively. The attitude can be represented by a sequence of three right-handed rotations from the reference frame to the body frame. If  $\psi, \theta$  and  $\phi$  represent the rotations about the  $z$  axis and the intermediate  $y$  and  $x$  axes, respectively, a vector  $u^a$  in the reference frame can be transformed to a vector  $u^b$  with the rotation matrix  $C_{b/a}$ .

$$\mathbf{u}^b = \mathbf{C}_{a/b} \mathbf{u}^a \quad (1)$$

The rotation matrix is given by

$$\mathbf{C}_{a/b} = \begin{bmatrix} c\theta c\psi & c\theta s\psi & -s\theta \\ -c\phi s\psi + s\phi s\theta c\psi & c\phi c\psi + s\phi s\theta s\psi & s\phi c\theta \\ s\phi s\psi + c\phi s\theta c\psi & -s\phi c\psi + c\phi s\theta s\psi & c\phi c\theta \end{bmatrix} \quad (2)$$

where  $c$  and  $s = \cos$  and  $\sin$ , respectively.

For a 3-2-1 rotation sequence, Euler-angle representation has a singularity at  $\theta = \frac{\pi}{2}$ , where the roll and yaw angles are undefined. An alternate representation of attitude is with a

quaternion. Quaternions are generalizations of complex numbers in three dimensions, and are represented by

$$\mathbf{q} = [q_0 \quad \mathbf{q}_r]^T \quad (3)$$

where  $q_0$  and  $\mathbf{q}_r$  are the real part and the vector part of the quaternion. If the norm of the quaternion is unity, it is referred to as a unit quaternion. Just like the rotation matrix, a unit quaternion (or any quaternion in general) can be used to rotate a vector from a reference frame to a fixed-body frame. The rotation equation in terms of quaternion is expressed as

$$\begin{aligned} \mathbf{u}^b &= \mathbf{q}^{-1} \cdot \mathbf{u}^a \cdot \mathbf{q} \\ \mathbf{q}^{-1} &= \begin{bmatrix} q_0 \\ -\mathbf{q}_r \end{bmatrix} \end{aligned} \quad (4)$$

where  $\mathbf{q}^{-1}$  is the inverse of the unit quaternion  $\mathbf{q}$  and  $\mathbf{q}$  is the unit quaternion that rotates a vector from system  $a$  to system  $b$  [17]. The attitude quaternion can also be represented as a product of component quaternions in three axes.

$$\mathbf{q}_\phi = [\cos(\phi/2) \quad \sin(\phi/2) \quad 0 \quad 0]^T \quad (5)$$

$$\mathbf{q}_\theta = [\cos(\theta/2) \quad 0 \quad \sin(\theta/2) \quad 0]^T \quad (6)$$

$$\mathbf{q}_\psi = [\cos(\psi/2) \quad 0 \quad 0 \quad \sin(\psi/2)]^T \quad (7)$$

The quaternion  $\mathbf{q}$  can be derived from the component quaternions as

$$\mathbf{q} = \mathbf{q}_\psi \cdot \mathbf{q}_\theta \cdot \mathbf{q}_\phi \quad (8)$$

Poisson's kinematic equation in quaternion form that relates the rate of change of the attitude quaternion to the angular rate of the body frame with respect to inertial frame [17] is given by

$$\dot{\mathbf{q}}_{b/a} = 0.5 \cdot \mathbf{q}_{b/a} \cdot \boldsymbol{\omega}_{b/a} \quad (9)$$

If  $\mathbf{q}_1$  and  $\mathbf{q}_2$  are two quaternions, the relative orientation or the error quaternion between the two is

$$\mathbf{q}_e = \mathbf{q}_1 \cdot \mathbf{q}_2^{-1} \quad (10)$$

The two frames, whose attitude quaternions with respect to a reference frame, are  $\mathbf{q}_1$  and  $\mathbf{q}_2$  and coincide only if

$$\delta \mathbf{q}_e = 1 \text{ and}$$

$$\delta \mathbf{q}_e^r = 0 \quad (11)$$

where  $\delta \mathbf{q}_e$  and  $\delta \mathbf{q}_e^r$  are the real and vector parts of the quaternion error.  $\delta \mathbf{q}_e^r = 0$  is a sufficient condition for the two frames to coincide.

## Algorithm Description

The algorithm presented here uses measurements from three axis gyros and accelerometers. If  $\omega_T$  is the true angular rate and  $\omega$  is the measured angular rate, then

$$\omega = \omega_T + \varepsilon_B + \varepsilon + \eta \quad (12)$$

where  $\varepsilon_B$  is a time-varying bias,  $\eta$  is noise, and  $\varepsilon$  is other errors. If gyro bias can be captured with an active bias estimation scheme, then the estimate of the true angular rate is given by

$$\bar{\omega} = \omega - \bar{\varepsilon}_B - \varepsilon_\omega \quad (13)$$

where  $\bar{\varepsilon}_B$  is the current estimate of the gyro bias and  $\varepsilon_\omega$  is an angular rate correction derived from the attitude error. The estimate of angular rate is used to compute an attitude estimate from the gyros by the integration of equation (9). Expressed in matrix form, equation (9) is given by

$$\begin{bmatrix} \dot{q}_0 \\ \dot{q}_1 \\ \dot{q}_2 \\ \dot{q}_3 \end{bmatrix} = \begin{bmatrix} 0 & -\omega_x & -\omega_y & -\omega_z \\ \omega_x & 0 & \omega_z & \omega_y \\ \omega_y & -\omega_z & 0 & \omega_x \\ \omega_z & \omega_y & -\omega_x & 0 \end{bmatrix} \begin{bmatrix} q_0 \\ q_1 \\ q_2 \\ q_3 \end{bmatrix} \quad (14)$$

where  $\omega_x, \omega_y, \omega_z$  are estimates of the true angular rates in the  $x, y$  and  $z$  axes. Given an initial attitude estimate, equation (14) can be integrated to obtain the latest attitude estimate,  $\mathbf{q}_0$ . A reference attitude estimate is obtained from accelerometers. The accelerometer measurements are given by

$$\dot{\mathbf{v}}_I = \dot{\mathbf{v}}_B + \boldsymbol{\omega} \times \mathbf{v}_B + \mathbf{G} \quad (15)$$

where  $\mathbf{v}_B, \mathbf{v}_I$  are body and inertial velocities, respectively,  $\mathbf{G}$  is the gravity vector component in the body coordinates given by

$$\mathbf{G} = [g \sin \theta \quad -g \cos \theta \sin \phi \quad -g \cos \theta \cos \phi]^T \quad (16)$$

If a measure of forward velocity in the body frame is not available, the roll and pitch angles obtained from accelerometers are corrupted by the linear acceleration and the cross product terms involving angular rate and linear velocity. If the reference attitude quaternion is  $\mathbf{q}_l$ , the attitude error using equation (11) is given as

$$\mathbf{q}_e = \mathbf{q}_l \cdot \mathbf{q}_0^{-1} \quad (17)$$

If the attitude error is small,  $\mathbf{q}_{e0} \approx 1$  and  $\mathbf{v} = [q_{e1} \quad q_{e2} \quad q_{e3}]$  can be assumed to be the errors in roll, pitch and yaw attitudes. The quaternion error can be used to generate angular rate corrections using

$$\varepsilon_\omega = \mathbf{k} \cdot \mathbf{v} \quad (18)$$

where  $\mathbf{k}$  is an estimator gain. The angular rate correction is used as a feedback correction as given in equation (13).

The main features of QFLASP are

**1. Adaptive Switching/Filtering:** The data flow is altered at runtime. Thus, certain filters are activated or deactivated based on quality, consistency, and characteristics of data. The switching is implemented by means of Fuzzy Logic

(discussed in next section). The Fuzzy estimator consists of a fuzzification process, an inference mechanism, a Rule Base and a defuzzification process. The fuzzification process assigns a degree of membership to the inputs over the Universe of Discourse. As the error changes, the degree of certainty changes and other measures of  $\mu$  have non-zero values. Thus, the errors are encoded by the degree of certainty that are between certain error bounds. The values for the error bounds ( $E_1, E_2$ ) can be determined using center clustering techniques on actual crash-test experimental data. Likewise, input membership functions are determined for the change in error. This process is explained in detail in the next section.

**2. Adaptive Gain Tuning:** The gains of the body-rate error, inertial-rate error and delay are tuned during runtime. Thus, the algorithm tunes itself to provide an optimum solution. In fact, the QFLASP-B output accuracy improves with period of use. The residual drift in the gyros and accelerometers is removed by means of feed-forward filters and are implemented in an error-correction loop.

**3. Gravity Compensation:** Accelerometers measure specific force, i.e., the accelerometer does not measure gravity but rather the component of total acceleration minus gravity along its input axis. The gravity-compensation function in QFLASP acquires data from accelerometers, based on the characteristics and validity of data, using appropriate filtering and passes slaving information to a sensor-fusion algorithm.

The governing equation for IMU dynamics are given as

$$\begin{aligned}\dot{\theta} &= \omega_y \cos \phi - \omega_z \sin \phi \\ \dot{\phi} &= \omega_x + \omega_y \sin \phi \tan \theta + \omega_z \cos \phi \tan \theta \\ \dot{\psi} &= (\omega_y \sin \phi + \omega_z \cos \phi) \sec \theta\end{aligned}\quad (19)$$

The acceleration equations are given as

$$ax_{cg} = \dot{U} + \omega_y W - \omega_z V + g \sin \theta \quad (a)$$

$$ay_{cg} = \dot{V} + \omega_z U - \omega_x W - g \cos \theta \sin \phi \quad (b) \quad (20)$$

$$az_{cg} = \dot{W} + \omega_x V - \omega_y U - g \cos \theta \cos \phi \quad (c)$$

where  $\omega_x, \omega_y$  and  $\omega_z$  are body-angular velocities about  $x, y, z$  directions, respectively, and  $\theta, \phi$  and  $\psi$  are pitch, roll and yaw (inertial) angles.  $U, V, W$  are body velocities in the  $x, y, z$  directions, respectively, and  $ax_{cg}$ ,  $ay_{cg}$  and  $az_{cg}$  are inertial accelerations. It should be noted that equation (19) is a coupled equation in angular velocities but does not involve any acceleration term. Equation (20) involves accelerations as well as body rates. Thus, discrete version of equation (19) is solved in an outer loop and equation (20) is solved in the

inner loop to determine kinematic parameters—e.g., roll, pitch, yaw, inertial velocities, and positions—via integration.

## Quaternion Fuzzy Logic

QFLASP is a novel approach for removing sensor errors. FFLASP, like Fuzzy Logic from which it is derived, is a more intuitive process than Kalman Filtering [16], [17]. As an example, the quaternion errors and gyro biases are calculated by this algorithm and used in an adaptive loop to remove their effects. The Fuzzy estimator consists of a fuzzification process, an inference mechanism, a Rule Base and a defuzzification process. The fuzzification process assigns a degree of membership to the inputs over the Universe of Discourse. Referring to Figure 2, if the error ( $e$ ) in Euler angle  $k$  is zero, the degree of certainty,  $\mu_0$  (center membership function), is 1 and all others are zero. As the error changes, the degree of certainty changes and other measures of  $\mu$  have non-zero values. Thus, the errors are encoded by the degree of certainty of their error bounds.

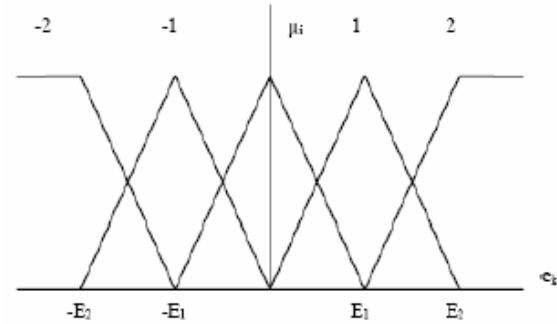


Figure 2. Membership Functions for Fuzzy Logic

Table 1. Rule Table for Fuzzy Logic

OUTPUT	"change in error"				
	2	1	0	-1	-2
"error"	2	2	2	1	0
	1	2	2	1	0
	0	2	1	0	-1
	-1	1	0	-1	-2
	-2	0	-1	-2	-2

The values for the error bounds ( $E_1, E_2$ ) can be determined using the center-clustering techniques on crash data. Likewise, input membership functions are determined for the change in error. For five error input membership functions and five change-in-error input membership functions, twenty five rules result as seen in Table 1.

Any membership function with a non-zero degree of certainty is said to be 'on' and the corresponding rule is also

active [16], [17]. If both the error and change in error were small enough to be within the smallest error bounds (- $E_1$  to + $E_1$  in Figure 2), the linguistic rule is considered as follows: If  $e$  is zero and change in  $e$  is zero then, correction is zero.

The certainty of the premise,  $i$ , is given by:

$$(1) \quad \mu_i = \min(\mu_{e0}, \mu_{\Delta e0})$$

In general, the rules are given as:

$$(2) \quad \text{If } \tilde{\mu}_{ei} \text{ is } A_{ei}^j \text{ and } \tilde{\mu}_{\Delta ei} \text{ is } A_{\Delta ei}^k, \\ \text{then } \varepsilon_i = g_i(\bullet) \text{ and } \dot{\varepsilon}_i = h_i(\bullet)$$

The symbol “•” simply indicates the AND argument. In QFLASP-B, the quaternion error is first reduced to the error in Euler angles:

$$\vec{\varepsilon}_q \rightarrow \{\varepsilon_\phi, \varepsilon_\theta, \varepsilon_\psi\} \quad (21)$$

The rules of Table 1 are then applied to each Euler angle error. The output correction for each Euler angle and Euler rate is calculated using a center-of-gravity method:

$$\hat{\varepsilon}_{\text{eulerangle}} = \frac{\sum_{i=1}^R g_i \mu_i}{\sum_{i=1}^R \mu_i}, \quad \hat{\dot{\varepsilon}}_{\text{eulerangle}} = \frac{\sum_{i=1}^R h_i \mu_i}{\sum_{i=1}^R \mu_i} \quad (22)$$

Corrections to the body rates can then be determined. To apply quaternion corrections, the estimated error quaternion must be reconstructed:

$$\vec{\varepsilon}_q \leftarrow \{\varepsilon_\phi, \varepsilon_\theta, \varepsilon_\psi\} \quad (23)$$

These corrections are then applied to the quaternion to remove quaternion error. Once the attitude is determined, angles and rate can be substituted into equation (20). Equation (20) can be integrated to calculate the velocity and position. It is noted that the Fuzzy logic approach discussed here is generic and can be extended to minimize accelerometer systemic errors.

While similar results to the QFLASP-B can be obtained using a Kalman Filter, the operational software overhead is considerable. In our own tests, the Kalman Filter took 3.5 ms to run per iteration, while QFLASP-B took under 1 ms per iteration on a Texas Instrument C33 DSP with a clock speed of 60 MHz. Similarly, the Kalman Filter code required memory of nearly 10,000 words, while the QFLASP-B was under 3,000 words. Both requirements were driven in the

Kalman Filter by the matrix inversion, which is absent in the QFLASP-B.

## Simulation and Experimental Results

Here, the authors tested the QFALSP-B algorithm through ADAMS-LifeMOD simulations. In these test cases, QFLASP-B performance for head-orientation computation and torso-orientation computation in a frontal crash situation was investigated. The forward kinematics problem was posed and solved in ADAMS [18] that gives body rates and accelerations. These body rates and accelerations were fed into QFLASP in order to solve the inverse kinematics problem. These simulations will help to ensure that:

1. QFLASP-B switches are working properly. There is no time delay in operating switches. A delay in switching would result in inaccurate or incorrect solutions.
2. QFALSP does not encounter singularities. The advantage of QFLASP-B over FLASP-Euler angle formulation is that it can handle 90° pitch situations. Unfortunately, the computation is time-consuming and may introduce group delay that would corrupt the solution.
3. At this preliminary stage, it is not possible conduct to extensive lab testing that would validate QFLASP-B for all possible crash scenarios. It is anticipated that these simulations will reveal problems with QFLASP-B and help tune the algorithm better.

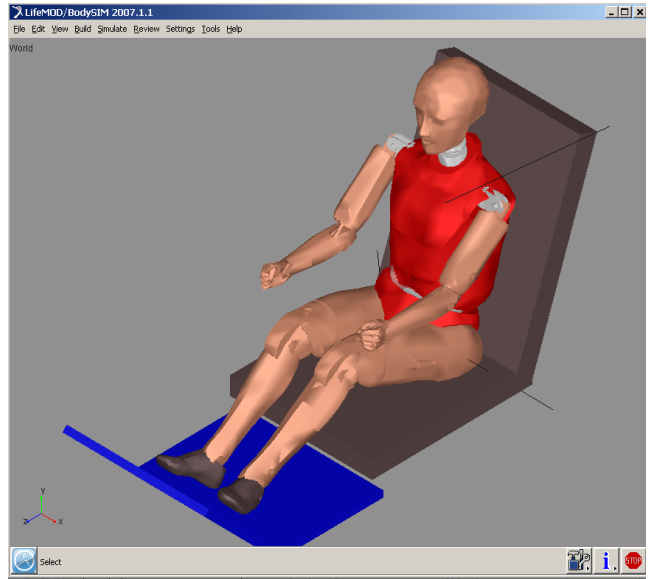


Figure 3. ADAMS-LifeMOD Setup for virtual crash testing

It was noted that the forward dynamics data can be corrupted using gyro, accelerometer-bias models so that this dataset would be very close to experimental data. This cor-

rupted data can be fed into QFLASP-B to evaluate the effectiveness of the algorithm. For this sample simulation, the dummy was postured as an occupant driving the car with 3-point seat belts attached (refer to Figure 3). A translational joint was created between the ground and car seat to simulate impact (standard SAE shock pulse). An equilibrium analysis was carried out so that the model settles under the action of gravity.

An appropriate coordinate transformation matrix was used to preprocess the head angular rate (shown in Figure 4) and head acceleration data obtained from ADAMS simulations before feeding them to QFLASP-B. Head angular velocity in body coordinates is shown in Figure 4. It is noted that  $\omega_x$  reaches a maximum value of 1500 deg/s. The head orientations computed by QFLASP-B from raw accelerometer and gyro data are shown in Figure 5. It can be observed in Figure 5 that the forward ADAMS attitude solution (obtained from MSC-ADAMS-LifeMod inertial marker) matches quite closely with the inverse QFLASP solution.

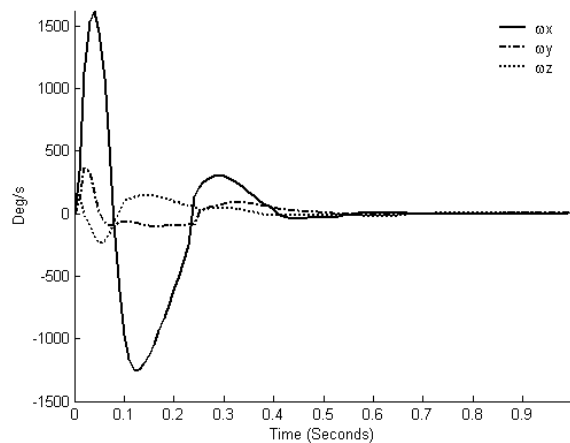


Figure 4. Head Angular Velocity in body frame

In the second simulation, torso response is evaluated in a frontal crash. As before, the dummy was constrained by a 3-point lap shoulder belt and a standard SAE shock pulse was applied. Central torso body accelerations about the x, y and z axes are plotted in Figure 6(a). Central Torso body angular velocities are plotted in Figure 6(b). The attitude solution is presented in Figure 6(c). It should be noted that due to lap-shoulder belts, the central torso motion is restricted. The body accelerations and body rates obtained from ADAMS-LifeMod simulations were fed into QFLASP-B to get torso orientations in inertial coordinates.

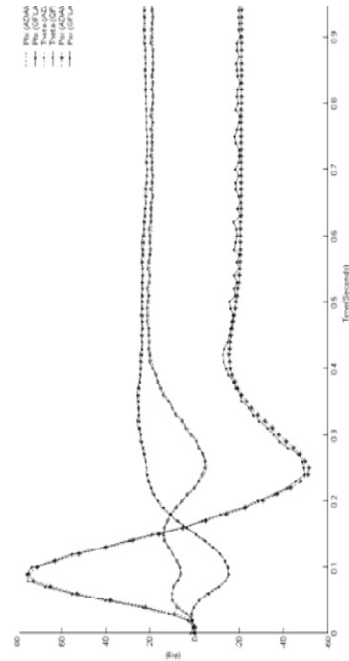
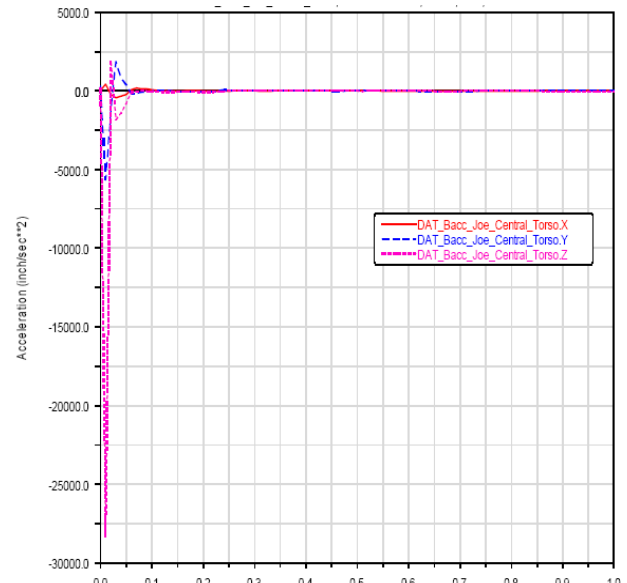
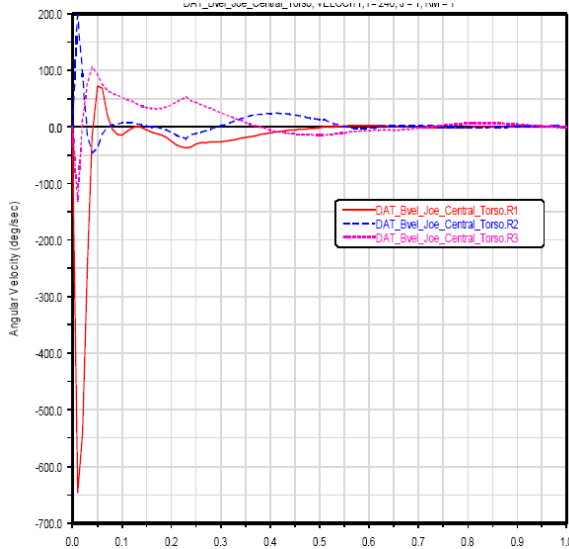


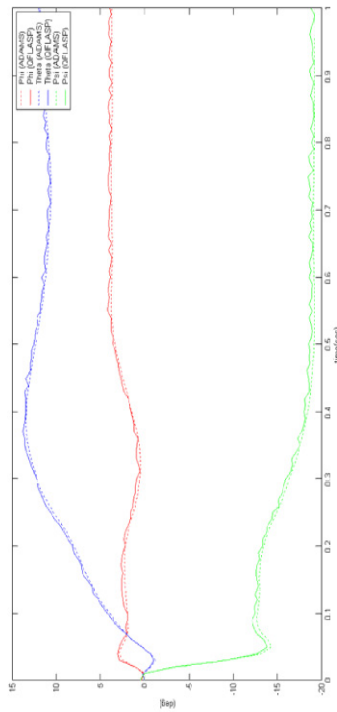
Figure 5. Head Inertial Forward Kinematics- ADAMS solution (indicated by dotted lines) and Inverse Kinematics-QFLASP Solution (indicated by solid lines).



a) Central Torso Body Accelerations vs. time (seconds)



**b) Central Torso Body Angular Velocity vs. time (seconds), (R1-rotation about x, R2-rotation about y, R3-rotation about z axis)**



**c) Central Torso Inertial Forward Kinematics- ADAMS solution (dotted line) and Inverse Kinematics-QFLASP Solution (solid line).**

**Figure 6. Central Torso Accelerations, Body Angular velocity and inertial solution IMU Coordinates**

It should also be noted that the ADAMS solution sensed by a marker in an inertial frame matches quite closely to the attitude solutions computed by QFLASP-B, as shown in Figure 6(c).

## Experimental Validation

In preliminary studies, the algorithm was tested for head kinematics. The purpose of this test was to evaluate head-restraint responses. There was about 20 msec of pre-crash data (about 250 points), which was used for bias capture. The test was done on a Hybrid III 50th percentile dummy with NAP and angular sensors. The advantage of such a configuration is that it is possible to compute head orientations using the NAP algorithm [1] and also acceleration and rate data can be fed into QFLASP-B. Thus, head orientations can be computed with two different techniques. The setup with sensor-mounting locations is shown in Figure 7. The dummy was subjected to standard SAE crash pulses and the raw sensor data in body coordinate system is shown in Figure 8. It is important to note that for meaningful results, the IMU coordinate system (at the CG of the head) should be mapped to the SAE coordinate system.

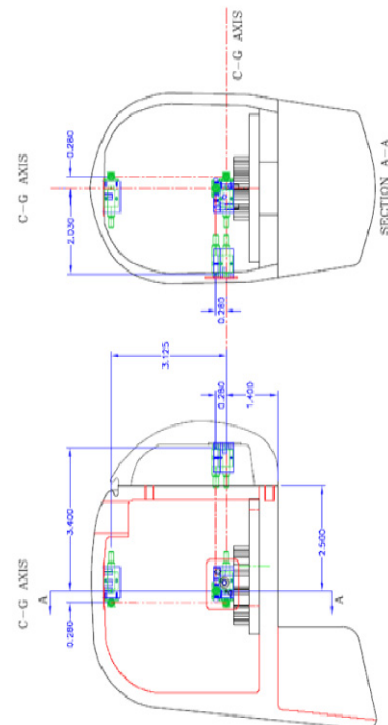


**Figure 7. Setup for Head Kinematics Test (sensor mountings locations shown in green)**

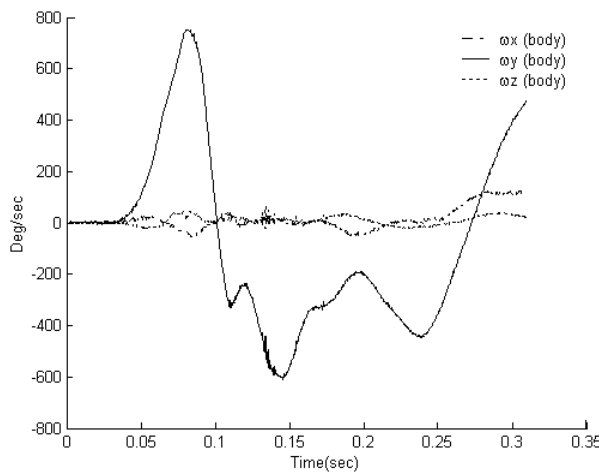


**Figure 8. Raw Rate Sensor Data in Body Coordinates**

An appropriate coordinate transformation matrix was used to preprocess the data before feeding them into QFLASP-B. In Figure 8, it can be observed that rates about the 'y' axis are very high at about 800 deg/s. The orientations computed by QFLASP-B are shown in Figure 9. It can be noted that pitch varies from  $+20^\circ$  to  $-30^\circ$  (rebound motion). However, roll and yaw are within  $5^\circ$ . These results compare favorably

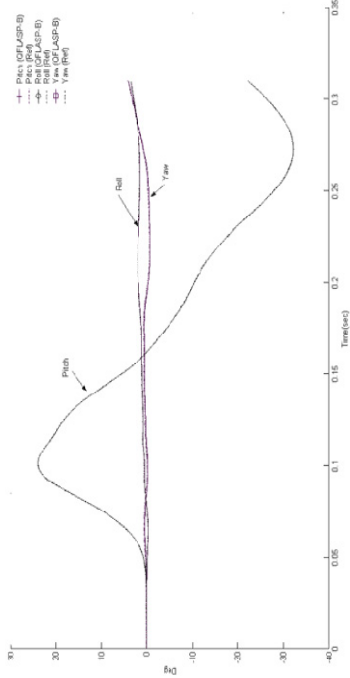


**Figure 9. Attitude Solution in Head Restraint Test NAP Solution (indicated by dotted lines) and QFLASP-B Solution (indicated by solid lines)**

with the reference NAP solution shown in Figure 8. However, due to less computation overhead, the speed of execution of QFLASP-B is much higher and QFLASP-B uses body accelerations for slaving (or to correct attitude solution using accelerometer data). Therefore, unlike the NAP processing algorithm, QFLASP-B can be operated in runtime for a longer duration or on a much cheaper DSP platform, if required. Other kinematic parameters such as angular accelerations, linear accelerations and inertial angular velocity can be easily derived using this approach, which can be used to compute injury measurements. It can be seen that this inertial measurement allows for computing relative orientations of various body parts, such as head rotation with respect to neck, in a fixed reference frame.

## Discussion and Conclusions

In this study, the authors presented a novel approach for sensing dummy kinematics in crash events using inertial measurement via Fuzzy logic. Sensing of dummy kinematic parameters in a crash event is crucial for evaluating the crashworthiness of vehicles. These kinematic parameters were used to compute various injury parameters, to understand the severity of injuries, to study the effectiveness of seat belts and airbags, and other occupant safety devices. The inertial-sensing approach discussed here is based on sensing rates and accelerations in 3 mutually perpendicular directions and using a Fuzzy-Logic-based algorithm for computing inverse kinematic inertial solutions. This superior signal-processing algorithm compensates for sensor errors like noise and drift present in typical low-cost MEMS sensors and provides equally accurate solutions normally obtained by expensive testing methods/sensor suites. This quaternion-based approach is free from singularities at  $90^\circ$  and, unlike the Kalman filter, does not involve matrix inversions. The hardware and software aspects of inertial sensing along with simulations and preliminary experimental results were also discussed. In simulations, forward-kinematics problems were posed and solved in MSC -ADAMS to obtain body rates and accelerations. These accelerations and rates were fed into QFLASP to obtain an inverse kinematic inertial solution. Two simulation cases, head-orientation calculation and torso-orientation calculation, were presented. In both cases, the MSC-ADAMS solution obtained via a marker in an inertial frame matches very closely with the QFLASP solution.

In preliminary experimental tests, the QFLASP algorithm was tested to compute head orientation and compared against the solution computed by a standard NAP sensor suit. The NAP solution and QFLASP solution matched quite well. Currently, efforts are underway to test QFLASP in a variety of crash situations. QFLASP can be implemented on

a low-cost DSP at much higher update rates. It is anticipated that this Inertial Tracking/Measurement approach will enable test engineers to use low-cost MEMs sensors for crash testing and provide an inexpensive alternative for measuring kinematic parameters in a crash event.

## Acknowledgments

The authors thank Dr. Michael Greene and Mr. Victor Trent of Archangel Systems for their help in this project. Support from MSC Software and the US Department of Transportation is also gratefully acknowledgement.

## References

- [1] J. Hill, M. Regan, R. Adrezin, and L. Eisenfeld, "System for Recording the Bowel Sounds of Premature Infants," ASME Biomed 2008 Conference, June 2008.
- [2] A. J. Padgaonkar, K. W. Krieger and A. I. King, "Measurement of angular acceleration of a rigid body using linear accelerometers.", *Journal of Applied Mechanics* 42, pp. 552–556, 1975
- [3] JRW Morris" Accelerometry - A technique for the measurement of human body movements." *Journal of Biomechanics*, 6, pp. 729–736, 1973.
- [4] R. E. Mayagoitia , P. H. Veltink," Accelerometer and rate gyroscope measurement of kinematics: an inexpensive alternative to optical motion analysis systems". *Journal of Biomechanics*, 35(4), pp. 537-542, 2002
- [5] A. J. van den Bogert, L. Read and B. M. Nigg, "A method for inverse dynamic analysis using accelerometry". *Journal of Biomechanics*. 29(7), pp. 949-954, 1996.
- [6] K. Aminian K. and B. Najafi, "Capturing human motion using body-fixed sensors: outdoor measurement and clinical applications.", *Computer Animation and Virtual Worlds*, 15, pp.79–94, 2004.
- [7] E.B. Bachmann "Inertial and magnetic tracking of limb segment orientation for inserting humans into synthetic environments". PhD Thesis, Naval Post-graduate School, 2000.
- [8] H. J. Luinge "Inertial sensing of human movement". PhD Thesis, University of Twente, 2002.
- [9] [www.archangel.com](http://www.archangel.com)
- [10] [www.sparkfun.com](http://www.sparkfun.com)
- [11] [www.analog.com](http://www.analog.com)
- [12] E. Foxlin "Inertial head-tracker sensor fusion by a complementary separate bias Kalman filter". In Proceedings of VRAIS '96, pp. 185–194, 1996.
- [13] R. G. Brown, *Introduction to Random Signals and Applied Kalman Filtering*, Wiley Publishing, 1996.
- [14] M. S. Grewal, L. R. Weill and A. P. Andrews ,*Global positioning systems, inertial navigation, and integration*, Wiley-Interscience, 2000
- [15] Wahba, G., "A Least-Squares Estimate of Spacecraft Attitude". *SIAM Review*, 7, 3, pp. 409-421, 1965
- [16] Greene M. and Trent V., "Software algorithms in air data attitude heading reference systems," *Aircraft Eng. And Aerospace Tech.*, West Yorkshire, Emerald Pub., 75(5), pp. 472-6, 2003.
- [17] K. Narayanan and Greene M., " A Unit Quartornion and Fuzzy Logic Approach to Attitude Estimation, In the proceedings of ION NTM 2007 pp. 731-735
- [18] [www.msccsoftware.com](http://www.msccsoftware.com)

## Biographies

**SANGRAM REDKAR** is an Assistant Professor in Engineering Technology at Arizona State University (ASU) Dr. Redkar may be reached at [sangram.redkar@asu.edu](mailto:sangram.redkar@asu.edu)

**TOM SUGAR** is an Associate Professor in the Engineering Department at ASU. Dr. Sugar may be reached at [thomas.sugar@asu.edu](mailto:thomas.sugar@asu.edu)

**ANSHUMAN RAZDAN** is an Associate Professor in the Engineering Department at ASU. Dr. Razdan may be reached at [ar@asu.edu](mailto:ar@asu.edu)

**UJWAL KONERU** is a graduate student in the Department of Computer Science at ASU. Mr. Koneru may be reached at [ujwal.koneru@asu.edu](mailto:ujwal.koneru@asu.edu)

**BILL DILLARD** is the Director of Emerging Technologies at Archangel Systems, Auburn, AL. He can be reached at [bill@archangel.com](mailto:bill@archangel.com)

**KARTHIK NARAYANAN** is the lead software engineer at Archangel System. He can be reached at [karthik@archangel.com](mailto:karthik@archangel.com)

# PRE-AMP EDFA ASE NOISE CHARACTERIZATION FOR OPTICAL RECEIVER TRANSMISSION PERFORMANCE OPTIMIZATION

Akram Abu-aishah, University of Hartford; Hisham Alnajjar, University of Hartford

## Abstract

Amplified Spontaneous Emission (ASE) noise mitigation from a pre-amp Erbium-Doped Fiber Amplifier (EDFA) to the Photon Detector (PD) in optical receivers can be reduced by minimizing the EDFA ASE noise at the optical receiver level to achieve optimal optical receiver transmission performance. The experimental work presented here focuses on the pre-amp EDFA noise performance characterization and analysis at the optical receiver level. This is the ultimate performance characterization method for the pre-amp EDFA, and it was performed through testing of the optical receiver transmission performance under different pre-amp operating conditions.

## Introduction

The main motivation for this work was to present a set-up and a procedure that can be used to characterize pre-amp EDFA noise and to present the results obtained using such a set-up and procedure. This work adds to the current knowledge in this field by the results obtained and presented here. This study concluded that the pre-amp EDFA needs to be optimized at the same input power and the same signal-to-noise factor at which it is to operate. The input power performance was in line with the one analyzed for Figure 4, where an increase of the input signal power resulted in an improvement of the optical receiver transmission performance.

The basic design of an optical receiver consists of an EDFA, an optical band-pass filter, a photon detector, a limiting amplifier, and an electrical low-pass filter [1]. Pre-amp EDFA are becoming an integral part of optical receivers since their performance is interrelated to the performance of the photon-detector receiver. The photon detector used in optical receivers is either a PIN diode or an Avalanche Photo Diode (APD). APDs have higher sensitivity than PIN diodes, but they exhibit excess noise that degrades the optical receiver transmission performance. On the other hand, PIN diodes have better noise characteristics than APDs; therefore, optimal optical receiver transmission performance can be achieved by using a combination of a pre-amp EDFA for good sensitivity and a PIN photon detector for low noise.

The generation of ASE noise in a pre-amp EDFA is an effect of the spontaneous de-excitation of the excited erbium electrons. Because the electrons have finite excited state lifetimes, some of the electrons return spontaneously to the ground state, emitting photons that have no coherence characteristics with respect to the incoming optical signal. These photons are different from the photons generated by stimulated emission.

The collection of spontaneously-generated photons, being multiplied by the fiber amplifier, forms background noise. This background noise is known as amplified spontaneous emission, and it is the dominant noise element in pre-amp EDFA. ASE and its effect on the deterioration of the signal-to-noise ratio for pre-amp EDFA can be measured in different ways [2].

## Erbium Atomic Structure

Erbium atomic structure has three energy levels that are of interest for the study of its amplification characteristic for use in communications. In three-level erbium atomic structure, population inversion can be achieved using laser pumping at 980nm to excite electrons to the upper erbium atomic state. When excited to the upper state, Erbium electrons rapidly decay non-radioactively to the meta-stable state. If electrons in the meta-stable state are not stimulated within the electron lifetime in that state, electron transition to the lower states results in spontaneous emission. Spontaneous emission is a random emission that introduces noise. The behavior of the erbium-doped fiber atomic structure is described in the following level rate equations [3]

$$\frac{dN_3}{dt} = -\frac{N_3}{\tau_{32}} + (N_1 - N_3) * \sigma_p * S_p \quad (1)$$

$$\frac{dN_2}{dt} = -\frac{N_2}{\tau_{21}} + \frac{N_3}{\tau_{32}} - (N_2 - N_1) * \sigma_s * S_s \quad (2)$$

$$\frac{dN_1}{dt} = \frac{N_2}{\tau_{21}} - (N_1 - N_3) * \sigma_p * S_p + (N_2 - N_1) * \sigma_s * S_s \quad (3)$$

Here,  $N$  is the population density at the given level [1/cm<sup>3</sup>],  $S$  is the photon flux [1/cm<sup>2</sup> \* s],  $\tau$  is the spontaneous lifetime [s], and  $\sigma$  is the transition cross section [cm<sup>2</sup>]. The first equation describes the population change rate for the upper state, the second equation describes the population change rate for the meta-stable state, and the third equation describes the population change rate for the ground state. The steady-state atomic populations  $N_1$  and  $N_2$  are functions of the pumping rate, which represents the pump absorption rate between levels 1 and 3, and of the absorption and stimulated emission rates between levels 1 and 2. Figure 1 shows the three-level erbium atomic structure, and it shows the level transitions when erbium is used in a single-stage 980nm pumped pre-amp EDFA [4]. The sum of the population in the three states of the erbium atomic structure is equal to the total population, and that can be expressed in the equation

$$N = N_1 + N_2 + N_3 \quad (4)$$

Under a steady-state condition, electron state transition in Erbium atoms is given by

$$\frac{dN_1}{dt} = \frac{dN_2}{dt} = \frac{dN_3}{dt} = 0 \quad (5)$$

The basic principle of signal amplification in erbium-doped fiber is based on the fact that when an optical signal passes through the erbium-doped fiber, the signal is amplified due to stimulated transition between electronic states in the presence of electromagnetic radiation at the correct wavelength to achieve population inversion. In order for signal amplification to occur [5], a frequency  $f_{12}$  is needed:

$$f_{12} = \frac{E_1 - E_2}{h} \quad (6)$$

where  $h$  is Plank's constant = 6.626x10E-34 [J/s]

Stimulated photons are in coherence with the input signal, and that results in signal amplification. In free space, the radiation wavelength is given by

$$\lambda_{21} = hc / (E_2 - E_1) \quad (7)$$

When this radiation interacts with a photon in the lower energy level, the photon is transformed into the upper atomic level. If a photon in the excited state is not stimulated within the 10ms lifetime of the excited state, it will spontaneously decay to the ground state, producing ASE. When this photon travels through the erbium-doped fiber, it is amplified, resulting in amplified spontaneous emission. All of the excited electrons can spontaneously relax from the upper state to the ground state by emitting a photon that is unrelated to the

signal photons. This spontaneously-emitted photon can be amplified as it travels down the fiber and stimulates the emission of more photons from excited electrons.

Amplified spontaneous emission can occur at any frequency within the fluorescence spectrum of the amplifier transitions. The dominant noise source in any EDFA is amplified spontaneous emission [6]. This spontaneous emission reduces the amplifier gain by consuming the photons that would otherwise be used for stimulated emission of the input signal.

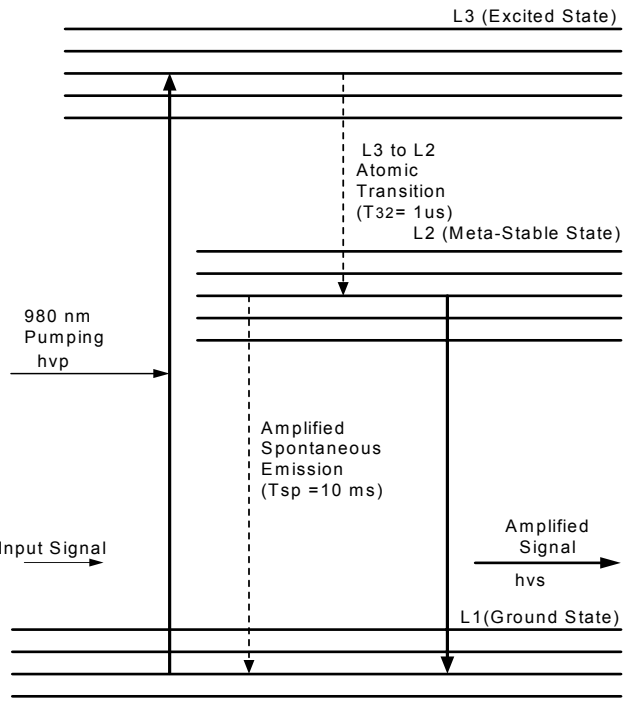


Figure 1. 980nm pumping in Erbium atomic structure

The total amplified spontaneous emission at any point in the fiber is the sum of all amplified spontaneous emission power from the previous sections in the fiber and the amplified spontaneous emission at the given fiber point. To minimize ASE noise, the pump power should be just enough to achieve population inversion. Population inversion can be achieved when the population in the excited state,  $N_2$ , is greater than the population in the ground state,  $N_1$ . The threshold pump power required to achieve population inversion can be obtained by setting the rate equation of level 2 to 0 and setting  $N_1$  to be equal to  $N_2$ . A long meta-stable state lifetime and a large absorption cross section are needed to have a low pump threshold to achieve population inversion. A detailed analysis of EDFA and photodiode noise elements was performed by different researchers [7], [8].

# Optical Receiver Transmission Performance Testing and Analysis

Optical receiver transmission performance, commonly known as bit error rate (BER) performance, is the gauge by which optical receivers are characterized. It characterizes the ability of the receiver to perform up to the transmission performance specifications under the same test conditions as those where the receiver operates in the field [9]; therefore, transmission performance will be used to analyze the pre-amp EDFA noise characterizations under different operating conditions.

Optical receiver optimal transmission performance analysis under different operating conditions is the ultimate method for characterizing pre-amp EDFA noise performance. The pre-amp EDFA design needs to be optimized at the pre-amp level and the EDFA level. Then, the pre-amp EDFA performance is determined by how well it performs in the optical receiver. The set-up of Figure 2 was used to perform the transmission performance tests for this study using the following definitions:

DCA	Digital Communications Analyzer
OSA	Optical Spectrum Analyzer
PPG	Pulse Pattern Generator
LPF	Low Pass Filter
BPF	Band Pass Filter
O/E	Optical to Electrical
E/O	Electrical to Optical
CW	Continuous Wave
ED	Error Detector

For optimal optical receiver transmission performance, the pre-amp EDFA design must be coordinated with the photon detector design to minimize amplified spontaneous-emission noise mitigation from the pre-amp EDFA to the photon detector and the photon detector signal-spontaneous beat noise. The pre-amp input power, output power, and operating wavelength should be taken into account. This allows designers to choose the right erbium-doped fiber length and pump power combination, and it helps minimize amplified spontaneous emission at the output of the EDFA.

Optical receiver optimal transmission performance analysis under different operating conditions is the ultimate method for optimizing pre-amp EDFA performance in the optical receiver. The pre-amp EDFA design needs to be optimized at two levels: the pre-amp/photon detector subsystem

level and the optical receiver level. Several characterization experiments were performed to analyze the effects of changing the pre-amp operating conditions on the optical receiver transmission performance. Testing the pre-amp-based optical receiver at a fixed signal-to-noise ratio of 9 dB at 1550 nm, the transmission performance was recorded at different input/output combinations. A graphical representation of its transmission performance, after normalizing BER, is given in Figure 3.

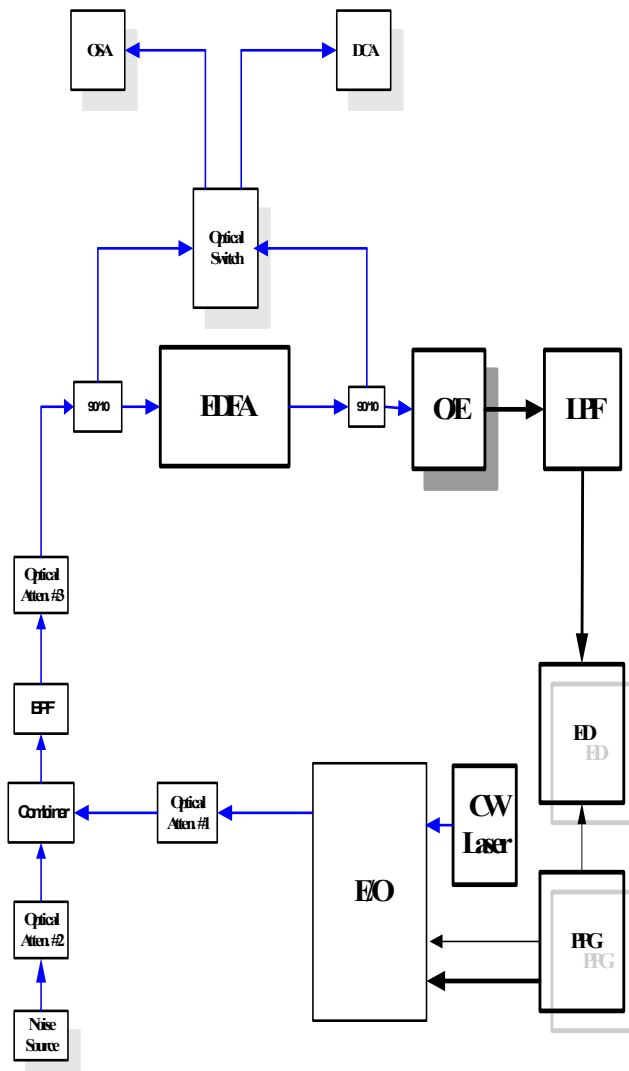
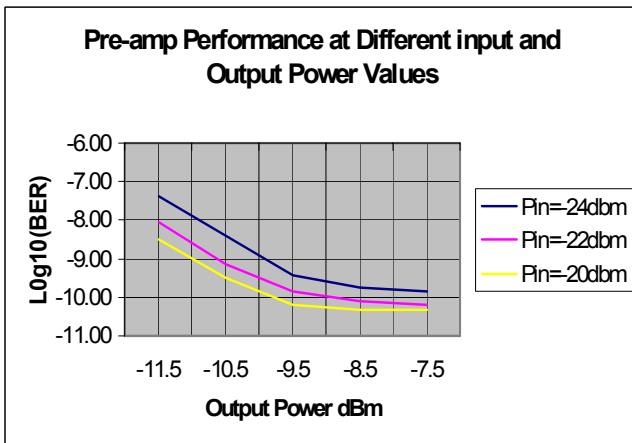
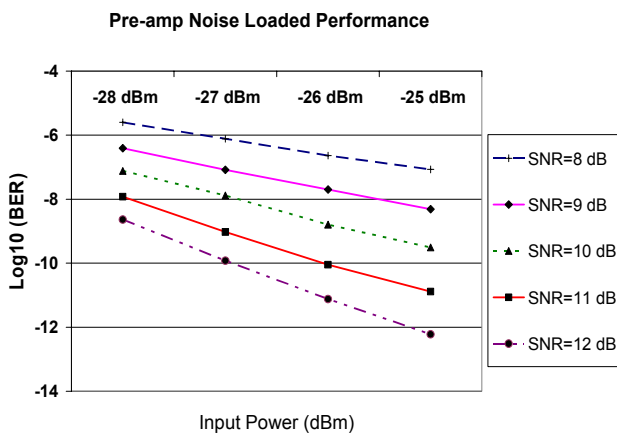


Figure 2. Optical receiver transmission performance test set-up



**Figure 3. Optical receiver performance change at different input and output power levels**

From the results in Figure 3, it can be seen that the optical receiver transmission performance improves as the pre-amp output power is increased. This improvement is due to the fact that more output power requires more pump output, and more output power excites more electrons to the upper state. This excitation results in the population inversion that is needed for the amplification process. When testing the pre-amp-based optical receiver at different input powers and at different signal to noise ratios at fixed output power and input signal wavelength, the transmission performance changes due to the changes in the operating conditions were monitored, and the results are given in Figure 4. A graphical representation of the system transmission performance is given in Figure 4, which shows that the optical receiver transmission performance improves as the pre-amp input signal power is increased.



**Figure 4. Optical receiver performance at different input powers and different input signal to noise ratios**

The results obtained in Figure 4 can be explained at the atomic-structure level since an increase in the input optical power causes a more stimulated emission of the excited electrons. This stimulated emission of electrons, in a form of photons, leaves fewer electrons to move to the ground state spontaneously. This means that the pre-amp is generating less amplified spontaneous emission, which reduces the signal spontaneous noise in the optical receiver photon detector, and that decrease in spontaneous emission results in improved optical receiver transmission performance.

## Conclusion

The results of the tests presented here show a need for fine-tuning pre-amp EDFA at the optical receiver level in order to achieve optimal optical receiver transmission performance. Optical telecommunication engineers can benefit greatly from this work since it presents new test results that are clear indicators of the behavior of pre-amp EDFA in long-haul optical telecommunication systems. For optimal optical receiver transmission performance, the pre-amp EDFA design must be coordinated with the photon detector design to minimize amplified spontaneous emission noise mitigation from the pre-amp EDFA to the photon detector. This will minimize the photon detector signal-spontaneous beat noise.

## References

- [1] Gred Keiser, 2000 "Optical Fiber Communications" Third Edition. McGraw-Hill Publishing
- [2] W. Moench, "Measuring the Optical Signal-to-Noise Ratio in Agile Optical Networks," OFC, 2007.
- [3] J. T. Verheyen, 1995, "Laser Electronics," third edition, Prentice Hall.
- [4] Jeff Hecht, 2006 "Understanding Fiber Optics" Fifth Edition, Prentice Hall.
- [5] J. Gowan, 1993 "Optical Communication Systems," second edition, Prentice Hall, Inc.
- [6] P. C. Becker, N. A. Olsson, and J. R. Simpson, 1999, "Erbium-Doped Fiber Amplifiers, Fundamentals and Technology," Academic Press, NY.
- [7] R. Tucker and H. Kingston, 1995, "Optical Sources Detectors and Systems Fundamentals and Applications," Academic Press, Inc.
- [8] R. S. Tucker and D. M. Baney, 2001 "Optical Noise Figure: Theory and Measurement," OFC, Anaheim, CA.
- [9] A. Abu-aisheh, and H. Alnajjar, "Design Coordination of Pre-amp EDFA and PIN Photon Detectors for Use in Telecommunications Optical Receivers," Pro-

---

ceedings of the 2008 IAJC-IJME International Conference. Nashville, Tennessee. November 2008.

## Biographies

**AKRAM ABU-AISHEH** is an Assistant Professor of Electrical and Computer Engineering at the University of Hartford. He is currently the assistant chair of the Electrical and Computer Engineering Department and director of the electronic and computer engineering technology program. Dr. Abu-aisheh has a doctorate in optical communications from the Florida Institute of Technology and a master of science and a bachelor of science in electrical engineering from the University of Florida. Dr. Abu-aisheh may be contacted at [abuaish@hartford.edu](mailto:abuaish@hartford.edu)

**HISHAM ALNAJJAR** is an Associate Professor of Electrical and Computer Engineering at the University of Hartford, where he is also the Associate Dean of the College of Engineering, Technology, and Architecture. Before that, he served for nine years as the Chair of the Electrical and Computer Engineering Department at the University of Hartford. Dr. Alnajjar has a doctorate from Vanderbilt University and a master of science from Ohio University. His research interests include sensor array processing, digital signal processing, and power systems in addition to engineering education. Dr. Alnajjar may be contacted at [alnajjar@hartford.edu](mailto:alnajjar@hartford.edu)

# LOW POWER SELF SUFFICIENT WIRELESS CAMERA SYSTEM

Faruk Yildiz, Sam Houston State University

## Abstract

The potential ability to satisfy overall power and energy requirements of an application using ambient energy can eliminate some constraints related to conventional power supplies. Power scavenging may enable electronic devices to be completely self-sustained so that battery maintenance can eventually be eliminated. Ambient energy scavenging could extend the performance and the lifetime of the portable electronic devices. These possibilities show that it is necessary to investigate the effectiveness of ambient energy as a source of power. This research studied the waste mechanical energy from hydraulic door closers and its conversion and storage into electrical energy. The converted and stored energy powers a wireless camera for surveillance around the door during the specified time period. Human presence (to open or close the door) is required to activate the hydraulic door closer to charge the storage device. Based on an ambient energy source, an electrical energy-harvesting circuit was designed and tested for a low-power camera system. The hydraulic door closer, as an ambient energy source, and typical camera components were investigated, according to their power generation and consumption, to make analytical comparisons between energy generation and consumption. The steps of investigation of the hydraulic door closer, door opening/closing phases, selection of a viable storage device, and camera integration were conducted to create a low-power, self sufficient, and energy-efficient wireless camera system.

## Introduction

Ambient energy sources can be considered for use in the replacement of batteries in some electronic applications to minimize product maintenance and operating costs [1-5]. In addition, power scavenging may enable electronic devices to be completely self-sustaining so that battery maintenance can eventually be eliminated. These possibilities show that it is important to examine the effectiveness of ambient energy as a source of power [6-10]. Recently, researchers performed several studies on alternative energy sources that could provide small amounts of energy to low-power electronic devices [11-15]. These studies were focused on investigating and obtaining power from different mechanical, electromagnetic, hydraulic, and thermodynamic energy sources such as rotation, vibration, light, sound, airflow, heat, waste mechanical energy and temperature variations. This research studied a mechanical ambient energy source, waste me-

chanical (rotational) energy, from a hydraulic door closer in order to power a wireless camera monitoring the door. A person has to open the door in order for the hydraulic door closer mechanism to function.

The waste mechanical energy is converted to electrical energy using appropriate devices and provides energy to a low-power wireless camera system. Based on the nature of this ambient energy source, an electrical energy harvesting and conversion circuit was designed and tested for a self-sufficient, low-power wireless camera application. The components of the energy harvesting, conversion, storage, and wireless camera system were investigated and chosen by students to scavenge maximum energy. The block diagram of the overall energy-harvesting and powering system is shown in Figure 1.

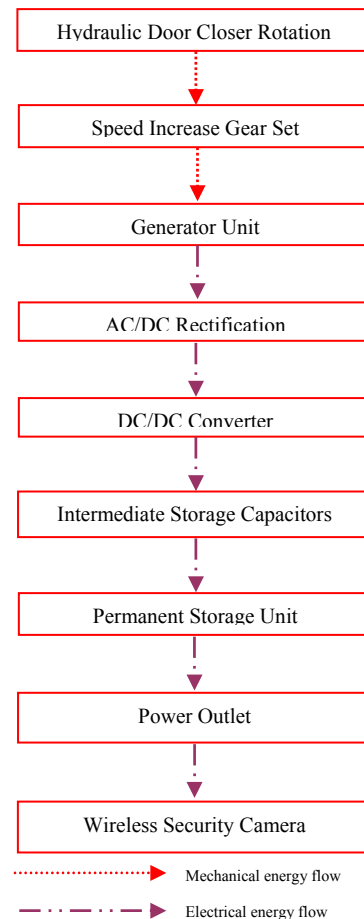


Figure 1. Block diagram of overall energy harvesting model

## Hydraulic Door Closer Mechanism

For the purpose of this experimental study, a hydraulic door closer was secured and tested from the Physical Plant at the University [16]. The hydraulic door closer was separately mounted on a wooden structure to simulate the operation of the door opening and closing system. The arms of the hydraulic door closers were moved manually by hand to represent an opening/closing phase of the door by human power. A door closer mounted on the wooden structure for testing purposes (Figure 2) shows the mechanical energy source with a circle. There are two phases of the door system operations: the first phase is the opening phase, generally activated by human power; the second stage is the closing phase, controlled by a spring and a hydraulic damping mechanism.



Figure 2. Hydraulic door closer

In the first phase, the arm of the door closer was moved up to  $90^\circ$  to represent the opening stage of the door (the reason for rotating the arm  $90^\circ$  degrees is to simulate the maximum angle that the door can be opened in reality). The opening and closing angles of the door may vary between  $0^\circ$  and  $90^\circ$ , depending on the person operating the door and the mechanical speed adjustment of the door closer. Another consideration of the system was the closing phase of the door. Since door closing is controlled by an internal spring and hydraulic damping mechanism, the closing speed of the door was adjusted on the hydraulic door closer.

## Gear Train

The role of the speed-increase gear set was to increase the speed of rotation, which was produced by the hydraulic door closer to provide sufficient input speed to a direct-current (DC) generator. This step-up in speed was necessary because it was found that without an increase in speed, the rotational speed from the hydraulic door closer was not sufficient for the electric generator to provide enough power for the energy-harvesting system. The different gear boxes that were purchased for speed-increase purposes had been originally designed for speed reduction and varied based on the differ-

ent assembly techniques. By changing the positions of gears and shafts, speed-reduction gear boxes were converted to speed-increase gear boxes [17]. These gear boxes were modified to be powered with mechanical energy (human power) instead of electrical energy in order to increase the mechanical speed. The pictures of the unassembled gearbox components and the assembled gear boxes are shown in Figures 3(a) and 3(b), respectively.



Figure 3a. Gear box components



Figure 3b. Assembled gear boxes

Each gear box had different interchangeable speed ratios and assembly techniques specified by the manufacturer's data sheets. The assembly of the gearbox components was accomplished by choosing the highest speed ratios to provide sufficient input speed to the generator unit. The reason for using a gearbox with high gear ratios is because of intermittent and slow rotational mechanical energy from the hydraulic door closer. In order to supply sufficient mechanical rotation to the generator unit for viable power generation, higher ratio gearboxes were necessary. These gear boxes were mounted with metal joints to the hydraulic closers, where waste mechanical energy was obtained during the opening/closing operations of the door closer [18]. Gear ratios and the number of gear sets in gearboxes were determined by considering the average opening/closing angle, speed of the door, and the nominal input required by the generator unit.

## Generator Unit

As a generator unit, two types of DC electric motors were selected and tested because of their power-generation efficiency for low-power electronic applications. A photograph of the two motors and their basic specifications are shown in Figure 4.



Figure 4. Generator units

These motor units were connected to output shafts of gear boxes to gain enough speed to generate electricity. The input rotations and power generation of the generator units were important factors due to constraints and the nature of input rotation from the hydraulic door closer [19]. Power, torque, and speed constraints were very important to consider because of their relationship and the need to measure the power loss between them. Depending on motor specifications, a voltage could not be induced until a specific speed (RPM) was achieved because most electrical machines start inducing voltage at specific speed ratings. In order to run the generator faster and gain more voltage, a higher gear ratio was needed. When the generator starts charging a battery, the load increase slows down the generator speed (RPM). Therefore, every effort was made to increase the speed [20].

## Storage Unit

For the purpose of energy harvesting from the hydraulic door closer, only small-range (1.2V and 3.6V) rechargeable batteries were used to store the energy for test purposes. According to the electronic application device specifications, battery current and voltage can be adjusted by serial and parallel connections. The rechargeable battery type selection for this research was a challenge because of the charging time, source, and leakage-rate constraints. After careful consideration, different types of rechargeable batteries were purchased from different manufacturers. A photograph of the rechargeable batteries is shown in Figure 5.



Figure 5. Rechargeable batteries

The battery regulator in the energy-harvesting circuit was designed and built to respond to the battery charge level and to maintain optimum efficiency. In this experiment, nickel-cadmium (NiCd) batteries were chosen for testing because they have relatively low capacity when compared to other

rechargeable batteries such as lead acid, nickel metal hydride (NiMH), lithium ion (Li-ion), and lithium ion polymer (Li-ion polymer).

## Energy Harvesting Circuit Design

A power harvesting and conditioning circuit was built to implement energy conversion and the battery charging system. This circuit, which was designed to handle a low source power, regulated the voltage level from the generator unit to charge the 1.2V and 3.6V rechargeable batteries for low-power electronic applications. Before implementation of the experiment, computer simulations were conducted with LTSPICE Switcher CAD III advanced circuit simulation software [21]. The alternating-current (AC) voltage output of the generator unit was rectified by a full-wave bridge rectifier circuit that included four Schottky diodes and capacitors connected to the cathode of the diodes to filter the rectified voltage output of the latter [22, 23].

After full-wave rectification, where the AC was converted to DC, the voltage was increased by a DC-DC boost converter [24]. Consideration of energy harvesting components resulted in a decision to integrate an LTC3429 integrated circuit regulator chip, which had a 0.8V threshold input voltage to start running its internal circuitry. The actual energy-harvesting circuit design is shown in Figure 6.

Since the generator unit in this experiment generated electricity up to  $3V_{AC}$ , the voltage was configured to vary from 0V - 3V in the simulation interface. The frequency required for the circuit trigger was 500Hz. The SwitcherCAD III simulation tool provided an advanced simulation toolbox, which allowed simulating each component's voltage and current levels in the circuit. In order to make the circuit perform according to the input and output voltage and current characteristics specified in the simulation model, replacement values of the capacitor and resistor were needed. Since rechargeable batteries were used, which needed  $1.2V_{DC}$  and  $3.6V_{DC}$  input voltage, the boost converter increased intermittent voltage from  $\sim 0.8V$  and then fixed the voltage level at  $1.2V_{DC}$  and  $3.6V_{DC}$ .

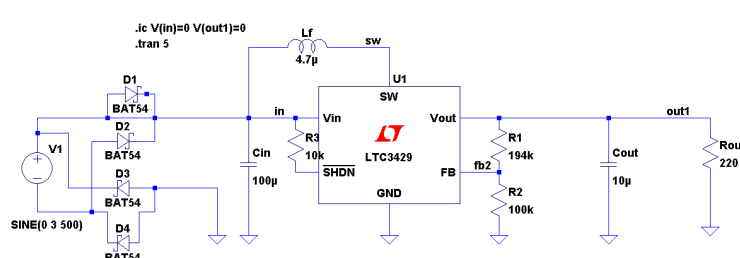


Figure 6. Energy-harvesting circuit with DC-DC boost converter

The following calculations were performed to determine resistor values for the boost converter unit to supply necessary voltage to the batteries.

$$V_{OUT} = 1.23V [1 + (R1/R2)] \quad (1)$$

Where,

1.23 = Manufacturer constant; and  
R1 and R2 = Resistor values for the voltage divider.

In the first case, to charge a 3.6V NiCd battery at 60mAh, R1 needed to equal 194kohm with R2 equal to 100kohm, such that

$$V_{OUT} = 1.23V [1 + (194k/100k)] = 3.61V$$

Because of the voltage drops and leakage current on the energy-harvesting circuit,  $V_{OUT}$  (battery charging voltage) was increased and adjusted to 3.8V in order to maintain voltage to the battery.

In order to increase this output voltage to 3.8V, the following changes were made:

$$V_{OUT} = 3.8V \quad R1 = 209k\Omega, R2 = 100k\Omega \\ 1.23V [1 + (209k/100k)] = 3.8007V$$

The output current for the battery charging circuit then was  $I_{OUT} = 16mA$  at  $R = 220\Omega$  load.

Therefore, 16mA of current was needed for the standard charging of the 3.6V rechargeable battery in 10 hours. Critical circuit values such as input voltage, output voltage, and output current were implemented and a simulation screen shot is shown in Figure 7.

In Figure 7, three important parameters of the energy-harvesting circuit were simulated at the same time to show consistency of voltage and current levels. It can be seen that input voltage,  $V_{IN}$ , fluctuates slightly due to the non-constant output voltage from the generator unit, which is consistent with the characteristics of the hydraulic door closer.

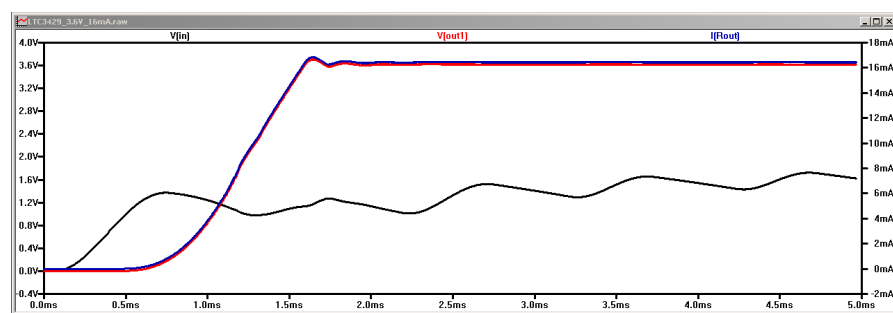


Figure 7. Simulation of critical parameters for battery charging

$V_{IN}$  = Input voltage before boost converter (after rectification);  
 $I_{OUT}$  = Output current for the load (battery charging current); and  
 $V_{OUT}$  = Voltage level after boost converter (battery charging voltage).

## Testing & Verification

Initially, all batteries were discharged with different resistive loads connected to their battery terminals. Resistor values were chosen based on battery capacity during the discharge process to avoid discharging the batteries to levels from which they could not recover. The discharging process of the batteries on the breadboard is shown in Figure 8 with different resistors.



Figure 8. Battery discharging process

At the mechanical part of the system, gearboxes and electric generators were connected to the hydraulic door closer (Figure 9).

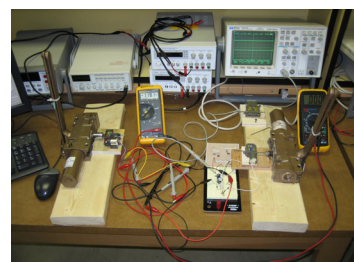


Figure 9. Overall energy-harvesting test system

The door closer was moved manually a number of times, then the battery voltage levels were recorded (Table 1). A cycle of thirty opening/closings was used for measuring the battery voltages. The overall door-opening stage was conducted to represent 180 people opening the door. Measurement of the batteries was recorded six times for each of thirty runs representing human power used to open the door. Each battery was charged using a 1:344 gearbox ratio including the generator unit. After rectification of the AC signal, the high-ratio gearbox was found to be more reliable for reaching the minimum voltage level for the battery charging process. Test results concluded that it is possible to harvest energy from a hydraulic door closer. The voltage level increased considerably when batteries were discharged at the beginning. After a certain voltage level, the charge (capacity) on the batteries only showed a slight increase. For example, to charge a completely discharged rechargeable battery, 10-15hrs [25] is needed to reach its highest capacity at a nominal charging rate. Comparing an off-the-shelf charger with our energy-harvesting system, a considerable number (500-5000) of door openings would be needed to fully charge the battery. In the following application, a wireless camera system monitoring the door is expected to have sufficient energy to fully operate according to the calculations in the next section.

## Self-Sufficient Wireless Camera Application

A hydraulic door closer as an ambient energy source was considered as a viable energy source for a wireless camera system. It was proven above that a hydraulic door closer is capable of providing enough charge to a small battery (depending on a sufficient number of people opening the door). The relationship between the brief battery charge time and number of door openings was analyzed for completely discharged batteries.

**Table 1. Energy harvesting-system battery charging test results.**

Gear-set ratio Generator Battery	Initial bat- tery voltage (V) temp (T)		Thirty runs across six measurements Volt (V <sub>DC</sub> ) Measuring Temp (T)													
			30 run		60 run		90 run		120 run		150 run		180 run		Final Volt- age*	
	V	T	V	T	V	T	V	T	V	T	V	T	V	T	V	T
Ratio 1:344 FA-130 (1.5V)	0.02	55.4	0.43	71	0.74	73	0.84	73	0.89	73	1.31	74	X	X	<b>1.21</b>	<b>53</b>
	0.19	57.2	0.84	69	0.96	75	0.99	75	1.06	75	1.16	75	X	X	<b>1.03</b>	<b>62</b>
	0.03	59	0.92	66	0.94	69	0.96	75	0.98	77	1.01	75	X	X	<b>0.94</b>	<b>68</b>
	0.02	57.2	0.21	69	0.35	73	0.47	73	0.64	73	0.81	73	X	X	<b>0.91</b>	<b>64</b>
	0.87	44.6	2.46	73	3.01	73	3.11	73	3.17	73	3.31	73	3.62	73	<b>3.29</b>	<b>59</b>
	0.52	48.2	2.65	62	2.87	69	2.99	73	3.12	73	3.23	73	3.56	73	<b>3.30</b>	<b>60</b>
	0.13	59	0.95	73	0.98	73	1.03	73	1.12	73	1.22	73	X	X	<b>1.11</b>	<b>60</b>

\* Final battery voltage level reached.

In the case of a low-power wireless camera system, the battery initially starts operating at full charge. The analysis in the previous section was done on completely discharged batteries. If daily charges balance daily consumptions and the standard leakage current of the low-power wireless camera system, then the hydraulic door closer source should be viable for this application. For this reason, estimates were made on the relationship between overall current consumption and current gain, where  $I_1$  was current consumption and  $I_2$  was current gain during a 24-hour period.

$$I_1 \text{ (LOSS/24HRS)} = (I_{\text{BATTERY\_LEAKAGE}}) + (I_{\text{HARVEST\_LEAKAGE}}) + (I_{\text{SWITCH\_MOSFET}}) + [(I_{\text{WORKING}}) * (T) * (P_{\# \text{ OF RUNS}})] \quad (2)$$

Where,

- $I_1 \text{ (LOSS/24HRS)}$  = Overall current loss per 24 hours;
- $I_{\text{BATTERY\_LEAKAGE}}$  = Leakage current from the battery (hr\*24 hrs);
- $I_{\text{HARVEST\_LEAKAGE}}$  = Discharge rate from the circuit components;
- $I_{\text{SWITCH\_MOSFET}}$  = Minimum standby current consumed by the MOSFET;
- $I_{\text{WORKING}}$  = Current consumption of the wireless camera per run;
- $T$  = Time required for each run of the system per second; and
- $P_{\# \text{ OF RUNS}}$  = Total number of runs of the system in 24 hours.

The equation above helps to calculate the overall current consumption including leakage current. The following equation allows us to calculate the total current gained from the hydraulic door closer source:

$$I_2 \text{ (GAIN/24HRS)} = EG * NP \quad (3)$$

Where,

$I_2$  (GAIN/24HRS) = Total current recovered and stored human power through the hydraulic door closer per 24 hours;  
 $I_G$  = Current gathered per person who opened the door (current per charge);  
 $NP$  = Number of the people who opened the door in 24 hours.

For this application, the current gained from a hydraulic door closer ( $I_2$ ) should be greater than or equal to the overall current loss ( $I_1$ ) in 24 hours ( $I_1 \leq I_2$ ). Otherwise, the wireless camera system's operation will be inconsistent, due to the lack of sufficient current (~60mA) to run the camera circuitry. Another important consideration is how much energy is recovered and stored per person. The following equation can be used to estimate the stored energy per person:

$$W = E \text{ (Joule)} * P \text{ (per person)} * T \text{ (hrs)} * \text{Time (one day/hrs)} \quad (4)$$

Where,

$W$  = Overall energy stored;  
 $P$  = Number of people per 24 hour;  
 $E$  = Energy recovered from one person;  
 $T$  = Time taken to store energy; and  
Time = Time span for one day.

In order to calculate the total energy stored in a day (24 hours), it was first calculated that 40J of energy could be recovered per person (average weight 80-kg pushing at 1.0m/s) according to SI units for energy (J), power (W), and kinetic energy of pushing (moving) an object using equations 5, 6, 7, and 8, respectively. A 1-watt system consumes 1 joule of energy each second. In circuit design, the watt-hour (Wh) is generally more useful as a unit of energy than the joule (watt-second) since our devices generally run for hours, not seconds [26].

$$\text{Joule (J)} = \text{unit of energy} \quad (5)$$

$$1J = 1N \cdot m = 1kg \cdot m^2/s^2 = 1V \cdot C = 1W \cdot s$$

$$\text{Watt (W)} = \text{unit for power} \quad (6)$$

$$1W = 1J/s = V \cdot C/s = V \cdot A$$

$$1J = 1W \cdot s = 1.16 \times 10^{-5} W \cdot h \quad (7)$$

$$1W \cdot h = 3600J$$

$$U = \frac{1}{2}mv^2 \quad (8)$$

Where,

$U$  = Kinetic energy of a moving object;  
 $m$  = Mass; and  
 $v$  = Velocity.

$$U = (1/2)(80kg)(1m/s)^2 = 40J = 11mWh$$

In this case, the total energy stored in a battery can be calculated for 50 people as

$$W = 40J \text{ (person)} * 50 \text{ people (per day)} * \text{One day (24 hours)} * 24 \text{ hours}$$

So,  $40J * 50 \text{ people} = 2000J$ , which can be stored per day.

For the purpose of calculating power, the specifications of the wireless camera system components were determined and tested. Consumption rates are described in this section. The photograph of the low-power wireless camera is shown in Figure 10 [27]. The C328 JPEG compression module functions as a video camera or a JPEG compressed still camera. Users can send a snapshot command from the host in order to capture a full-resolution single-frame still picture (OV76xx sensor). The picture is then compressed by the JPEG engine (OV528) and transferred to the host computer. The microcontroller platform allowed us to utilize the system in two ways. The first was to utilize a system without transceivers in order to store camera surveillance information on the additional flash disk on the door. In this way, nothing is transmitted to the host computer, which is more energy efficient but may have security concerns keeping the data related to movement around the door. This idea may eliminate the transceiver unit to reduce energy consumption when transmitting and receiving data.

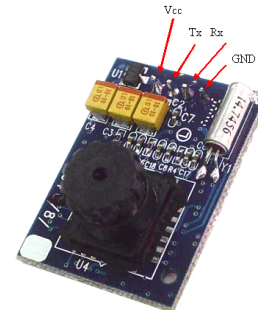


Figure 10. Low-power wireless camera

A ZigBee (802.15.4) wireless communication standard was used to transmit the data (captured pictures) to the remote host computer, where the data are evaluated and stored. In the first approach (using a flash disk around the door to eliminate a transceiver), the energy needed for the overall system was less than the second approach (using a wireless communication standard) and should be considered since our power source was not constant and was limited by use of the small-scale battery. However, for both approaches, the energy-harvesting system would be sufficient if there were enough human presence as mentioned in previous sections (500-5000 door openings). The viability of this energy-harvesting system is depend-

ent on how often the camera takes and transmits the pictures, which changes energy consumption each time the camera transmits. The block diagrams of the devices for the door and the computer for the complete self-powered wireless camera system are shown in Figures 11 and 12, respectively. The circuit (receiver) at the host computer can receive energy from the computer ports without any other external power supplies. The only part of the system which needs to be powered is the circuitry of the camera at the door. After extensive research, energy-friendly components to estimate energy consumption for a wireless camera system were identified and are listed in Table 2. All of the components in the block diagrams are numbered and matched with the components in Table 2 for ease in comparing and understanding the specifications.

The estimated energy leakage in 24 hours was calculated according to the specifications in Table 2. There are certain components in the system, which are always on standby, either to sense the presence around the door or because of the part's functionality. These components experience quiescent drain currents while they are on standby, including the MOSFET and energy-harvesting circuit, to keep the system up and running.

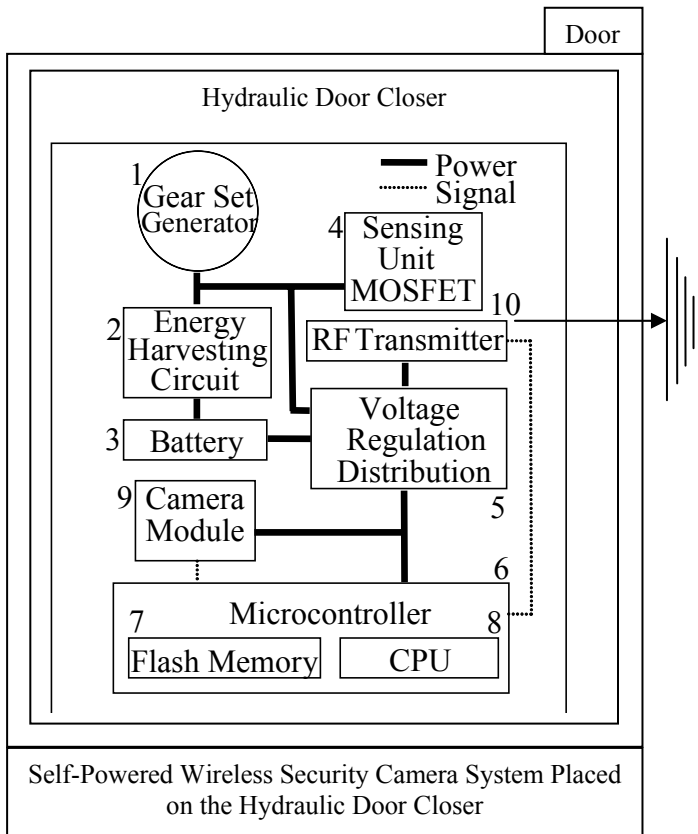


Figure 11. Wireless camera system at the door site

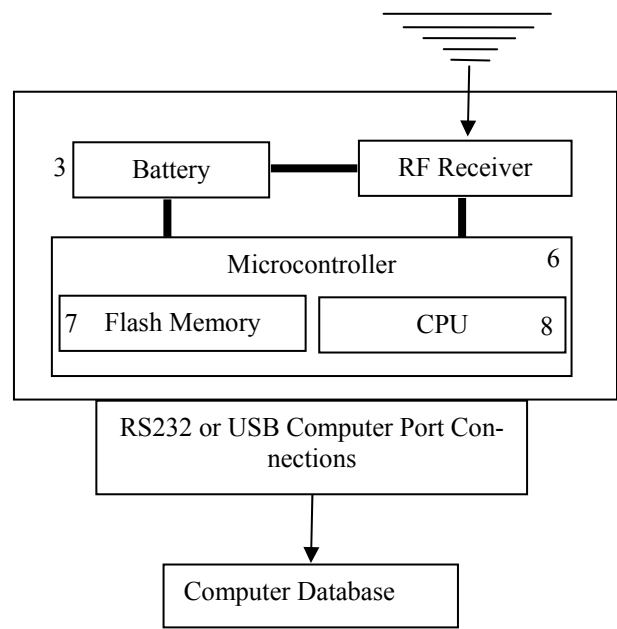


Figure 12. Wireless camera receiver at the remote host computer port

Before calculating the overall operating current for all components, the total leakage and quiescent currents were calculated according to equation 9.

$$\begin{aligned}
 I_{\text{L}}(\text{LOSS/24HRS}) &= (I_{\text{BATTERY\_LEAKAGE}}) + (I_{\text{HARVEST\_LEAKAGE}}) \\
 &\quad + (I_{\text{SWITCH\_LEAKAGE}}) \\
 &= [(288\mu\text{A}) + (432\mu\text{A}) + (4.8\text{nA})] \\
 &= 720.48\mu\text{A}/24\text{hrs}
 \end{aligned} \tag{9}$$

A value of  $720.48\mu\text{A}$  was estimated to be the standard leakage current from the system in the standby mode over a 24-hour period. The total leakage and quiescent currents were added to the operating currents in 24 hours in order to calculate overall current consumption. The steps below indicate the order of operation when a camera is taking and sending a picture to the remote host computer.

1. Subject walks through the door.
2. Subject activates the energy-harvesting circuit and MOSFET switches.
3. Charging system charges battery and closes wake-up switch (solid-state MOSFET).
4. Microcontroller powers up and closes the hold switch.
5. Microcontroller takes a photo with a camera module.
6. System transmits the photo to the remote host computer.
7. Microcontroller releases hold and powers down.

**Table 2. Specifications of the parts for the self-powered wireless camera system**

#	Part	Name	Voltage In/Out (V)	Supply & Operating Currents	Quiescent (Standby) & Leakage Currents	Charging and Operation Times	Total Quiescent & Leakage Currents
1	Gearbox Generator	Tamiya (Manufacturer) Micromo motors (Manufacturer)	N/A 1.5V	~0.20A	N/A	N/A	N/A
2	Energy Harvesting Circuit	Linear Technology IC & Electronic components	1.2V	~12mA	~18µA*	24hrs	~432µA
3	Battery	Typical NICD	1.2V	~110mAh	~12µA	24hrs	~288µA
4	Sensing Unit MOSFET	N-P Channels 585-ALD1115SAL	0.7/-0.7	~3/-1.3mA	~0.4nA	24hrs	~4.8nA
5	Voltage Regulator	Linear Technology	Varies ( $V_{OUT}$ )	~Varies	~Varies	24hrs	N/A
6	Micro-Controller	PIC16F677-I/P	2V-5.5V	~11µA	~50nA	24hrs	OFF
7	Flash/EEPROM	Integrated memory in Microcontroller	N/A	N/A	N/A	N/A	OFF
8	CPU	Integrated in Microcontroller	N/A	N/A	N/A	N/A	OFF
9	Camera Module	C328-7640 (S)	3.3V	~60mA	~100µA	24hrs	OFF
10	Radio Transmitter	MRF24J40-I/ML	0.3V-3.6V	~22mA	~2µA	24hrs	OFF

\* Leakage into output of energy harvesting circuit from battery.

The typical system event as explained above takes three seconds to send a photo (the time increases if more photos are transmitted to the base station). The advantage of this system is that the camera system does not work during the daytime (unless requested) and can be programmed only to wake-up and activate the system during the specific time periods at night. This makes the system more energy-efficient and viable at low-power operating rates. The overall operating system estimation is given below and assumes that the system is activated only at night.

$$I_{WORKING} = [(I_{Microcontroller}) + (I_{Camera}) + (I_{RF Transmitter}) + (I_{MOSFET}*2) * (I_{Photo})] \quad (10)$$

Where,

$I_{WORKING}$  = Overall operating current for one object;

$I_{Microcontroller}$  = Current consumption of microcontroller;

$I_{Camera}$  = Current consumption of camera module;

$I_{RF Transmitter}$  = Current consumption of transmitter;

$I_{MOSFET}$  = Current consumption for two switches (MOSFETs); and

$P_{Photo}$  = Number of photos for one object sent to the computer database.

The calculation of energy consumption of the camera system to transmit a photo for one object is

$$\begin{aligned} I_{WORKING} &= [(11\mu A) + (60mA) + (22mA) \\ &\quad + (4.3mA*2) * (1)] \\ &= 90.11mA \\ &\quad \text{(current needed to send a photo)} \end{aligned}$$

The overall leakage and quiescent currents for the system components during system operation were calculated

using  $I_1$  in equation 2. Since  $I_{\text{WORKING}}$  was calculated separately and added to the overall current consumption in 24 hours, we get the following:

$$\begin{aligned} I_{1(\text{LOSS}/24\text{HRS})} &= [(288\mu\text{A}) + (432\mu\text{A}) + (4.8\text{nA})] \\ &\quad + [(90.11\text{mA}) * (1) * (3)] \\ &= 273\text{mA} \text{ (current consumed in order to transmit a photo in 24 hours)} \end{aligned}$$

The calculated value for  $I_1$  is converted to the power value in order to make a comparison between the power gain and the power loss.

$$\begin{aligned} P_{1(\text{LOSS}/24\text{HRS})} &= 0.2731\text{A} * 3.6\text{V} \\ &= 0.983\text{W} \end{aligned}$$

As calculated above, the total power drained from the storage unit is estimated as 0.983W in 24 hours. The total energy gained from the hydraulic door closer depends on the number of people who open the door in 24 hours. Since the door opening/closing phases take two seconds, the number of people opening the door is multiplied by two seconds.

$$\begin{aligned} P_{2(\text{GAIN}/24\text{HRS})} &= EG * NP \\ &= [(3.6\text{V} * 0.016\text{A}) * (200 * 2)] \\ &= 23.04\text{W} \end{aligned}$$

$P_1$  and  $P_2$  were calculated and converted to the energy value in order to make a comparison ratio if energy gain is greater than energy loss in order to balance the system power.

$$E_{\text{GAIN}} = \frac{E_{\text{INPUT}}}{E_{\text{OUTPUT}}} \quad (11)$$

Where,

$E_{\text{GAIN}}$  = Overall energy gain/loss ratio

$E_{\text{OUTPUT}}$  = Energy consumption by the wireless camera system

$E_{\text{INPUT}}$  = Energy gained from the human powered hydraulic door closer

$$EG = \frac{23}{0.983} \cong 23$$

As estimated above, the energy gain from the hydraulic door closer mechanism is 23 times greater than the overall energy consumption of the wireless camera system. The estimation comparison was performed running the system across its full operating range. Since the energy gain is 23 times greater than the camera system, the latter can be run 23 times with the harvested energy. The energy gain/loss

graph shown in Figure 13 compares the power values for various numbers of images.

As indicated in Figure 13, the power gained would be sufficient to power a wireless camera system. The energy-harvesting circuit and generator unit, including the gear box, can be improved by increasing the gear ratio and motor power output to increase the amount of energy scavenged from the hydraulic door closer. The energy loss can be decreased by replacing the circuit components with the more energy-friendly parts of the self-powered wireless camera system. Moreover, if the number of door openings increases, the battery charging time would be decreased. More door openings would keep the battery charged to supply sufficient power to the electronic devices without any intermittent power failures.

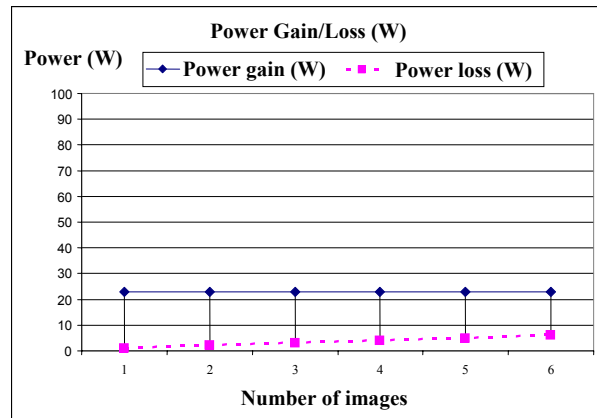


Figure 13. Energy gain/loss for the wireless camera system

## Conclusion

The design of an energy-harvesting system from a hydraulic door closer was very challenging, due to non-constant energy flow. As an analytical estimation, an electronic camera application was designed to compare the energy gained and lost. The power generated in 24 hours was able to run the camera system within specific time frames. Depending on the number of door opening/closings, the power produced can be increased, resulting in more energy in the storage device. Taking the viability of the system into consideration, this energy-harvesting system would be shared with a hydraulic door-closer manufacturer for further investigations. The mechanical design of the energy harvesting system will be redeveloped and placed inside the hydraulic door closer by decreasing the size of the components during a subsequent phase of the project. The camera module could also be placed closer to the hydraulic door closer to avoid voltage drops across the wires.

This experimental study will be a part of a new alternative energy course starting in the spring of 2010, and is designed to teach students how to discover ambient energy sources. Faculty of technology programs can use this research as a part of their courses in various content areas such as electromechanical, electronics etc. This unique experimental study can also transfer technology to the classroom in the form of energy-conversion techniques for enhancement of related undergraduate curricula.

## References

- [1] Hinrichs A. R., Kleinbach M. (2002). *Energy: Its Use and the Environment*. 3rd Edition, Orlando, Florida: Harcourt, Inc.
- [2] Holmes, A. S. (2004). Axial-Flow Microturbine with Electromagnetic Generator: Design, CFD Simulation, and Prototype Demonstration. Proceedings of 17th IEEE International Micro Electro Mechanical Systems Conf. (MEMS 04), IEEE Press, 568–571.
- [3] Mitcheson, P. D., Green, T. C., Yeatman, E. M., & Holmes, A. S. (2004). *Analysis of Optimized Micro-Generator Architectures for Self-Powered Ubiquitous Computers*. Imperial College of Science Technology and Medicine.
- [4] Paradiso, J., & Feldmeier, M. (2001). *A Compact, Wireless, Self-Powered Pushbutton Controller*. Ubicomp: Ubiquitous Computing, LNCS 2201, Springer-Verlag, 299–304.
- [5] Rabaey, J. M., Ammer, M. J., Da Silva Jr, J. L., Patel, D., & Roundy, S. (2000). *Picoradio supports ad hoc ultra-low power wireless networking*. IEEE Computer, pp. 42–48.
- [6] Roundy, S. J. (2003). Energy Scavenging for Wireless Sensor Nodes with a Focus on Vibration to Electricity Conversion, A dissertation, The University of California. Berkeley.
- [7] Roundy, S., Steingart, D., Fréchette, L., Wright, P. K., & Rabaey, J. (2004). *Power Sources for Wireless Networks*. Proceedings of 1<sup>st</sup> European Workshop on Wireless Sensor Networks (EWSN '04), Berlin, Germany.
- [8] Stevens, J. (1999). *Optimized Thermal Design of Small Thermoelectric Generators*. Proceedings of 34<sup>th</sup> Intersociety Energy Conversion Eng. Conference. Society of Automotive Engineers, 1999-01-2564.
- [9] Shenck, N. S., Paradiso, J. A. (2001). Energy Scavenging with Shoe-Mounted Piezoelectrics, IEEE Micro, 21, 30-41.
- [10] Starner, T., & Paradiso, J. A. (2004). *Human Generated Power for Mobile Electronics*. Low-Power Electronics Design, C. Piguet, ed., CRC Press, chapter 45, 1–35.
- [11] Starner, T. (1996). Human-powered wearable computing. *IBM Systems Journal*, 35 (3), 618-629.
- [12] Torres, E. O., Rincón-Mora, G. A. (2005). Energy-harvesting chips and the quest for everlasting life. IEEE Georgia Tech Analog and Power IC Design Lab.
- [13] Yeatman, E.M. (2004). *Advances in Power Sources for Wireless Sensor Nodes*. Proceedings of International Workshop on Wearable and Implantable Body Sensor Networks, Imperial College, 20–21.
- [14] Yaglioglu, O. (2002). Modeling and Design Considerations for a Micro-Hydraulic Piezoelectric Power Generator. Master's thesis, Department of Electrical Eng. and Computer Science, MIT.
- [15] Yildiz, F., Zhu, J., & Pecen, R. (2007). *Techniques of Harvesting Ambient Energy Sources & Energy Scavenging Experiments, Design and Implement an Energy Harvesting Device*. Proceedings of the NAIT Conference, Panama City, Florida.
- [16] LCN Hydraulic Door Closer Systems. <http://www.lcnrollers.com/literature.asp>
- [17] Electric motors and generators. [http://www.physclips.unsw.edu.au/jw/electri\\_cmotors.html#DCmotors](http://www.physclips.unsw.edu.au/jw/electri_cmotors.html#DCmotors)
- [18] Tamiya America, Inc. (2009). Retrieved January 5, 2009, from [www.tamiyausa.com](http://www.tamiyausa.com)
- [19] Mabuchi motor specifications. *Data sheets for typical application requirements*. [http://www.mabuchi-motor.co.jp/cgi-bin/catalog/e\\_catalog.cgi?CAT\\_ID=fa\\_130ra](http://www.mabuchi-motor.co.jp/cgi-bin/catalog/e_catalog.cgi?CAT_ID=fa_130ra)
- [20] McGraw Hill(2007) *Encyclopedia of Science and Technology* (10<sup>th</sup> ed.), "Gear", p. 742-744. McGraw-Hill Professional.
- [21] LTspice/SwitcherCAD III. (2009). <http://www.linear.com/designtools/software/index.jsp#Spice>
- [22] Schottky Diode. Glossary of Terms. <http://www.elpac.com/resources/glossary/index.html>
- [23] Bridge Rectifier. <http://hyperphysics.phy-astr.gsu.edu/Hbase/electronic/rectbr.html>
- [24] DC-DC Converter Basics. [http://www.powerdesigners.com/InfoWeb/design\\_center/articles/DC-DC/converter.shtm](http://www.powerdesigners.com/InfoWeb/design_center/articles/DC-DC/converter.shtm)
- [25] Battery University, Charging Batteries. <http://www.batteryuniversity.com/partone-11.htm>
- [26] Harrison, R. Low Power Circuit Design (2004). <http://www.ece.utah.edu/~harrison/lpdocs/lecture1.pdf>
- [27] The C328 JPEG Compression Module. <http://www.electronics123.com/s.nl;jsessionid=0a0101421f43f658c31cc7964576b2ca8a8355e9af4d.e3eSc3iSaN0Le34Pa38Ta38ObNv0?it=A&id=2581&sc=8&category=241>

---

## Biography

**FARUK YILDIZ** is an Assistant Professor of Industrial Technology at Sam Houston State University. He earned his B.S. (Computer Science, 2000) from Taraz State University, Kazakhstan, MS (Computer Science, 2005) from City College of The City University of New York, and Doctoral Degree (Industrial Technology, 2008) from the University of Northern Iowa. Dr. Yildiz is currently teaching Electronics, Alternative Energy, and Computer Aided Design classes at Sam Houston State University. His interests are in energy harvesting, conversion, and storage systems for renewable energy sources. Dr. Yildiz may be reached at [fy001@shsu.edu](mailto:fy001@shsu.edu)

# PRESERVING HISTORICAL ARTIFACTS THROUGH DIGITIZATION AND INDIRECT RAPID TOOLING

Arif Sirinterlikci, Robert Morris University; Ozden Uslu, Microsonic Inc.; Nicole Behanna, Robert Morris University;  
Murat Tiryakioglu, Robert Morris University

## Abstract

This case study presents digitization and replication of a historical plaster pattern of Robert Morris, one of the founders of the United States of America. Details of the scanning stages and engineering solutions developed for successful digitization such as fabrication of a rotary table and its inductance to the scanning software are introduced. The three rapid prototyping technologies that produced resin, thermoplastic, and metal composite copies in this study are discussed in detail. Subsequently, the use of Room Temperature Vulcanization molds to cast polyurethane copies is demonstrated. A detailed comparison for the three rapid prototyping technologies as well as producing polyurethane copies is provided.

## Background

The process of replicating historical artifacts is not new. With the development of 2-D computer scanning technologies, historians, librarians, archivists, museum curators, and amateur enthusiasts have been digitizing historical works such as books, records, documents, and making them available to the public [1]. In the past decade, the technology has greatly advanced from these 2-D computer scanners to 3-D digitizers. This technological advancement has broadened the users of reverse engineering to medical technologists, historians, anthropologists, paleontologists, primatologists, and forensic scientists. In this context, virtual reconstruction for forensic applications has been one of the growing application fields of reverse engineering, replacing the hard work of skull reconstructionists [2].

The virtual reconstruction process starts with digitization of physical elements such as bone fragments of a primate or a crime victim. These digitized elements are manipulated by eliminating noise, filling in missing geometric data, and assembling them within the CAD environment. The next step beyond the virtual reconstruction is to realize the CAD model via rapid prototyping. One of the other growing applications of the virtual reconstruction is the generation of custom implants or scaffolds for replacement of missing sections of human bones [3], which has relied on rapid prototyping and tooling in fabrication of these substitutes and implants.

Data acquisition from fragile historic artifacts residing in museums faced the following challenges during scanning of the objects [4]:

- The artifact could not be touched by hand or an instrument.
- The artifact could not be moved.
- The job would need to be accomplished during the normal museum hours due to very high after-hours security requirements.

This paper outlines the details of a study conducted at Robert Morris University to replicate the bust of the founding father after whom the university was named.

## Case Study: Bust of Robert Morris

Robert Morris (1734–1806) was a Pennsylvania merchant who helped finance the American Revolutionary War. Morris signed the Declaration of Independence, served in the Continental Congress, and gave away his fortune to help fund the Colonial Army. During the war, he served as Superintendent of Finance, working to establish the first national bank and improve the emerging nation's credit. Morris later served as one of Pennsylvania's earliest senators [5].

This study presents a case on scanning and duplicating a pattern used in fabrication of Robert Morris statutes and busts for museums and parks. The pattern, shown in Figure 1, was restored at the Carnegie Museum of Art in Pittsburgh, Pennsylvania. In the summer of 2007, the Robert Morris University (RMU) Engineering Department was given the task of digitizing and duplicating the pattern without causing any damage to it. Because it was made from plaster and almost 100 years old, it had to be handled very carefully and could not be used as a molding master pattern. The pattern was scanned prior to restoration with the intention of rescaning after the completion of restoration. A sand mold was also originally planned to be fabricated through rapid manufacturing technologies for obtaining full-scale replicas to market or to give as gifts. For completing such an application, 3-D scan data should be highly accurate to avoid sacrificing any detail made by the artist.

## Hardware and Software Technologies Used

For digitization, a Minolta Vivid 910 scanner and Geomagic Studio software were used. The camera could scan large free-form objects with a dimensional accuracy of 0.1270 mm. To assist in the scanning process, a Parker Automation 200 RT Series motor-driven rotary table with a diameter of 203.20 mm and a maximum load capacity of approximately 68 kg was available, but not used. Because of the geometric complexity of the bust, special attention had to be paid to cavities and shiny surfaces. Because the scanner did not have the flexibility to reach hard-to-access details, the scanning process became more tedious than originally expected.

## Scanning Process

The main difficulty encountered during the scanning process was the special care requirement in handling a historical artifact with a value more than \$100,000. The pattern would fit in a  $0.9144\text{ m} \times 0.9144\text{ m} \times 0.9144\text{ m}$  work envelope and weighed approximately 27.22 kg. Such a large object with a vulnerable structure due to its fragile, aged body required that a special scanning platform be fabricated. Figure 2 shows the rotary table built to accommodate this large part in a stable manner. Even though the original rotary table can handle up to approximately 68 kg, its footprint was not large enough for the pattern [6].

Once placed on the platform, the object would not be moved. Because the original platform spins automatically to enable data capture through  $360^\circ$  during the scanning process, it was necessary that the manual platform rotate as well. The investigators calibrated the new rotary table as if it was the one connected to the PC with the Geomagic Studio software and accomplished each shot by matching the angle of rotation at the software tool and the manually driven table. Various rotation angles were used. After a brief study, a rotation interval of  $30^\circ$  was selected as the stepping angle for the consecutive scans. As the Geomagic software was instructed to rotate the original rotary table  $30^\circ$  for the next scan, the investigators manually moved the second table with the actual piece  $30^\circ$ .

The captured data were processed within the Geomagic Studio reverse engineering software. This handling process consisted of three phases: point, polygon, and shape. The following functions were utilized during the data manipulation stage:

- Point Phase (filtering points, registration, reducing noise, filling holes, and merge)

- Polygon Phase (cleaning, filling holes, boundary editing, relaxing boundary, defeature, decimating polygons, sandpaper, relaxing polygons, sharpening wizard, and manifold operation)
- Shape Phase (saving the file in STL format)



Figure 1. Historical Pattern of Robert Morris after Restoration

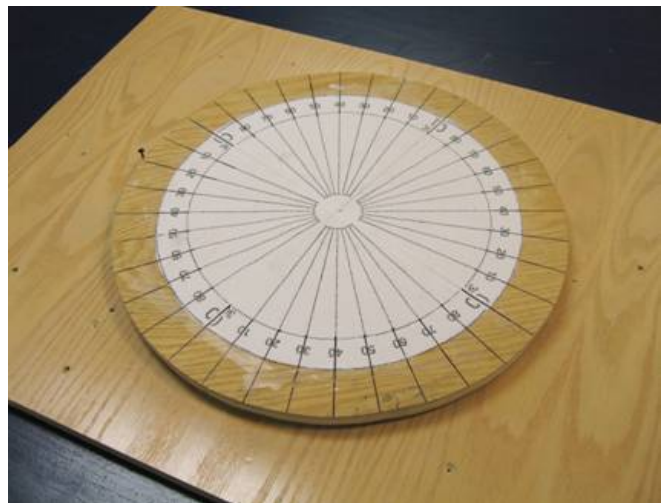


Figure 2. Custom Rotary Table Made to Scan the Robert Morris Bust

The most tedious data handling steps were registering individually scanned surfaces and cleaning up spikes and inaccurate areas due to the size and complexity of the scanned object. Upon completion of the reverse engineering process, the file was saved in STL (Stereolithography) format, which is a triangular-based image of an object's 3-D surface ge-

ometry. The STL file size was approximately 200 MB. The polygon model of the pattern and the STL file resulting from the polygon model are presented Figures 3 and 4, respectively.

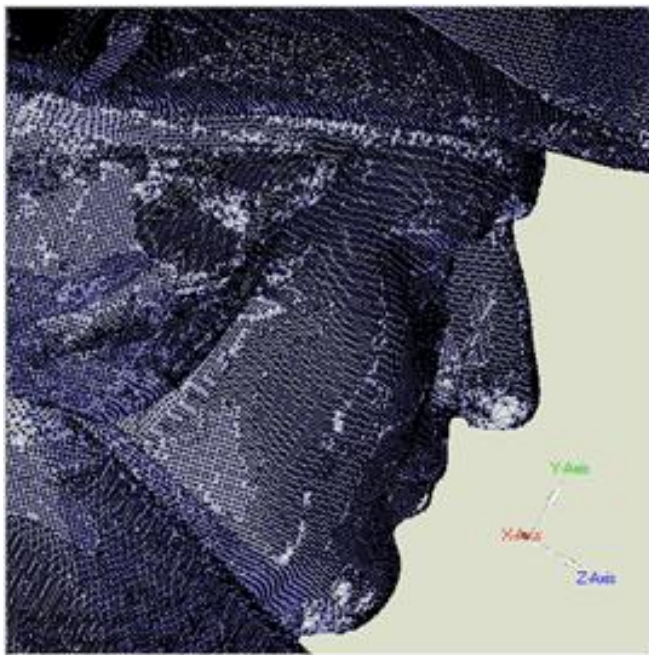


Figure 3. Results of the Scanning – the Polygon Model

The STL file was later used to create 3-D physical replicas of the original piece. Replicas were produced employing the following equipment: (i) 3D Systems Viper Si Stereolithography (SLA) machine, (ii) Stratasys Dimension Elite Fused Deposition Modeling (FDM) machine, and (iii) EX ONE ProMetal RXD (R1) 3-D Metal Printing machine, all housed in the RMU Engineering Department.

## Prototyping of the Bust

The Viper SLA failed to build the part initially due to PC hardware failure at the machine. It was later realized that the Viper SLA's controller unit had to be upgraded to process such a large STL model. The number of triangles had to be reduced to control the STL file size for handling without losing the details or accuracy of the data as well. The hardware upgrades helped improve the physical capabilities of the SLA system and resolved the main issue before the prototyping stage. The DSM-Somos WaterShed 11120 clear SLA resin was used to produce the scaled Robert Morris bust shown in Figure 5. Next, the Dimension Elite FDM machine produced the bust with the same scale using ABS plastic without any problems. However, employing ProMetal's RXD (R1) was not possible due to its small build envelope. Consequently, The EX ONE Company helped RMU build the replica by using an R2 machine that had adequate

build volume. Thirty micron 420 stainless steel (S4) powder was used to fabricate the metal replica. After the build process, the piece was infiltrated with bronze to make it durable enough for handling. Both the FDM- and ProMetal-built parts are presented in Figure 6.

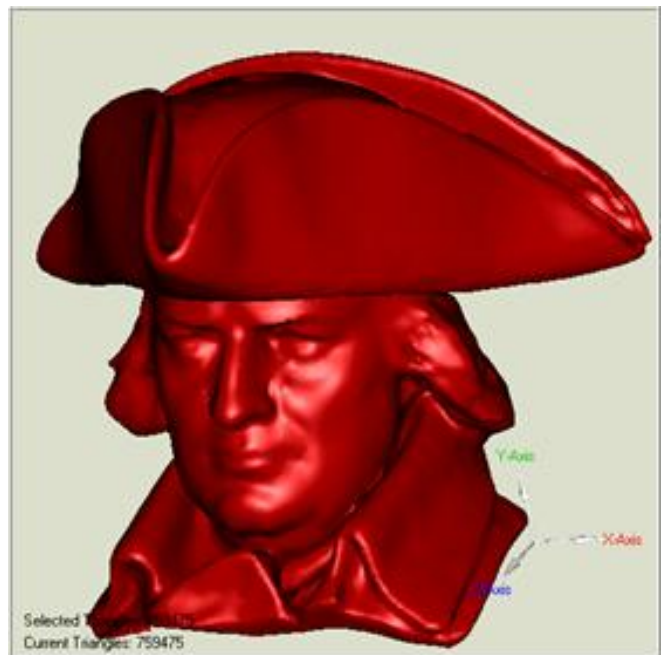


Figure 4. The STL File



Figure 5. SLA Part Made with DSM-SOMOS Watershed 11120



**Figure 6. ABS and S4/Bronze Reproductions Made with FDM (left) and ProMetal 3D Printing (right) Technologies**

## Indirect Rapid Tooling Project

Indirect rapid tooling can be realized by utilization of various processes including Room Temperature Vulcanization (RTV) based on silicon rubber molding. Employing a metal composite pattern, the authors fabricated tin-cured silicon rubber molds to cast polyurethane replicas of the RP pattern.

The RP pattern was built in the ProMetal's R2 machine using a stainless steel (S4) base with bronze infiltration, as seen in Figure 6. A two-piece silicone rubber mold was built around the pattern. The molding material selected was SMOOTH-ON's Moldmax 40 (40A tin silicone) [7]. Approximately 20 hours was deemed suitable for curing time to obtain a solid mold. However, the molding was held longer to ensure complete curing. Moldmax 40 was ideal for transferring the details of the RP pattern. It also carried the characteristics of other advanced silicone molding materials: (i) good release properties and mold life for casting polyurethane, (ii) low shrinkage and good dimensional stability, (iii) good tear resistance, (iv) high elongation for easy removal of complex parts, and (v) medium mixed viscosity and medium hardness.

The material selected for the RTV process was the fast setting Smooth Cast 320, which is a polyurethane material, also from SMOOTH-ON. It sets in about 10–15 minutes and works well with the selected mold material [8]. Mann Technologies 200 Easy Release Agent was also employed in the process. The mold halves and a polyurethane replica produced by them are presented in Figure 7, and a finished and painted replica is presented in Figure 8.

Table 1 illustrates the dimensional accuracy of the processes used including ProMetal, SLA, FDM, and RTV Silicon Rubber Molding, fabrication lead times and costs for making a single Robert Morris bust replica. The cost of making an RTV mold, the cost of the ProMetal R2 piece, and the lead time for the ProMetal process are given in the table as well. The following details were taken into account while constructing Table 1:

- The fabrication lead times include post-processing times for each process.
- The part and molding cost for the RTV process include the material cost and the labor involved.
- For the RP processes, there can be two types of cost estimation: (i) rough quote based on the weight of the RP part, and (ii) precision quote based on the build time [9]. The precision quote considers the cost elements incurred during three stages: pre-process, process, and post-process. These stages include CAD design, file preparation for RP hardware, set up of the RP hardware, cleaning and finishing processes, post-curing, taxes, and profits.
  - The Robert Morris pattern fits in an envelope of (x-axis) 117.60 mm x (y-axis) 102.10 mm x (z-axis) 91.70 mm. Its volume was calculated as  $2.2780 \times 10^5 \text{ mm}^3$  by the 3D Systems SLA Viper software, and  $2.2696 \times 10^5 \text{ mm}^3$  by the Stratasys' FDM/Dimension machine. The material cost for the SLA Viper System was \$61.23, and the material cost for the FDM/Dimension was \$60.96.
  - While the FDM/Dimension machine costs \$20/hr for use, the same cost factor for the SLA viper is \$47.29/hr. ProMetal R2 operational cost is not known precisely but can be estimated to be within the \$20 to \$30 range.

Based on the information supplied in Table 1, it can be concluded that producing the part via FDM Dimension incurs the least cost compared with the other two RP processes.

However, the SLA process is the fastest and delivers the best accuracy of the three technologies. Nevertheless, these RP technologies are still not cost effective for directly replicating artifacts with a relatively large part envelope, even after scaling down dimensions of the pieces. For instance, for a batch of 50 SLA-made busts, the cost will still be \$387/piece. Moreover, all three RP technologies require long build times and therefore cannot be relied upon for increasing productivity even with smaller batches.

**Table 1. Comparison of Prospective Replica Materials and Associated Processes**

Material/ Process	S4/ ProMetal	Somos 11120/ SLA	ABS/ FDM	PU/ RTV
Mold Cost (\$)	-	-	-	1,547
Dim. Accuracy	$\pm 0.127$ mm and $\pm 0.2\%$ for shrinkage	**Varies between $\pm 0.0508$ mm - $\pm 0.2540$ mm [10]	$\pm 0.2540$ mm [11]	0.1016 mm/mm for shrinkage
Lead Time (hr)	*53	14.50	19.02	24.20/ 0.20
Part Cost (\$)	1,500	652 [12]	408 [13]	1,560

\*Lead time includes debinding of the binder and the infiltration of bronze. Post processes may take up to three times of the actual RP process time. Shot blasting may also be used in improving surfaces.

\*\* Horizontal and vertical accuracy, and accuracy for the first vertical inch and afterward, are included.

\*\*\* RTV mold fabrication lead time and molding lead time are presented.



**Figure 7. A Polyurethane Replica and Its Silicon Rubber Mold Halves**

In this study, the ProMetal R2 model was utilized as a pattern in making the RTV molds. This adds to the cost of the RTV molding process, and the resulting replica is the most expensive with a cost of \$1,560. However, this figure



**Figure 8. Finished Robert Morris Bust Replica with an Added Base**

is only for one part. Because the mold can be used for a batch of 50 parts, this cost can be reduced to approximately \$44/piece. Similar results can be obtained for SLA/RTV molding or FDM/RTV molding couplings. Because SLA delivers the best dimensional accuracy, surface finish, and is second best in cost, it can be used with the RTV process for making replicas. SLA/RTV coupling results in a cost of approximately \$27/piece for a batch of 50 parts. In the case of the RTV molding, close to 50 pieces can be made in an eight-hour shift once an RTV mold is built. Two molds will produce twice as many, though a batch this size will take a substantially longer time to build directly with the RP systems used in this study. However, the only drawback of the RTV molding process is having less dimensional accuracy compared with the replicas made directly at the RP systems.

## Conclusions and Future Work

One of the most promising uses of reverse engineering technology is heritage conservation. Reverse engineering and rapid prototyping can be employed in preserving history. This study is an account of efforts made to preserve an important artifact at Robert Morris University. Even though it was a non-conventional project for the investigators due to its sensitive nature, various engineering problem-solving methods were applied in the scanning and replication processes. In the near future, the investigators plan to employ the capabilities of the RMU Engineering laboratories to work on collaborative efforts with forensics scientists or anthropologists. There is an ongoing development effort to include some of these subjects within the ENGR 4801 - Reverse Engineering and Rapid Prototyping course curriculum.

The digitized data resulting from the reverse engineering process could be used in preparation of digital and interac-

tive exhibits and bringing these artifacts to many more people through Web resources. By helping the preservation process, the engineering field will have a great role in preserving our past. By also creating such incredibly detailed and identical replicas of historical artifacts, we can ensure that the artifacts will never be lost.

In terms of the indirect tooling applications, an RP/RTV molding combination seems to be the logical answer for making replicas of historical busts at this dimensional scale. Once an RTV mold is fabricated, replicas can be made about one every 10–15 minutes at a fraction of the cost of RP processing methods. The only drawback of such a system is again the tool life. It is very limited, and may require replacement after only 50 pieces. Additional manufacturing volume requirements make use of a set of molds necessary, also adding to the overall cost. However, in this case study, the authors showed that making a limited number of replicas, perhaps 50 to 100, is justifiable in terms of the costs and the quality obtained through the process.

Future work by the authors will include: (i) influence of part dimensional requirements (scale) on process selection for rapid manufacturing, and (ii) effect of manufacturing volume requirements on process selection for rapid manufacturing. Future work may also involve rapid-tooling approaches other than RTV molding including sand casting or injection molding.

## References

- [1] R. Rosenzweig, “Digital History: A Guide to Gathering, Preserving, and Presenting the Past on the Web.” Philadelphia, PA. University of Pennsylvania Press. 2005.
- [2] American Academy of Forensics Sciences, Resources, [http://www.aafs.org/default.asp?section\\_id=resources&page\\_id=choosing\\_a\\_career](http://www.aafs.org/default.asp?section_id=resources&page_id=choosing_a_career), retrieved December 1, 2008.
- [3] D. Zollikofer, “Virtual Reconstruction: A Primer in Computer-Assisted Paleontology and Biomedicine.” Hoboken, NJ. John Wiley and Sons. 2005.
- [4] Leica-Geosystems, Project Brief [http://www.leica-geosystems.com/corporate/en/ndef/lgs\\_64189.htm](http://www.leica-geosystems.com/corporate/en/ndef/lgs_64189.htm), retrieved December 1, 2008.
- [5] Robert Morris University, History and Heritage, <http://www.rmu.edu/public-relations-and-marketing/content/history-and-heritage.aspx?it=&ivisitor=>, retrieved December 1, 2008.
- [6] A. Sirinterlikci, O. Uslu, and Z. Czajkiewicz, “Replicating Historical Artifacts: Robert Morris Case Study.” SME 3D Scanning Conference, Lake Buena Vista, FL. May, 2008.
- [7] Smodev, Mold Max Series, [http://tb.smodev.com/tb/uploads/Mold\\_Max\\_Series\\_TB.pdf](http://tb.smodev.com/tb/uploads/Mold_Max_Series_TB.pdf), retrieved December 1, 2008.
- [8] Smooth-On, Smooth Cast 320, <http://www.smooth-on.com/index.php?cPath=1210>, retrieved December 1, 2008.
- [9] L. Ding, “Price Quotation Methodology for Stereolithography Parts Based on STL Model,” *Computers and Industrial Engineering*, 52, 2007, pp. 241–256.
- [10] R. Noorani, “Rapid Prototyping: Principles and Application.” Hoboken, NJ. John Wiley. 2006.
- [11] T. Grimm, “3D Printer Dimensional Accuracy Benchmark,” *Time Comprehension Technologies*, September/October 2005, p. 1–4.
- [12] Kelynnamsla, Calculator, <http://www.kelynnamsla.com/calculator.php>, retrieved December 1, 2008.
- [13] Fdmonly, Cost Estimator, <http://fdmonly.com/estimator.asp>, retrieved December 1, 2008.

## Biographies

**ARIF SIRINTERLIKCI** received B.S. and M.S. degrees in Mechanical Engineering from Istanbul Technical University, Turkey, in 1989 and 1992, respectively, and a Ph.D. degree in Industrial and Systems Engineering from the Ohio State University in 2000. Currently, he is an associate Professor of Engineering at Robert Morris University in Moon Township, Pennsylvania. His teaching and research areas include rapid prototyping and reverse engineering, robotics and automation, bioengineering, and entertainment technology. He has authored articles in the Journals of Manufacturing Systems, STEM Education, Technology Interface, Service Learning in Engineering Education, and Agile Manufacturing. He has been also active in ASEE and SME, serving as an officer of the Manufacturing Division and Bioengineering Tech Group. Sirinterlikci may be reached at [sirinterlikci@rmu.edu](mailto:sirinterlikci@rmu.edu).

**OZDEN USLU** received a B.S. degree in Economics from Istanbul University, Turkey, and an M.S. degree in Engineering Management from Robert Morris University in 2007. He is currently the Technical Director of Microsonic Inc., a global ear-mold manufacturer, located in Ambridge, Pennsylvania. As an expert of rapid prototyping and reverse engineering, Uslu has delivered various industrial courses in the field. Uslu can be reached at [ozden@microsonicinc.com](mailto:ozden@microsonicinc.com).

**NICOLE BEHANNA** received a B.S. degree in Logistics Engineering from Robert Morris University in 2008. Cur-

---

rently, she is a project manager at the RMU Center for Applied Research in Science and Engineering (CARES). In addition to managing various research and engineering projects, Behanna delivers training courses. Behanna can be reached at [behanna@rmu.edu](mailto:behanna@rmu.edu).

**MURAT TIRYAKIOGLU** is a University Professor of Engineering at Robert Morris University. He has a Ph.D. in Engineering Management from the University of Missouri-Rolla and a Ph.D. in Metallurgy and Materials from the University of Birmingham, UK. Tiryakioglu is widely published within materials science and engineering, especially in metallurgy. Tiryakioglu can be reached at [tiryakioglu@rmu.edu](mailto:tiryakioglu@rmu.edu).

# FULLY-REVERSED CYCLIC FATIGUE OF A WOVEN CERAMIC MATRIX COMPOSITE AT ELEVATED TEMPERATURES

Mehran Elahi, Elizabeth City State University

## Abstract

Ceramic matrix composites provide characteristics suitable for high-temperature applications such as jet engines, due to their high strength and toughness, low density, creep and thermal shock resistance. The use of continuous fiber-reinforced ceramic-matrix composites for propulsion applications requires evaluation of performance and durability of these materials under static and cyclic loading at elevated temperatures. This paper presents the results of an experimental study as part of a larger investigation, to characterize cyclic fatigue response of a SiC/SiC composite-material system. In this study, the author investigated and characterized the behavior of fiber-reinforced silicon-carbide matrix composites at 1800 °F under fully-reversed cyclic loading with a frequency of 1 Hz. Results for various stress levels representing various states of damage are presented. Results of tests for cross-ply and quasi-isotropic laminates are presented and compared.

## Introduction

Reinforcement of ceramic materials with high modulus and high strength fibers has resulted in tougher materials with improved properties such as strength, fracture resistance [1], fatigue resistance, creep resistance and thermal shock resistance [2]-[3]. These improved properties prompted many researchers to look into potential uses of these materials in structures with launch technology propulsion applications [4], nuclear applications [5], or as fasteners [6], among others. For propulsion applications, with operating temperatures well above 1800 °F, evaluation of performance and durability of any candidate material under static and cyclic fatigue loading is required. This study followed the previous work by the author and is intended to characterize the thermo-mechanical behavior of a model material, silicon-carbide fiber (Nicalon) reinforced enhanced silicon-carbide matrix composite (Nicalon<sup>1</sup>/E-SiC) processed by a chemical vapor infiltration technique (CVI) [7].

## Investigative Approach

The emphasis was mainly on the cyclic fatigue behavior of this material at elevated temperatures.

Potential damage modes and failure mechanisms as a function of applied load levels—stacking sequence, specimen geometry, and test temperature—are discussed. This study was part of a larger investigation and followed the earlier experimental research [7]. In the near future, the results of this study will be used for calibration of a prediction model, which is based on a damage-accumulation concept and uses remaining strength as a damage metric, to predict life and remaining strength.

Fully-reversed cyclic loads are considered by many to be the most damaging to fiber composites because of activation of both tensile and compressive damage modes. Depending on the relative competition of these damage modes, either tensile or compressive-failure will be the controlling mode. Therefore, fully-reversed loading provides an opportunity to observe different damage mechanisms in composite laminates. In a load-controlled mode, bow-tie shaped specimens with stacking sequences of [(0,90)/(0,90)]<sub>2s</sub> (cross-ply) and [(0,90)/(+45,-45)]<sub>2s</sub> (quasi-isotropic) were subjected to a sinusoidal waveform with a frequency of 1 Hz, and a fatigue ratio of R=-1 under atmospheric air at 1800 °F (Figure 1).



Figure 1. Geometry of test specimens

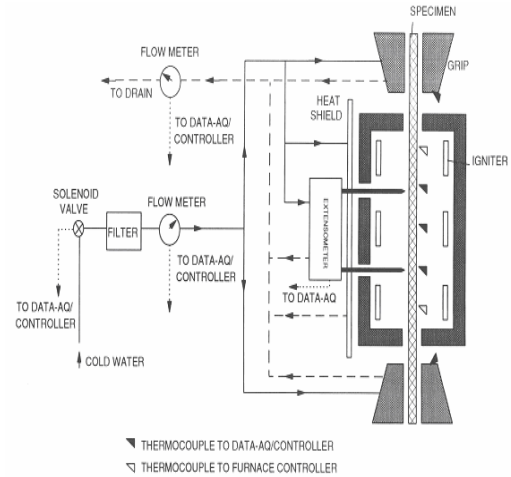


Figure 2. Schematic of the test set-up for elevated-temperature axial testing

The proposed test matrix for cross-ply and quasi-isotropic laminates is presented in Table 1. Based on the availability of specimens at least two specimens were tested at each stress level. A run-out (RO) test, according to the High-Speed Civil Transport (HSCT) standards for cyclic fatigue of ceramic matrix composites [8], was set at  $10^5$  cycles. The remaining material properties of run-out specimens were obtained by conducting quasi-static tensile tests at temperatures under stroke control.

**Table 1. Test matrix for cyclic tests of  $[(0,90)/(0,90)]_{2s}$  and  $[(0,90)/(+45,-45)]_{2s}$  laminates for  $R=-1$ ,  $f=1$  Hz,  $T=1800$  °F**

# of Specimens	Loading Mode	Max. Stress Level	% Life Cycled
2	Load	$\sigma_1$	100
2	Load	$\sigma_2$	100
2	Load	$\sigma_3$	100

## Material and Specimen Geometry

Test specimens were fabricated of 2-D woven flat coupons made of Ni/E-SiC composite material. This material was processed by an isothermal chemical vapor infiltration technique (ICVI) manufactured by Du Pont Lanxide Composites, Inc. The reinforcement phase was ceramic grade Nicalon fiber (0/90 plain weave cloth) and the matrix material was enhanced SiC (containing boron-based particles for protection of fibers against oxidation). Each ply had a thickness of 0.0105", a density of 0.83 lbs/in<sup>3</sup>, a fiber volume fraction of 40%, and a porosity of 12%. Specimens were cut from 12"×12" panels with cross-ply and quasi-isotropic stacking sequences into bow-tie shapes using a water-jet technique. Based on their width, specimens were categorized as wide specimens (average thickness = 0.09", gage section width = 0.75", grip section width = 0.85", and length = 6.0"), and the narrow specimens (thickness = 0.09", gage section width = 0.40", grip section width = 0.50", and length = 6.0"). Finally, for protection against oxidation, a layer of SiC (80-100  $\mu$ m) was deposited on the outer surface.

Utilizing an elevated-temperature axial testing system (Figure 2) and tensile test results of cross-ply and quasi-isotropic laminates at 1800 °F obtained from the first phase of this investigation [7], fully-reversed cyclic fatigue tests were carried out at 1800 °F under three different stress levels. According to the tensile stress-strain curve for these laminates (Figures 3 & 4), these stresses correspond to locations of well below, right at, and well above the Proportional Limit Strength (PLS). Based on a PLS of 12.7 ksi (measured using a 0.005% offset strain method), stresses of  $\sigma_1=10$  ksi,

$\sigma_2=13$  ksi, and  $\sigma_3=15$  ksi were chosen as the maximum applied stress levels. The 10 ksi stress level is located within the linear elastic range; the 13 ksi stress level is located in a region where material is going through the transition from linear elastic regime to nonlinear regime; and, the 15 ksi stress level is located in a nonlinear regime past the transition region.

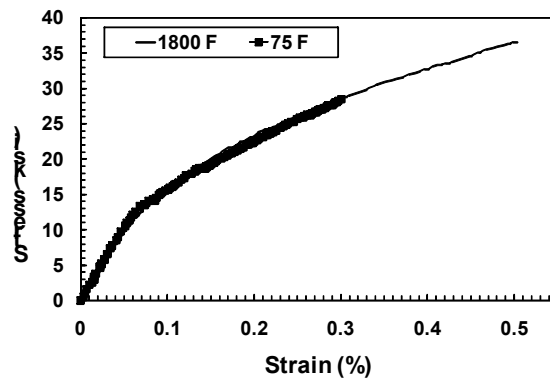


**Figure 3. Room and elevated temperature tensile responses of  $[(0,90)/(0,90)]_{2s}$  laminates**

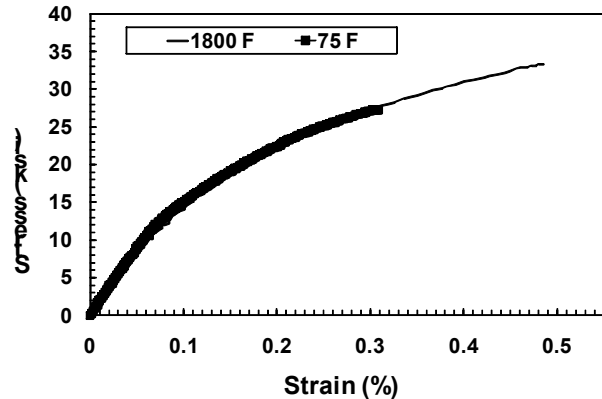


**Figure 4. Room and elevated temperature tensile responses of  $[(0,90)/(+45,-45)]_{2s}$  laminates**

## Cross-Ply Laminates

From a total of seven specimens designated for this testing category, two were tested at 10 ksi, two at 13 ksi and three at 15 ksi stress levels. At least one 0.75"-width specimen was included in each stress level. All of the 10 ksi tests lasted more than  $10^5$  cycles (representing an exposure time of 28 hours at temperature) and were considered as run-outs. Typical stress-strain loops were collected using an x-y plotter (Figure 5). Close inspection reveals that the application of the first loading cycle resulted in a small amount of hysteresis on the tensile-loading side of the curve, which lasted almost  $5 \times 10^4$  cycles and gradually disappeared upon further cycling. This energy dissipation is believed to be associated with the presence of matrix micro-cracks at this load level.

Damage mechanisms such as stretching of fibers, breaking of fibers, sliding of interfaces, and crack deflection can also contribute, either alone or in combination, to energy dissipation. The small magnitude of hysteresis area at this load level did not permit an accurate measurement although stiffness measurements were made. During these tests, damage and damage evolution were confined to the tensile side of loading. This was expected as the Ultimate Compression Strength (UCS) for this material is reported to be almost twice as large as the Ultimate Tensile Strength UTS [9].

Tensile tests under stroke control at 1800 °F were conducted on the run-out specimens. Large scatters in initial elastic modulus values (Young's elastic modulus prior to cycling) were present, which might have contributed to variation in material response (especially in strain to failure). The scatter in initial elastic modulus values was believed to be directly related to the degree of porosity for these material systems. A nominal value ranging from 10% to 12% has been reported. In the initial elastic region, matrix contributes substantially to the modulus of composite. Presence of any porosity results in lower actual matrix volume fraction, thereby causing a reduction in the elastic modulus. This may explain why there is larger scatter in elastic modulus than tensile strength.

The 10 ksi tests did not result in failure of specimens. Initial elastic modulus, representing the virgin state of material, was measured and recorded. Measured remaining properties indicated an average final elastic modulus (Young's elastic modulus after cycling) of 16.13 Msi, a remaining strength (Sr) of 26.16 ksi, and a remaining strain-to-failure of 0.278% (Table 2). These values represented a decrease of 7%, 27%, and 47% from the corresponding average values obtained from the tensile test of virgin specimens at 1800 °F. Due to the presence of large scatter in initial elastic modulus, the percent reduction in modulus was based on the average initial elastic modulus of the same (17.38 Msi in case of the 10 ksi test) specimens, which is much smaller than 20.50 Msi reported previously). The PLS and its associated strain remained basically unchanged. Specimens with wider gage width provided higher remaining properties.

The 13 ksi tests resulted in failure of all specimens, where an average life of 26,000 cycles was recorded (representing an exposure time of 8 hours). Typical stress-strain loops were collected and results are presented in Figure 6. The stress-strain hysteresis loops indicated significant amounts of damage, generated upon application of the first loading cycle. This was expected as the 13 ksi stress level caused significant matrix cracking. An average value of 18.37 Msi was obtained for initial elastic modulus. Similar to 10 ksi tests, damage initiated on the tensile side of loading. Upon further cycling, damage evolved and grew slowly into the

compression side. The presence of a small amount of hysteresis on the compression side may, in part, be explained by the fact that the 13 ksi stress level was large enough to produce fiber matrix de-bonding, matrix crack, fiber fracture, and fiber pull-out. Depending on the position of broken fibers and the large matrix cracks upon unloading, some of these broken fibers did not go back into the matrix from which they were pulled. The ends of the broken fibers were deflected such that they prevented full crack closure.

This argument was supported by the absence of stiffness degradation on the compression side of stress-strain curves, where the unloading compressive modulus provided the same value as loading compressive modulus. The hysteresis area increased steadily from the second cycle with the highest hysteresis occurring on the last cycle before final failure. It was not possible to capture the last few cycles before final failure without running the risk of computer storage overflow. The specimen with larger gage width lasted longer.

Depending on the gage width, the 15 ksi tests showed large scatter in cycles to failure values. The wider specimens lasted almost twice as long as the narrow specimens. Narrow specimens showed similar cycles to failure averaging at 12,350 cycles (representing an exposure time of almost 3.75 hours). It was decided to discard the life of the wide specimens and use the average life of narrow specimens as the reference life. This life is almost half of the life for 13 ksi tests. The measured initial elastic modulus values were very close, averaging 18.03 Msi. Typical hysteresis loops were collected and are presented in Figure 7. As is indicated by the size of the hysteresis loops, 15 ksi stress levels generated more damage in the material than the other two stress levels. Similarly, damage was initially confined to the tensile loading side (at least for the first 100 cycles).



Upon further cycling, hysteresis grew into the compression side. As to the nature of hysteresis on the compression side, the same argument as for the 13 ksi tests may be applied here. It should be noted that in all of these tests, tensile failure proved to be the dominant failure mode and always occurred in the specimen's discoloration zone.

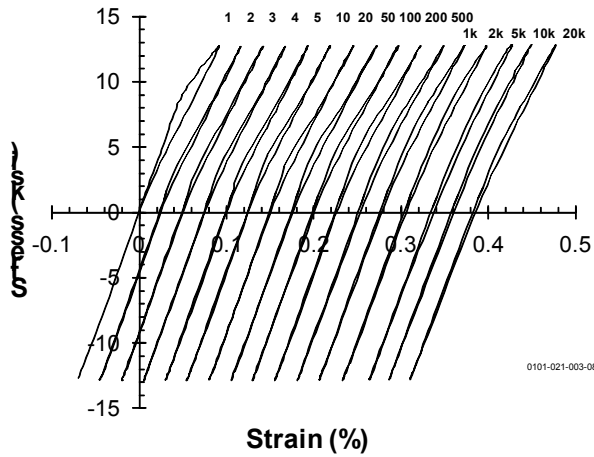


Figure 6. Stress-strain loops for a  $[(0,90)/(0,90)]2s$  laminate for  $\sigma_{max}=13$  ksi,  $R=-1$ , and  $f=1$  Hz at  $1800^{\circ}\text{F}$

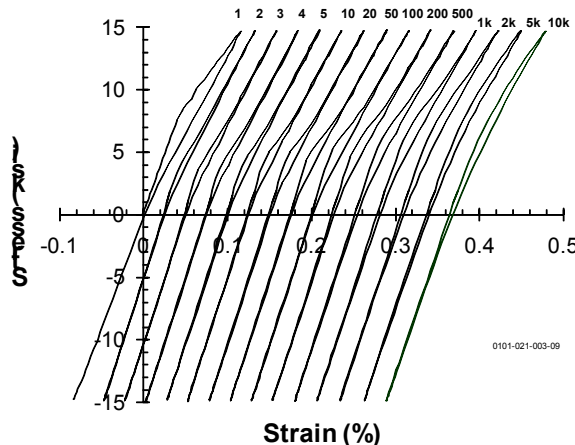


Figure 7. Stress-strain loops for a  $[(0,90)/(0,90)]2s$  laminate for  $\sigma_{max}=15$  ksi,  $R=-1$ , and  $f=1$  Hz at  $1800^{\circ}\text{F}$

Normalizing the applied stresses with respect to UTS, the S-N diagram (stress-cycle relationship), when plotted with a semi-log axis, indicates a straight line (Figure 8). This line may best be represented by  $(Sa/Su) = 1.0008 - 0.0624 \log(N)$ , where  $Sa$ ,  $Su$ , and  $N$  represent the applied stress, ultimate tensile strength, and number of loading cycles, respectively. These results indicate that matrix cracking played the most important role. With stress levels at or above the PLS, the composite has a short life. Also, porosity seemed to influence the fatigue response. This assessment was supported by the presence of large amounts of porosity at the fractured

surfaces. Moschelle et al. [10] have reported similar observations based on room-temperature fatigue test results of regular Nicalon/SiC.

Table 2. Fatigue test results of  $[(0,90)/(0,90)]2s$  laminates for  $R=-1$ , and  $f=1$  Hz, at  $1800^{\circ}\text{F}$

Spec.I. D. & Width	$\sigma_{max}$ (ksi) & Cycles	$Ei$ & $Ef$ (Msi)	PLS (ksi) & Strain (%)	$Sr$ (ksi) & Strain (%)
025-09 (0.40")	10.0 RO, OX	16.41 & 14.99	11.70 & 0.075	24.85 & 0.263
020-09 (0.75")	10.0 RO, IX	18.34 & 17.26	13.59 & 0.079	27.51 & 0.293
Ave. Value	<b>10.0</b> <b>RO</b>	<b>17.38</b> <b>&amp; 16.13</b>	<b>12.65</b> <b>&amp; 0.077</b>	<b>26.18</b> <b>&amp; 0.278</b>
024-07 (0.40")	13.0, OX 23515	18.10 & NA	NA	NA
020-08 (0.75")	13.0, OX 28486	18.63 & NA	NA	NA
Ave. Value	<b>13.0</b> <b>26000</b>	<b>18.37</b> <b>&amp; NA</b>	<b>NA</b>	<b>NA</b>
021-08 (0.40")	15.0, OX 12679	18.12 & NA	NA	NA
023-10 (0.40")	15.0, OX 12022	17.93 & NA	NA	NA
018-10 (0.75")	15.0, IX 21825	NA	NA	NA
Ave. Value	<b>15.0</b> <b>12350</b>	<b>18.03</b>	NA	NA

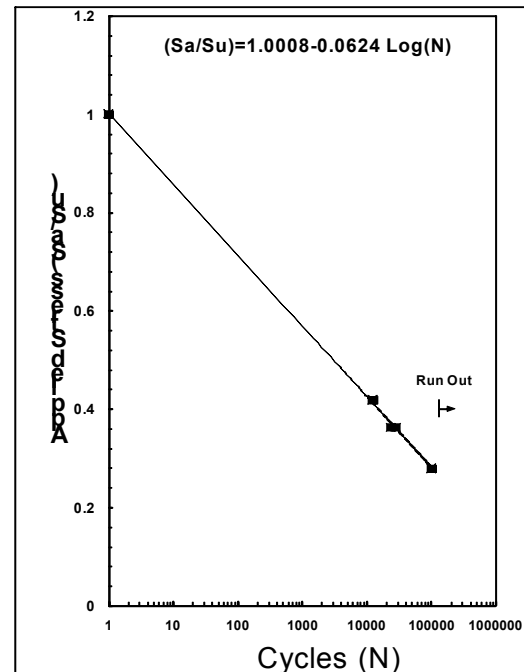


Figure 8. Cyclic fatigue response of  $[(0,90)/(45,-45)]2s$  laminates for  $R=-1$ , and  $f=1$  Hz at  $1800^{\circ}\text{F}$

## Quasi-Isotropic Laminates

Similar to cross-ply laminates, all of the 10 ksi tests resulted in run-outs. The stress-strain loops indicated similar characteristics as the cross-ply laminates (Figure 9) with an average initial elastic modulus of 17.76 Msi. Based on quasi-static tensile tests at 1800 °F, an average final elastic modulus of 16.35 Msi, a remaining strength of 25.56 ksi, and a remaining strain to failure of 0.289% were recorded (Figure 12).

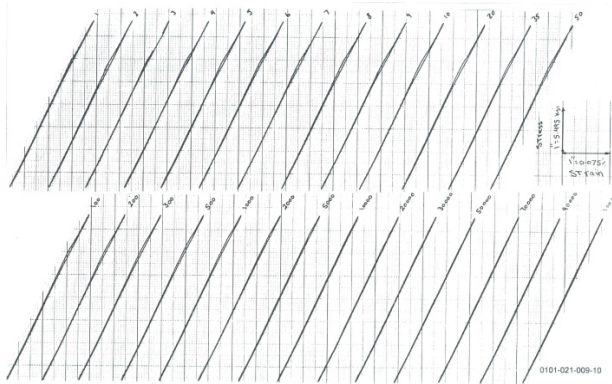


Figure 9. Stress-strain loops for a  $[(0,90)/(45,-45)]2s$  laminate for  $\sigma_{max}=10$  ksi,  $R=-1$ , and  $f=1$  Hz at 1800 °F

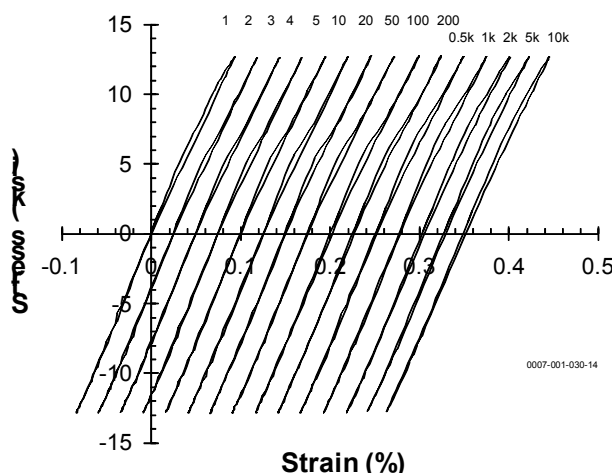


Figure 10. Stress-strain loops for a  $[(0, 90)/(45, -45)]2s$  laminate for  $\sigma_{max}=13$  ksi,  $R=-1$ , and  $f=1$  Hz at 1800 °F

The 13 ksi tests resulted in an average life of 25,140 cycles (an exposure time of 7.25 hours). This is very similar to the average life of cross-ply laminates. An average initial elastic modulus of 18.26 Msi was obtained. The typical stress-strain loops are presented in Figure 10. The evolution of hysteresis resembled those of cross-ply specimens and the same argument for the presence of hysteresis may be applied. The 15-ksi stress-level tests resulted in an average life

of 14,800 cycles (an exposure time of 4.36 hours). Similar to cross-ply laminates, this life was almost half of the life achieved by 13 ksi tests. Unlike 13 ksi tests, the life for 15 ksi tests was slightly higher than its cross-ply counterpart. An average value of 16.97 Msi was recorded. Typical stress-strain hysteresis loops are shown in Figure 11.

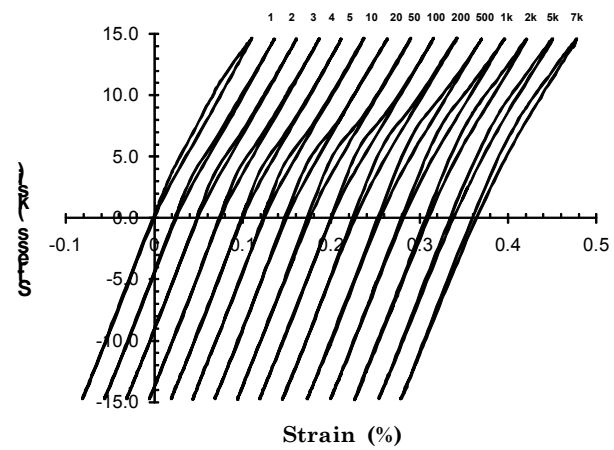


Figure 11. Stress-strain loops for a  $[(0,90)/(45,-45)]2s$  laminate for  $\sigma_{max}=15$  ksi,  $R=-1$ , and  $f=1$  Hz at 1800 °F

Spec.I .D. & Width	$\sigma_{max}$ (ksi) & Cycles	$Ei$ & $Ef$ (Msi)	PLS (ksi) & Strain (%)	Sr (ksi) & Strain (%)
009-09 (0.40) RO, IX	10.0 10.0 RO, IX	18.63 & 16.82	12.36 & 0.077	26.38 & 0.300
009-10 (0.40) RO, IX	10.0 10.0 RO, IX	16.89 & 15.87	12.36 & 0.082	24.73 & 0.277
Ave. Value	<b>10.0</b> <b>RO</b>	<b>17.76</b> <b>&amp; 16.35</b>	<b>12.36</b> <b>&amp; 0.079</b>	<b>25.56</b> <b>&amp; 0.289</b>
030-01 (0.40) OX 24300	13.0 13.0 OX 24300	18.01 & NA	NA	NA
030-02 (0.40) OX 25980	13.0 13.0 OX 25980	18.51 & NA	NA	NA
Ave. Value	<b>13.0</b> <b>25140</b>	<b>18.26</b> <b>&amp; NA</b>	<b>NA</b>	<b>NA</b>
030-03 (0.40) OX 15614	15.0 15.0 OX 15614	17.56 & NA	NA	NA
030-04 (0.40) OX 13986	15.0 15.0 OX 13986	16.37 & NA	NA	NA
Ave. Value	<b>15.0</b> <b>14800</b>	<b>16.97</b> <b>&amp; NA</b>	<b>NA</b>	<b>NA</b>

Figure 12. Fatigue test results for  $[(0,90)/(+45,-45)]2s$  laminates with  $R=-1$ , and  $f=1$  Hz, at 1800 °F

In general, the off-axis lamination did not significantly influence the fatigue response. The S-N diagram showed characteristics similar to the cross-ply laminates. The fatigue S-N data may best be represented by a straight line such as

$(Sa/Su) = +1.0032 - 0.0595 \log(N)$ , as shown in Figure 13. The slope of this line was slightly lower than the one for the cross-ply case. Comparison of average remaining properties of cycled specimens with the corresponding un-cycled values indicated a reduction of 8%, 23% and 37% in elastic modulus, UTS and strain to failure, respectively. With an offset strain of 0.005% and a PLS of 12.36 ksi, with a corresponding strain of 0.079%, were also obtained. A comparison between remaining strength and remaining strain values of cross-ply and quasi-isotropic laminates did not show significant differences in property degradation as a function of stacking sequence (Figure 14).

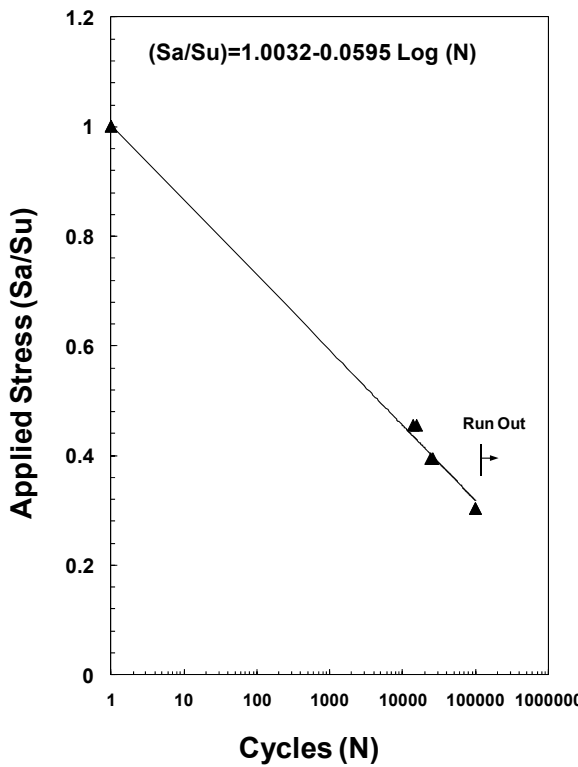


Figure 13. Cyclic fatigue response of  $[(0,90)/(45,-45)]2s$  laminates for  $R=-1$ , and  $f=1$  Hz at  $1800^{\circ}\text{F}$

## Summary

In fully-reversed cyclic fatigue tests, the compression part of loading, in general, does not influence the material response directly, but reduces the time that cracks stay open by half. Cross-ply and quasi-isotropic laminates show very similar fatigue behavior, remaining strength, and life. Results indicate that matrix cracking plays the most important role. With stress levels at or above the proportional limit strength, the composite has a short life. Also, porosity seems to influence the fatigue response significantly. This assessment was supported by the presence of a large amount of

porosity at the fractured surfaces. The fatigue threshold stress, the level at which run-out occurs, is believed to be lower than the proportional limit strength.

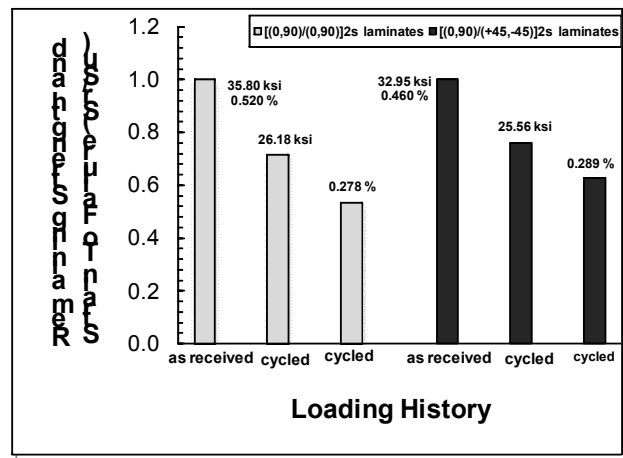


Figure 14. Remaining strength and strain for  $[(0,90)/(0,90)]2s$  and  $[(0,90)/(+45,-45)]2s$  laminates after 100k cycles,  $\sigma_{max}=10$  ksi,  $R=-1$ , and  $f=1$  Hz at  $1800^{\circ}\text{F}$

## Further Research

To have a better picture of the fatigue response for these materials, more tests are needed to complete the S-N diagram. The next phase of this research will also include identifying damage modes and failure mechanisms and to quantify damage accumulation in terms of stiffness degradation and remaining strength. The intention is to use the results of this study to enable and calibrate a prediction model. This model, which is based on a damage-accumulation concept and uses remaining strength as a measure of damage, will be utilized to predict life and remaining strength.

## References

- [1] E.L. Courtright, H.C. Graham, A.P. Katz, and R.J. Kerans, "Ultra High Temperature Assessment Study-Ceramic Matrix Composites," NASA Technical Report WL-TR-91-4061, Sep. 1992.
- [2] K.K. Chawla, "Composite Materials Science and Engineering" New York:Springer-Verlag, Inc., 1987, page 250.
- [3] L.C. Sawyer, M. Jamieson, D. Brikowski, M.I. Haider, and R.T. Chen, "Strength,Structure, and Fracture properties of Ceramic Fibers Produced from Polymeric Precursors: I, Base-Line Studies," J.Am.Ceram.Soc., 70 [11] 798-810 (1987).

---

- [4] Kiser, J.D., et al.: Durable High Temperature Ceramic Matrix Composites for Next Generation Launch Technology Propulsion Applications. Proceedings of the JANNAF 27th Airbreathing Propulsion Subcommittee Meeting, CPIA-JSC-CD-24, 2003. Available from Chemical Propulsion Information Agency (CPIA).
- [5] W. E. Windes, P. A. Lessing, Y. Katoh, L. L. Snead, E. Lara-Curzio, J. Klett, C. Henager, Jr., R. J. Shinnavski, "Structural Ceramic Composites for Nuclear Applications," Technical report, Idaho National Laboratory, INL/EXT-05-00652, Aug. 2005.
- [6] M.J. Verrilli, D. Brewer, "Characterization of Ceramic Matrix Composite Fasteners Exposed in a Combustion Liner Rig Test" Proceedings of ASME/IGTI TURBO EXPO 2002, June 3-6, Amsterdam, Netherlands.
- [7] M. Elahi, "Characterization of Tensile Properties of Woven Ceramic Composites at Room and Elevated Temperature," Proceedings of The 2008 IAJC-IJME International Conference, ISBN 978-1-60643-379-9.
- [8] Tension-Tension Load Controlled Fatigue Testing of Ceramic Matrix, Intermetallic Matrix and Metal Matrix Composite Materials, HSR/EPM-D-002-93 Consensus Standard, GE Aircraft Engines, 1 Neumann Way, Mail Drop G-50, Cincinnati, OH. 45215-6301.
- [9] M.H. Headinger, D.H. Roach, and D.J. Landini, "High Temperature Fatigue of Ceramic Matrix Composites," Presented at AeroMat 1994.
- [10] W.R. Moschelle, "Load Ratio Effects on the Fatigue Behavior of Silicon Carbide Fiber Reinforced Silicon Carbide," Ceram.Eng.Sci.Proc., Vol 15, [4], 1994, 13-22.

## Biographies

**MEHRAN ELAHI** is an associate professor in the Department of Technology at Elizabeth City State University. He received his B.S. and M.S. degrees in Mechanical Engineering from Mississippi State University, Starkville, MS, in 1992, and 1995, respectively. He received a Ph.D. from the Engineering Science and Mechanics Department at Virginia Tech, Blacksburg, VA, in 1996. His areas of interest are solid mechanics, composite materials, material characterization, fatigue and creep of engineering materials. Dr. Elahi may be reached at [melahi@mail.ecsu.edu](mailto:melahi@mail.ecsu.edu)

# SIMULATION OF A TENNIS PLAYER'S SWING-ARM MOTION

Hyounkyun Oh, Savannah State University; Onaje Lewis, Georgia Institute of Technology; Asad Yousuf, Savannah State University;  
Sujin Kim, Savannah State University

## Abstract

Human-factors modeling and the simulation of the human movement have been critical bases for finding the optimized motion in a variety of areas. This study investigated both aspects: the mechanical modeling of the human arm structure and the computational simulation and analysis of a tennis player's full-swing motion, while the player receives a ball. For this objective, the arm structure was regarded as a serial 6 degrees of freedom (DOF) mechanical manipulator with three rigid links. Each joint-angle data point was obtained in a discrete manner through the observation of a related video file. The data were then applied to the Denavit-Hartenberg (DH) Convention to lead the position vectors of the shoulder, elbow, wrist, and the center point of the racket. The smooth position functions along the DH parameter ( $q_1$  through  $q_6$ ) were achieved through the cubic spline interpolation theory. The 3-dimensitonal graphical simulations were produced based on these smooth functions in MATLAB. Additionally, in order to measure the tennis player's quality of performance, the constraint functions of stress and potential energy were evaluated. The results of the analysis were expected to provide valuable information on a tennis player's full-swing motion and also serve as a guide for making optimal movements.

## Introduction

Human-factors modeling and the simulation of the human movement have been widely used as critical tools for implementing optimized human motion in a variety of areas including the factory floors: management constantly seeks better ways of organizing work space [1]; building-construction areas are ergonomically designed with barrier-free equipment or safe structure for physically disabled persons [2]-[7]; the improvement of the efficiency of troop movement on military fields [8]-[10], and so on. In particular, one of the most wide-open areas, where the analysis of the human body's movement is used, may be in the field of sports [11]-[13]. The analysis of the technical deficiencies of an athlete can assist the coach or teacher in identifying the areas where the athlete needs to improve his/her performance. In addition, this analysis can be applied for reforming the athlete's habitual motion, which may potentially cause repetitive fatigue or sudden injury. This study also analyzed the athlete's performance.

In tennis, athletes seek to perfect their swing so that the ball is placed on the desired point as accurately and as fast as possible. In other words, people have always wondered what the perfect forehand swing is in tennis. However, no one has come up with an exact explanation of what it is. This is mainly because human subjects are extremely complex and have intrinsic limitations. As humans are unquestionably the random variable, subject to fatigue, and have limitations of strength and coordination, they must be treated with a considerable measure of safety and ethics. Theoretically, the subject of the perfect swing motion may be summarized as an individual's optimization problem depending on the various cost functions such as personal discomfort, fatigue, effort, potential energy, dexterity, etc. Nevertheless, people have tried to mimic the world's top players' motions throughout the decades for many reasons; perhaps out of curiosity of top players' abilities and long experiences, or perhaps to investigate the best way to improve their athletic techniques or formulate techniques that would reduce stress on their arms.

The main objectives of this study were the implementation of a computational simulation of the world's top tennis player's forehand stroke, and the provision of biomechanical information by analyzing the simulation. The authors address these objectives in the following order:

- A general modeling method for a mechanical rigid body
- Collection of data through the observation of a video file
- Conversion of discrete data into smooth functions
- Computational simulation of the motion based on the smooth data in MATLAB
- Analysis of the simulation and optimization factors

## Method of Kinetic Modeling

Biomechanical investigations often involve a simplified mechanical model of a human body. Mass-spring-damper models are often used to model human movements in which impacts occur. Musculoskeletal models are mostly used for describing individual muscles [14]. For kinetic analyses, one of the most commonly used models is the rigid-body model. Rigid-body models represent the human system in whole or part as a set of rigid segments controlled by joint move-

ments. In other words, the human body is considered as a system of serial rigid manipulators, which are connected at easily-identifiable joints. Theories of anatomical and experimental mechanisms characterize joints of these manipulators so that a position vector can describe the location of the specific point in terms of all joint displacements. For example, Dapena [15] developed a 15-link segment model in his optimization of a high jump; Yeadon [16] used a rigid 11-segmental model with 17 degrees of freedom to describe the aerial movements of the human body. Figure 1 illustrates how the authors in this study segmented the arm structure [13], [17], [18].

In this study, the authors considered a mechanical system of three articulated rigid links that were composed of the upper arm from shoulder to elbow, the lower arm from elbow to wrist, and the hand-to-racket link from wrist to the center of the racket. It was assumed that body segments are rigid-links, and joints are frictionless and hinged. Each link was connected with two revolute joints, as shown in Figure 1. Information from anthropometry in occupational biomechanics, which deals with the measure of size, shape, mass, and inertial properties of the human body segments, was also considered.

The mechanism developed by the authors, then, was considered to have 6 degrees of freedom (DOF). Of course, more detailed modeling may be possible by adding the third revolute joint on the shoulder or two prismatic joints between the neck point and shoulder. Even though such complex models are more accurate at describing human behavior, the model introduced here was adequate for defining the arm swing motion.

The construction of an operating procedure for the calculation of direct kinematics is naturally derived from the typical open-kinematics chain of the manipulator structure. One of the preferable methods comes from the Denavit-Hartenberg (DH) convention, which is based on the fact that each joint connects two consecutive links. This convention

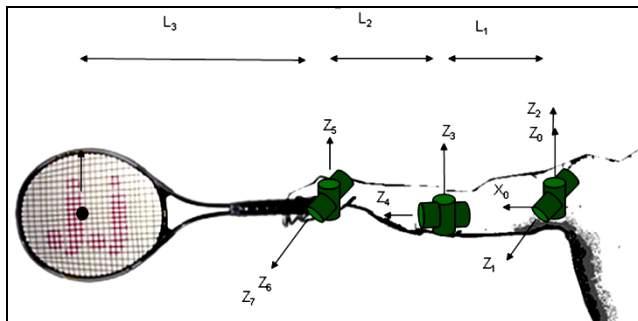


Figure 1. Modeling of segments & joints of the player's arm

considers first the description of kinematics relation between consecutive links and secondly the process to obtain the overall description of manipulator kinematics in a recursive fashion. Position vectors are determined in terms of all joint displacements [17], [18], and such a relation between adjacent links is expressed effectively from the DH method [19]. The DH method is based on the  $4 \times 4$  transformation matrix from the link  $i-1$  to the link  $i$ , which is defined by

$${}_{i-1}T_i = \begin{bmatrix} \cos q_i & -\cos \alpha_i \sin q_i & \sin \alpha_i \sin q_i & a_i \cos q_i \\ \sin q_i & \cos \alpha_i \cos q_i & -\sin \alpha_i \cos q_i & a_i \sin q_i \\ 0 & \sin \alpha_i & \cos \alpha_i & d_i \\ 0 & 0 & 0 & 1 \end{bmatrix} \quad (1)$$

where  $q_i$  is the joint angle between the axes  $X_{i-1}$  and  $X_i$ ,  $d_i$  is the distance between these axes along the axis  $Z_i$ ,  $a_i$  is the offset distance from the intersection of  $Z_{i-1}$  with the axis  $X_i$ , and  $\alpha_i$  is the offset angle between  $Z_{i-1}$  and  $Z_i$  along the axis  $X_i$ . Then, the homogeneous matrix

$${}^0T_n = {}^0T_1^{-1}T_2 \cdots {}^{n-1}T_n = \begin{bmatrix} {}^0R_n(\mathbf{q}) & \mathbf{x}(\mathbf{q}) \\ 0 & 1 \end{bmatrix} \quad (2)$$

specifies the location of the  $i^{\text{th}}$  coordinate frame with respect to the base coordinate system. Here, the matrix  ${}^0R_n(\mathbf{q})$  represents the rotation matrix and  $\mathbf{x}(\mathbf{q})$  represents the position vector. Thus, the position  $\mathbf{x}(\mathbf{q}^*)$  of the aimed end effector can be found by the rule

$$\begin{bmatrix} \mathbf{x}(\mathbf{q}^*) \\ 1 \end{bmatrix} = {}^0T_n(q_1, \dots, q_n) \begin{bmatrix} \mathbf{x}_0 \\ 1 \end{bmatrix} \quad (3)$$

where  $\mathbf{x}_0$  is the starting point of the base coordinate system.

In order to obtain the DH parameters, Figure 2 illustrates the transformed directions of each reference frame and Table 1 shows the DH table matching with the diagram of frames.

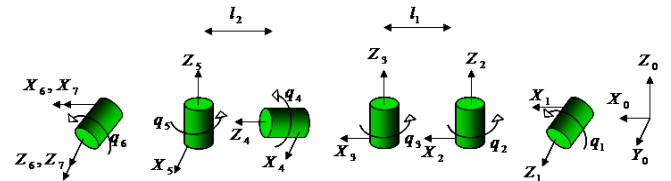


Figure 2. Segmental diagram of the arm for the DH methods

**Table 1. DH parameters for the arm structure**

	$q_i$	$d_i$	$\alpha_i$	$a_i$
${}^0T_1$	0	0	-90	0
${}^1T_2$	$q_1$	0	90	0
${}^2T_3$	$q_2$	0	0	$l_1$
${}^3T_4$	$90 + q_3$	0	90	0
${}^4T_5$	$q_4$	$l_2$	-90	0
${}^5T_6$	$-90 + q_5$	0	-90	0
${}^6T_7$	$q_6$	0	0	$l_3$

Based on this information, each position vector of the shoulder (considered the starting point) elbow, wrist and the center of the racket is given as

$$\text{Shoulder position} = [0, 0, 0]^T \quad (4a)$$

$$\text{Elbow position} = [l_1s_2, -l_1c_1c_2, -l_1s_1c_2]^T \quad (4b)$$

$$\text{Wrist position} = \begin{pmatrix} l_2s_2c_3 + l_2c_2s_3 + l_1s_2 \\ -c_1(l_2c_2c_3 - l_2s_2s_3 + l_1c_2) \\ -s_1(l_2c_2c_3 - l_2s_2s_3 + l_1c_2) \end{pmatrix} \quad (4c)$$

$$\text{Racket center position} = \begin{pmatrix} -l_3c_6c_4s_5s_2s_6 + \dots + l_2c_2s_3 + l_1s_2 \\ l_3c_6s_5c_4c_1c_2s_3 + \dots + l_2c_1s_2s_3 - l_1c_1c_2 \\ l_3c_6s_5c_4s_1c_2s_3 + \dots + l_2s_1s_2s_3 - l_1s_1c_2 \end{pmatrix} \quad (4d)$$

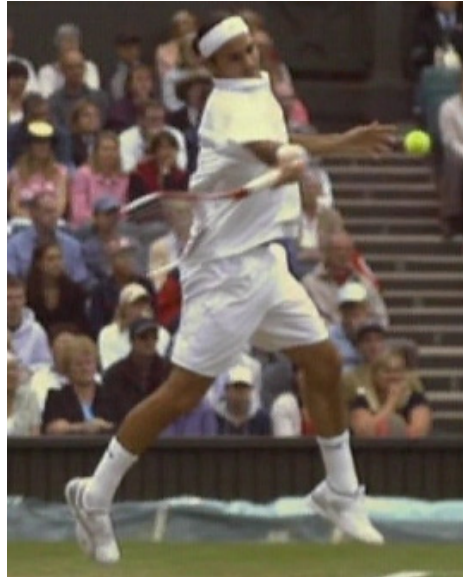
Here,  $c_i$  and  $s_i$  represent  $\cos(q_i)$  and  $\sin(q_i)$ , respectively. This analysis applied the used joint variables to the optimization problems.

## Data Correction

The video used in this study for simulation was captured from a shot, while the world's number one player, Federer, hit at Wimbledon. The file was initially slowed down by 1000 frames per second, in order to calculate the actual speed of the swing. Time and speed were measured using Windows Movie Maker. The video's frame rate was 25 frames per second and lasted 14 seconds. Thus, the actual swing time was calculated at  $x = 0.35$  seconds from

$$\frac{1000 \text{ frames/sec}}{25 \text{ frames/sec}} = \frac{14 \text{ seconds}}{x \text{ seconds}} \quad (5)$$

Each angle along the swing was broken up into 17 time-intervals with increments of 0.0206 seconds. The point of impact was at roughly 1.5 seconds but was not measured in increments of 0.0206 seconds. Figure 3 shows one cut of the video file and Table 2 shows the observed joint angles during the player's full motion.

**Figure 3. Screen capture from the video file****Table 2. Collected angle data from the video file (Unit: degree)**

	$q_1$	$q_2$	$q_3$	$q_4$	$q_5$	$q_6$
0.0000 sec	40	-35	20	-45	-40	-45
0.0206 sec	42	-30	15	-43	-45	-38
0.0412 sec	45	-25	10	-38	-55	-35
0.0618 sec	50	-15	5	-23	-60	-23
0.0824 sec	60	0	3	-15	-70	-15
0.1029 sec	50	10	0	-10	-90	-3
0.1235 sec	42	30	0	-8	-100	0
0.1441 sec	35	60	0	-3	-120	0
0.1647 sec	25	70	5	0	-95	10
0.1853 sec	23	80	15	10	-60	25
0.2059 sec	22	90	22	20	-10	30
0.2265 sec	21	105	32	30	0	20
0.2471 sec	20	120	50	45	0	20
0.2676 sec	18	145	90	80	0	20
0.2882 sec	15	160	92	85	0	20
0.3088 sec	13	165	94	95	5	20
0.3294 sec	7	180	97	100	10	20
0.3500 sec	6	180	100	105	15	20

It is important to note that the image from the video file was seen from one viewing point. As a result, the exact measurement of the joint angles was difficult or almost impossible. The actual measurement was achieved by watching the target angles from a real person, who was asked to make the same posture at each specific time set. This implies that small observational errors could be involved due to the role play. In addition, since the angles  $q_5$  and  $q_6$  were measured with the terminal side from the wrist to the center of racket, it was different from the actual wrist rotation and may overpass to the anatomical limitation of the wrist structure.

## Conversion of Discrete Data

It was difficult to simulate the smooth motion with the discrete data we obtained. An alternative way to resolve this problem is through numerical interpolation theories. These numerical methods allow investigators to determine the continuous swing motion by replacing the discrete data with smooth functions. The most simple and popular interpolation method is polynomial fitting [21]. This method is beneficial in that the function produced is continuously differentiable because of the property of polynomials. Each discrete angle sequence over the time interval is approximated with a distinct polynomial of less than 18 degrees.

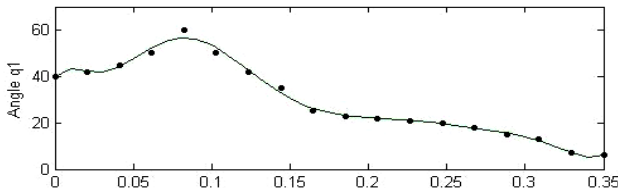


Figure 4. Polynomial interpolation of degree 10

Figure 4 shows how the polynomial fitting to angle  $q_1$  works with the polynomial of degree 10. As illustrated in Figure 4, the polynomial skips some nodes and does not work satisfactorily to cover the entire range of data. These mismatches occur even on the polynomials of higher degrees.

Instead, Figures 5 - 6 show the graphical simulations for the cubic spline interpolation for each angle parameter  $q_1$  through  $q_6$  in MATLAB. Even though this interpolation has only second differentiable properties, it was adequate to simulate a smooth motion.

## Simulation of the Swing Motion

Since Federer's arm size is not well-defined in the literature, lengths of the upper arm and the lower arm were selected at 28.04 cm and 30.69 cm, respectively, for  $l_1$  and  $l_2$  in

equations 4a-d. These values come from the data of Reeves's experimental subjects [22]. Taking normal sizes of upper and lower arms is also beneficial for general application to the public. The racket used for the simulation is the Topspin 660 Powerlite, manufactured since the late 1990s. The  $l_3$  value in the simulation, that is the length from the wrist point to the center of the racket, was  $53.20 + 3.00$  cm = 56.20 cm [23].

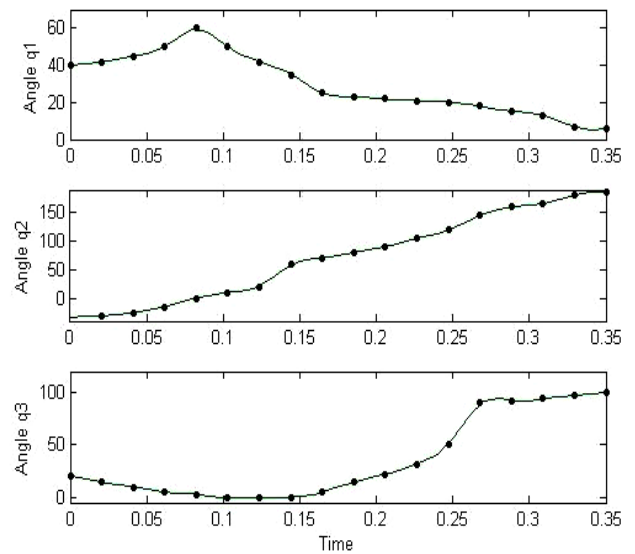


Figure 5. Cubic spline interpolation of  $q_1$  through  $q_3$

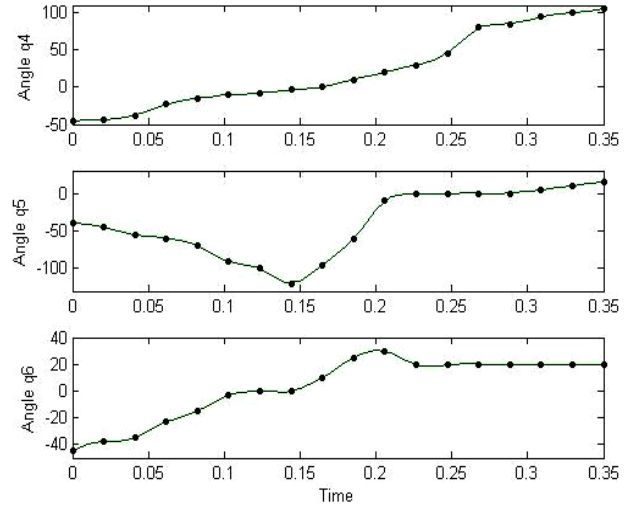


Figure 6. Cubic spline interpolation to  $q_4$  through  $q_6$

By observing the pictures of tennis players, the distance from the wrist point to the butt of the racket was determined to be 3.00 cm. Applying these values to equations 4a-d under the assumption that the player's shoulder is fixed at a height of 170 cm, Figure 7 shows how the player makes the full swing motion. Each group of three lines in Figure 7 is

marked at 0.0035-second intervals (100 marks/0.35 seconds). In the simulation, the dense plot explains the decrement of motion speed. The figure also shows that the player's swing proceeds along a very smooth trajectory and the player tries to make a fast and technically correct swing at the moment of impact.

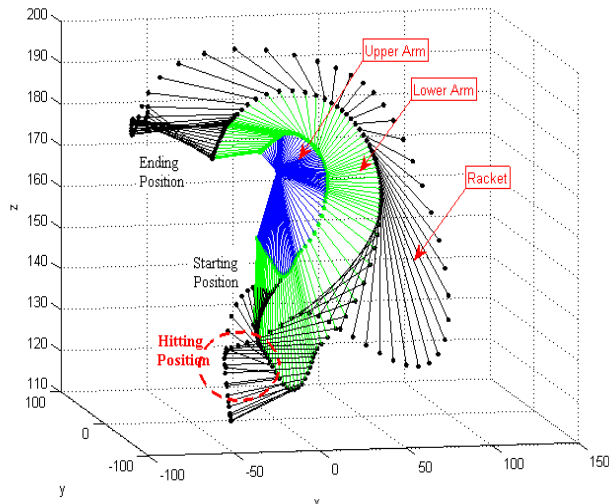


Figure 7. Simulation of the full swing motion over the time interval 0.35 seconds (Unit: cm)

## Analysis of the Swing

A critical aspect of the forehand stroke is how fast the ball comes off the racket. The final shot speed is determined by the sum of bounce speed and racket speed:

$$\text{Shot speed} = \text{Bounce speed} + \text{Swing speed} \quad (6)$$

Bounce speed is mainly concerned with the tennis racket's unique parameters such as the local weight, the center of percussion, frame stiffness, and string-bed stiffness [24], [25]. Even if the racket's contribution to the final shot is factored out, the swing speed—the speed of the racket just prior to impact—is the most significant factor and has a huge influence on the ball's final outgoing speed. In Figure 8, the dotted curve in the upper graph shows this swing speed. From the graph, it can be seen that the ball collision occurs between roughly 0.15 and 0.2 seconds. One can also see that the player is able to increase ball speed by concentrating on the point of impact.

The other graph in Figure 8 shows the acceleration of each joint point. Since the acceleration values are directly proportional to the input/output force combining with the segmental mass, it works as a significant factor for determining how the player controls the force over a full swing. As shown in the lower graph in Figure 8, the greatest force is applied at

the point of impact. After a required sequential motion, the player intended to decrease the force from the body at around 0.27 seconds.

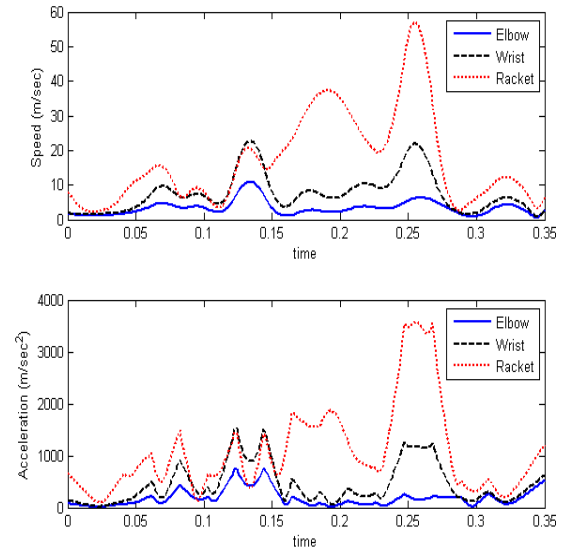


Figure 8. Speed (above) and acceleration (below) of the elbow point, the wrist point and the center of racket over the full swing

Humans act in such a way as to minimize certain types of cost functions or human performance measures such as reactivity, dexterity, musculoskeletal discomfort, fatigue, torque, stress, etc. A number of studies noted a variety of methods for finding such optimized paths through the process of optimization of base-motion prediction [26]-[30]. However, having found motion paths through simulation, this study focused on the evaluation of the existing cost functions. In particular, the authors considered stress functions and potential-energy functions according to vertical-directional shifting.

The stress function concerns discomfort, due to the displacement of joint angles; this was mathematically defined as an aggregate weighted function by

$$f_{\text{stress}}(q) = \sum_{i=1}^{\text{DOF}} \omega_i |q_i - q_i^N| \quad (7)$$

where  $q_i^N$  represents the  $i^{\text{th}}$  joint angle in the neutral/equilibrium position, which may be different from the body models [27]-[29]. With the assumption of humans' tendency to gravitate to a comfortable neutral position, it was assumed that  $q_1^N = 90^\circ$  and  $q_2^N = q_3^N = q_4^N = q_5^N = q_6^N = 0$ . The set of weights,  $\omega_i$ , were mostly based on intuition and experimentation, assigning relative importance to the segmental components. In this study, the authors tested the three

types of weights: 1) segmental mass-based weights; 2) accumulated mass-based weights; and, 3) segmental length-based weights. Again considering the segmental masses, 2.17 kg, 1.27 kg, and 0.48+0.35 kg for the upper arm, lower arm, and the hand-to-racket link, respectively [22], [23], the segmental mass-based weights were given as the ratio  $\omega_1: \omega_2: \omega_3: \omega_4: \omega_5: \omega_6 = 2.17:2.17:1.27:1.27:0.83:0.83$ . Meanwhile, with the assumption that the upper-arm motion is restricted by the mass of both the lower arm and hand, and the lower-arm motion is limited by the mass of the hand, the accumulated mass-based weights are given as  $\omega_1: \omega_2: \omega_3: \omega_4: \omega_5: \omega_6 = 4.27:4.27:2.10:2.10:0.83:0.83$ .

Finally the length-based weights are taken as  $\omega_1: \omega_2: \omega_3: \omega_4: \omega_5: \omega_6 = 28.04:28.04:30.69:30.69:56.02:56.02$ . Figure 9 shows the calculation of stress factors due to the joint angles  $q_1$  through  $q_6$  (upper graph) and the total stress value according to the weighted types (lower graph). As shown in Figure 9, biomechanical stress continues to increase along the swing regardless of weighted types. It was accepted as reasonable that the ending posture of the swing looked very uncomfortable when compared to the normal relaxed posture.

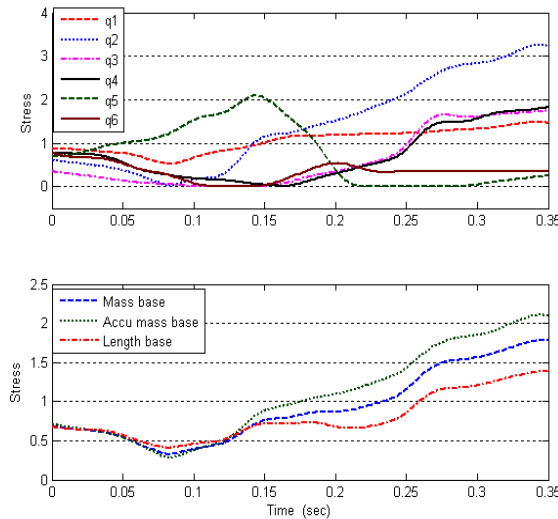


**Figure 9. Stress factors according to the joint angles (upper graph) and overall stress according to the different sets of weight (lower graph)**

The potential energy also works as a critical factor to constrain the human movement. It is mainly divided into two categories; potential energy stored in the muscles and potential energy due to gravity. This study focused on the latter, which was indirectly based on the vertical directional movement of each mass segment. Then, the total potential energy was calculated as a weighted sum of segmental potential energy as

$$f_{potential}(q) = \sum_{i=1}^{DOF} P_i = \sum_{i=1}^{DOF} (-m_i g h_i) \quad (8)$$

Here,  $h_i$  represents the height of each center of segmental mass [28]. However, if this potential energy function is used directly in order to minimize this factor, there would always be a tendency to bend over. Consequently, the change in potential energy from one of the initial configurations to one of the updated configurations was minimized. Such a potential energy is defined by

$$f_{delta-potential}(q) = \sum_{i=1}^{DOF} P_i = \sum_{i=1}^{DOF} (-m_i g)^2 (\Delta h_i)^2 \quad (9)$$

[29], [30]. Figure 10 illustrates the total potential energy (upper graph) and the change of potential energy (lower graph) along the full swing motion. As observed in Figure 10, the total potential energy was almost re-tracing the graph of the z-coordinate of the simulation. Meanwhile, the lower graph in the figure reflects the fact that at the impact moment, a huge amount of energy conversion occurs for power hitting. The reason that the energy change stays at the lower level after the point of impact is understood because the player must correctly control the ball.

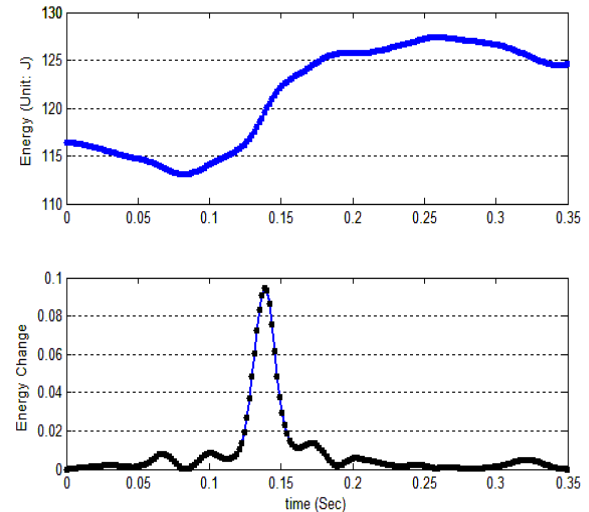


**Figure 10. Potential energy (upper graph) and the change in the potential energy (lower graph) along the full swing motion**

In addition to the constraint factors noted above, one can consider other constraint functions, which can be evaluated based on this simulation; for example,

$$f_{inconsistency}(q) = \sum_{i=1}^{DOF} \omega_i |q_i(t)| \quad (10a)$$

$$f_{nonsmoothness}(q) = \sum_{i=1}^{DOF} \omega_i (q_i(t))^2 \quad (10b)$$

[28], [29]. Although constraint functions were examined individually, in order to yield the maximum effect, such performance measures must be used in a combined manner. Obviously, a new weight for each function must also be developed according to the relative effectiveness of the motion restriction.

## Summary

Developing a model for the most effective technique was more difficult for open-skill sports. That is, the factors affecting the performance of the forehand stroke in tennis are numerous. Sometimes one may be confronted with combinations of factors, which the player is able or unable to control. These factors include player's location on the court, opponent's location on the court, the incoming direction and velocity of the ball, offensive or defensive situation, material status of the court and even weather. Even player's physical status and condition should be considered. Therefore, the best way to make the perfect forehand swings depends on how much the player practices against a certain situation.

This study described the overall procedures of how to computationally simulate the human movement through a tennis player's forehand swing and how to analyze the simulation biomechanically. Regardless of available equipment or lack of informed sources, the procedure of analysis of the player's motion is still valuable from the standpoint of the public's understanding of the subject.

There are many different issues concerning the human motion needing to be analyzed. Subsequent studies should include a direct extension of this modeling to more complex modeling, and a comparative analysis of these results to the optimization-based motion paths, so that a well-defined realistic human motion on the given tasks can be found.

## References

- [1] W. Kuehn, "Digital Factory - Simulation enhancing the product and production engineering process", proceeding of the 38<sup>th</sup> conference on winter simulation: Manufacturing applications: manufacturing systems design, pp 1899-1906, 2006
- [2] A. Fireman, and N. Lesinski, "Virtual Ergonomics: Taking human factors into account for improved product and process", 2009 Dassault Systemes Delmia Corp, 2009
- [3] K. Jung, O. Kwon, and H. You, "Development of a digital human model generation method for ergonomic design in virtual environment", Inter. J. of Industrial Ergonomics, Vol. 39(5), pp 744-748, 2009
- [4] S.A. Gill, and R.A. Ruddle, "Using virtual humans to solve real ergonomic design problems", Simulation 98. Inter. Conference. (Publ. No. 457), 1998
- [5] J. Yang, T. Sinokrot, K. Abdel-Malek, S. Beck, and K. Nebel, "Workspace zone differentiation and visualization for virtual humans", Ergonomics, Vol. 51(3), pp 395-413, 2008
- [6] P.A. Hancock, and R. Parasuraman, "Human factors and safety in the design of intelligent Vehicle-Highway Systems (IVHS)", J. of Safety Research, Vol. 23, pp. 181-198, 1992
- [7] N. Pelechano, and A. Malkawi, "Evacuation simulation models: Challenges in modeling high rise building evacuation with cellular automata approaches", Automation in Construction, Vol. 17(4), pp 377-385, 2008
- [8] D. Andrews, F. Moses, H. Hawkins, M. Dunaway, R. Matthews, and T. Singer, "Recent Human Factors Contributions to Improve Military Operations", Human Factors and Ergonomics Society Bulletin, Vol. 46(12), 2003
- [9] R.W. Pew, and A.S. Movor, "Modeling human and organizational behavior: application to military simulation", National Academic Press, 2001
- [10] X. Man, C. Swan, and S. Rahmatallah, "A Clothing Modeling Framework for Uniform and Armor System Design", Proc. SPIE, 2006
- [11] S.R. Carvalho, R. Boulic, and D. Thalmann, "Interactive low-dimensional human motion synthesis by combining motion model and PIK", Comp. Anim. Virtual Worlds, Published online in Wiley InterScience, 2007
- [12] S.M. Nesbit, and M. Serrano, "Work and power analysis in the golf swing", J. of Sports Science and Medicine, Vol. 4, pp 520-533, 2005
- [13] P. McGinnis, "Biomechanics of sports and exercise", Human Kinetics, 2005
- [14] G. Robertson at al, "Research Methods in Biomechanics", Human Kinetics, 2004
- [15] J. Dapena, "Simulation of modified human airborne movements", J. of Biomechanics, Vol. 14, pp 81-89, 1981
- [16] M.R. Yeadon, J. Atha, and F.D. Hales, "The simulation of aerial movement-IV: A computer simulation model", Journal of Biomechanics, Vol 23(1), pp 85-89, 1990
- [17] L. Sciavicco, and B. Siciliano, "Modeling and control of robot manipulators", McGraw-Hill, 1996
- [18] P. Allard, L. Stokes, and J.P. Blanchi, "Three-dimensional analysis of human movement", Human kinetics, 1995

---

[19] J. Denavit, and R.S. Hartenberg, “A kinematic notion for lower-pair mechanisms based on matrices”, *Journal of Applied Mechanics*, Vol. 77, pp 215-221, 1955

[20] K. Atkinson, and W. Han, “Elementary Numerical Analysis”, Wiley & Sons, Inc, 2004

[21] URL [www.tennis-warehouse.com/player.html?ccode=rfederer](http://www.tennis-warehouse.com/player.html?ccode=rfederer) (Last accessed on April 1, 2010)

[22] R.A. Reeves, O.D. Hicks, and J.W. Havalta, “The relationship between upper arm anthropometrical measures and vertical jump displacement”, *Int. J. of Exercise Science*, Vol. 2(4), 2008

[23] R. Cross, “Customising a tennis racket by adding weights”, *Sport Engineering*, Vol. 4, pp 1-14, 2001

[24] URL [http://twu.tennis-war-house.com/learning\\_center/racquetcontribution.php](http://twu.tennis-war-house.com/learning_center/racquetcontribution.php) (Last accessed on April 1, 2010)

[25] H. Brody, “Physics of the tennis racket”, *American J. of Physics*, Vol. 47(6), pp 482-487, 1979

[26] I. Rodriguez, R. Boulle, and D. Meziat, “A joint – level model of fatigue for the postural control of virtual humans”, *J. of Three Dimensional Images*, Vol. 17(1), pp 70-75, 2003

[27] T. Marler, S. Rahmatalla, M. Shanahan, and K. Abdel-Malek, “A new discomfort function for optimization-base posture prediction”, *2005 Digital Human Modeling for Design and Engineering Symposium*, June 2005 or *SAC international*, DN 2005-01-2680, 2005

[28] URL <http://www.santoshumaninc.com/pdf/vsr-motion.pdf> (last accessed on April 1, 2010)

[29] J. Yang, T. Marler, H. Kim, J. Arora, and K. Abdel-Malek, “Multi-objective optimization for upper body posture prediction”, *Proc. 10th AIAA/ISSMO Multidisciplinary Analysis and Optimization Conf*, 2004

[30] E.N. Horn, “Optimization-based dynamic human motion prediction”, master degree thesis, U. of Iowa, 2005

## Biographies

**HYOUNKYUN OH** is an Assistant Professor of Mathematics at Savannah State University. He instructs undergraduate mathematics courses, directs undergraduate research, and performs research involved with computational differential algebraic equations, human-factor based biomechanics, application of digital image processing, and optimization-based renewable energy systems. Dr. Oh may be reached at [hoh@savannahstate.edu](mailto:hoh@savannahstate.edu)

**ONAJE LEWIS** is currently a junior in Mechanical Engineering program at Georgia Institute of Technology at Savannah. His interests are in the mechanical design of vehicle body. Mr. Lewis may be reached at [onaje\\_lewis@hotmail.com](mailto:onaje_lewis@hotmail.com)

**ASAD YOUSUF** is Professor of Electronics Engineering Technology at Savannah State University. He earned his B.S. (Electrical Engineering, 1980) from N.E.D University, MS (Electrical Engineering, 1982) from the University of Cincinnati, and a Doctoral degree (Occupational Studies, 1999) from the University of Georgia. Dr. Yousuf is a registered professional engineer in the state of Georgia. He is also a Microsoft Certified Systems Engineer (MCSE). Dr. Yousuf has worked as a summer fellow at NASA, US Air Force, US Navy, Universal Energy Systems, Oakridge National Laboratory, and Lockheed Martin. Dr. Yousuf may be reached at [yousufa@savannahstate.edu](mailto:yousufa@savannahstate.edu)

**SUJIN KIM** has been serving as an Assistant Professor of Mathematics at Savannah State University. Her research interest involves wavelet theory in statistics and digital image processing through wavelet. Dr. Kim may be reached at [kims@savannahstate.edu](mailto:kims@savannahstate.edu)

# AN INNOVATIVE IMPLEMENTATION TECHNIQUE OF A REAL-TIME SOFT-CORE PROCESSOR

Reza Raeisi, California State University, Fresno; Sudhanshu Singh, California State University, Fresno

## Abstract

The objective of this project was to experience and develop rapid prototypes of a System-on-chip (SoC) by using a soft-core processor implementation on a Field Programmable Gate Array (FPGA). The research project described here was a partnership program between Altera Corporation and CSU, Fresno, to enhance the quality of both undergraduate and graduate education in the Electrical and Computer Engineering department. As engineering education is changing in response to the major technological changes in Electronics Design Automation (EDA) tools, the Altera Corporation donated the required EDA tools to build an industry-verified Digital Design Environment Laboratory.

Presented here is the use of these tools for a reconfigurable hardware-software co-design implementation of embedded systems on a FPGA using the  $\mu$ Clinux Real Time Operating System (RTOS). This software-hardware co-design technique is useful for the design of both soft-core and hard-core processors and is ideal for teaching an embedded-system design course. This technique allows students to customize the exact set of several Central Processing Unit (CPU) peripherals and the interfaces needed for engineering design applications.

## Introduction

One of the purposes of this research partnership project was to enhance and transcend graduate research in the field of soft-core processor embedded-system design. Also, to apply an industry-verified electronic design automation tool set for learning soft-core embedded systems in undergraduate education. Any device that includes a programmable computer, but itself is not a general-purpose computer, is termed as an embedded system. An embedded system is a special-purpose computer, which is designed to perform certain dedicated functions. This can be from portable devices such as cell phones and MP3 players, to a large stationary installation like bank teller machines or systems controlling power plants.

In general, embedded systems are not recognizable as regular computers, but instead are recognized as specific computers that usually do not interface with the real world through familiar personal-computer interface devices such as a mouse, keyboard or graphic-user interfaces. Instead, they

interface with the real world through unusual interfaces such as sensors and other communication links. Soft-core embedded systems are preferred for teaching over hardware-embedded and general computers because of their design flexibility and ease of development. Students have the option of customizing their own embedded systems with the required peripheral subsystems.

Most time-constrained resource allocations and task scheduling across a spectrum of subsystems, such as sensor and actuator processing, communications, CPU, memory and other peripheral devices, are today required to use RTOS in order to meet the system response. FPGA-based RTOS embedded systems using soft-core processors are increasingly used in a variety of applications such as aircraft autopilots, avionics and navigation systems, anti-lock braking systems, and traction control systems. They have been adapted more commercially nowadays and are gaining popularity in educational institutions for teaching embedded-system courses [1]. Hence, it is essential to apply this new pedagogy for teaching embedded systems. In this study, the authors integrated a small, fast and efficient real-time operating system (OS),  $\mu$ Clinux, with a soft-core processor and implemented them on FPGA platforms. The ultimate goal was to disseminate the use of soft-core processor experience for graduate research, classroom/laboratory teaching and learning in undergraduate education. The plan was to enhance the quality and complexity of the laboratory experiments, senior design and masters projects.

The focus of this study was the dissemination of the practical details of implementing and integrating a RTOS with a soft-core processor for interfacing with real-time applications through different I/O subsystems. Aside from this experience, another outcome of the project was the development of a digital-design environmental laboratory taking place to provide students a new perspective on digital design using better tools and equipment, than are currently being used in industry. The initial lesson learned from this experience led to the development of a new embedded-system design course "ECE 178". This is a senior-level course taken by students in the seventh semester of their program, before their senior-design project. This course has already gone through its approval stages at the University and was published in the 2009-2010 University general catalogs. It is scheduled to be taught during the spring of 2010, when an assessment of the course will be made.

---

## Processor Overview

Embedded systems are implemented using the following classification of processors:

1. Hard-core processors
2. Soft-core processors

The hard-core processor is embedded in the form of silicon inside an FPGA, where a soft-core processor will use the programmable logical structure of an FPGA to implement the processor. They both have the advantage of using the FPGA logical elements for configuring and implementing peripherals interface to both soft-core and hard-core processors. Both design approaches are very common among manufacturers, but using the soft-core-processor approach is more flexible in academic environments. The soft-core-design approach allows students to specify the processor organization, functionality, and different peripheral connectivity. Therefore, using a FPGA soft-core processor for student design projects is more practical and can save both time and money as they can use and customize a variety of peripherals at their disposal. However, the hard-core processor tends to be faster because of faster clock rates, consumes less power, but they are not reconfigurable and have large development costs. Above all, a soft-core processor targeting FPGA is flexible because its parameters can be changed at any time by reprogramming the device [2]. There are many different kinds of soft-core processors available on the market including:

1. ARM
2. Microblaze
3. Nios II

A soft-core processor version of ARM has been implemented in an FPGA called ARM Cortex-M1 by Dominic Pajak [2]. The ARM Cortex-M1 processor is a streamlined three-stage 32-bit Reduced Instruction Set Computer (RISC) processor that includes: configurable instruction and data memories, optional OS support and system timer, 1 to 32 interrupts, fast or small multiplier and removable debug features.

The MicroBlaze soft-core processor is included as part of Xilinx Embedded Development Kit (EDK). The EDK comes with a standard set of peripherals including timers, UARTs, interrupt controllers, and external flash and memory controllers. There are many OSs to support the Xilinx MicroBlaze soft-core processor including  $\mu$ Clinux.

The Nios II embedded processors were introduced in 2001 into the electronics industry by Altera as the viable commercial processor specially created for embedded-system designs in FPGAs [3]. Since then, it has been used widely in the industry and academia. It is a 32-bit soft-core processor, which is defined in a hardware descriptive language (HDL). It can be implemented in Altera's FPGA devices (DE-2) by using the Quartus II CAD system. The soft-core nature of the Nios II processor allows students to specify and generate a custom Nios II core, tailored for specific project requirements. Nios II is comparable to Xilinx MicroBlaze with RISC-type architecture. The Nios II platform was chosen because Altera Corporation agreed to be a partner in this study and provide the tools needed for the development of the embedded-systems project using  $\mu$ Clinux RTOS. Some features of the Nios II include: access to up to 2GB of external address space, optional tightly-coupled memory for instructions and data, pipeline architecture, dynamic branch prediction, up to 256 custom instructions, and JTAG debug-module capability.

Nios II processors also allow for:

1. Customization of the CPUs, peripherals and the interfaces.
2. Increased performance by implementing real-time embedded-system applications.
3. Lower laboratory costs by not spending additional money on a hardware microcontroller board.

The Nios II processor can be used with a variety of other components to form a complete system. Altera's DE-2 development and educational board contains several components that can be integrated into a Nios II system. An example of such a system is shown in Figure 1. Its arithmetic and logic operations are performed on operands in the general-purpose registers. The data are moved between the memory and these registers by means of Load and Store instructions. The word length of the Nios II processor is 32 bits. All registers are 32 bits long. The Nios II architecture uses separate instruction and data buses, which is often referred to as the Harvard architecture [4].

## Soft-core Processor Real-Time Operating System (RTOS) Implementation

Real-time and embedded systems operate in constrained environments in which computer memory and processing power are limited. They often need to provide their services within strict time deadlines to their users and to the surrounding world. It is these memory, speed and timing

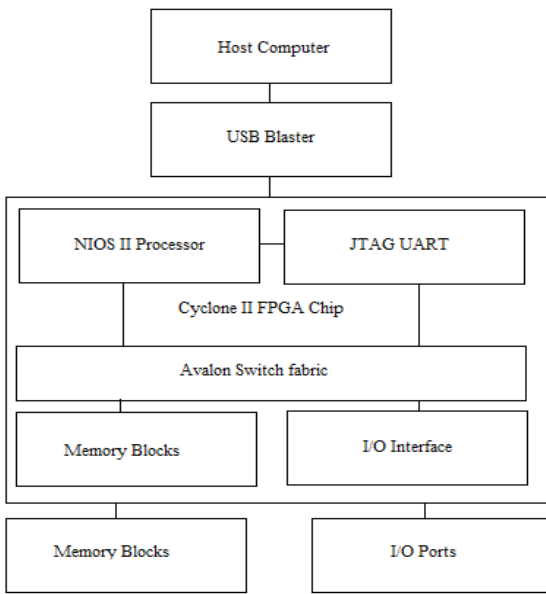


**Figure 1. Nios II system implemented on the DE-2 board**

constraints that dictate the use of real-time operating systems in embedded software. RTOS kernels hide from application software in the low-level details of system hardware, while at the same time providing several categories of services to the application software. These include: task management with priority-based preemptive scheduling, reliable inter-task communication and synchronization, non-fragmenting dynamic memory allocation, and basic timer services [5]. The  $\mu$ Clinux kernel supports multiple soft-core CPU platforms including Altera's Nios II architecture. The main advantage of this operating system is that it is an open-source project and it is smaller than the regular Linux kernels. Most features of Linux kernels are available, like process control, file system, networking, and device drivers [6].

Altera's DE-2 board block diagram is shown in Figure 2. The DE-2 board and Quartus II software are used to implement the Nios II soft-core processor that supports a flexible memory option and I/O device combination. Experiments implemented using the NIOS II soft-core processor are real-time tasks using interrupt programming, and connections with I/O devices such as audio, video, USB, network and memory expansion. Quartus II is used to configure the available memory on the DE-2 board for the execution of small application programs. However, for larger application programs, whose size is beyond the capacity of the available on-chip memory, a Bootloader is placed into the on-board memory. The Bootloader will start running on boot-up and can receive a larger program binary file—over a serial interface—from external memories such as, SRAM, SDRAM, and Flash, for execution on the soft-core processor.

The Nios II Integrated Development Environment (IDE) is the standalone program that helps us to accomplish our task of implementing  $\mu$ Clinux over the FPGA device. Nios II IDE 9.0 is the latest version of the software and can be downloaded from the Altera website. The distribution for  $\mu$ Clinux can be obtained from <http://Nioswiki.jot.com/WikiHome/>. The Nios II community develops and releases the latest kernels according to the Altera software release. Because of the licensing issue, the authors have built the  $\mu$ Clinux kernel in a Linux environment and then transferred the kernel image into the Windows to complete the project. Running the  $\mu$ Clinux on a DE-2 board requires two steps. First, the FPGA must be configured to implement the Nios II processor system [7], and second the  $\mu$ Clinux kernel image must be downloaded into SDRAM on the DE-2 board. Both configuration steps can be accomplished via the Nios II 9.0 command shell. Before starting the configuration of the DE-2 board, the power cable should be connected, the DE-2 board should be turned ON, and the USB cable connected between the PC and the USB blaster port on the DE-2 board.

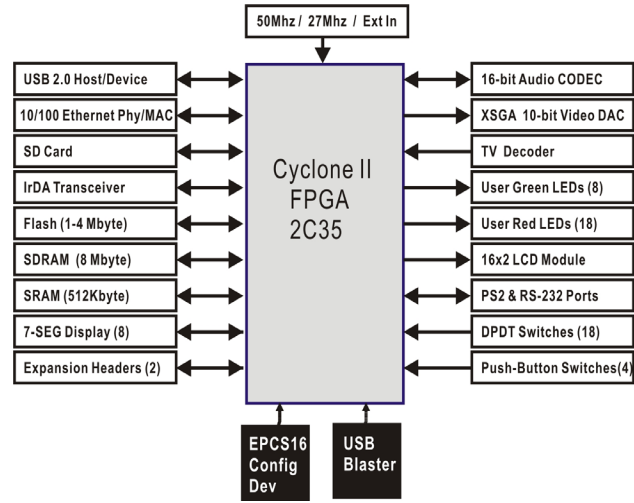


**Figure 2. Altera DE-2 board block diagram**

An existing Nios II project from the demonstrations directory of the enclosed DE-2 CD-ROM was used. The authors chose the DE2\_NIOS\_HOST\_MOUSE\_VGA project and used the *wget* command in the Linux terminal to download the  $\mu$ Clinux distribution. A basic  $\mu$ Clinux kernel image was built using the *make menuconfig* command. The completed image was located at Nios-linux/uClinux-dist/image/zimage. Zimage is a compressed form of a kernel image. The Linux kernel takes care of expanding the image at bootup. On Linux systems, *vmLinux* is a statically-linked executable file that contains the Linux kernel in one of the executable file formats supported by Linux, including ELF, COFF and a.out. To configure the FPGA and download the zImage to

the processor, the following command steps were written into the Nios II 9.0 command shell [7].

**Step 1. ConFigure the FPGA:**

*Nios2-conFigure-sof DE2\_NIOS\_HOST\_MOUSE\_VGA.sof*

**Step 2. Download and run the kernel image:**

*Nios2-download*

*-g zImage\_DE2\_NIOS\_HOST\_MOUSE\_VGA\_v1.6*

After the kernel image was downloaded onto the DE-2 board,  $\mu$ Clinux in *Nios2-terminal* became active and was ready, as shown in Figure 3.

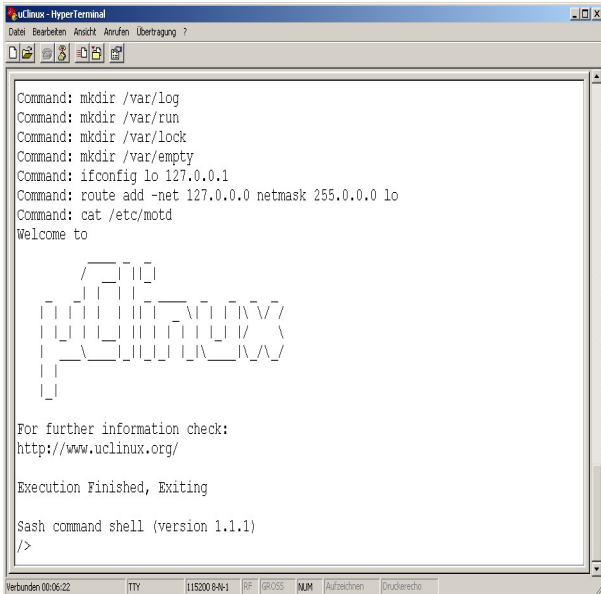


Figure 3. uClinux Implementation on Nios II

## Application of the Soft-Core Processor

Once the  $\mu$ Clinux is configured, the Nios II system was ready for use. The next step was to customize the kernel and add a user application. Next, after logging into the Linux platform, the *make menuconfig* operation was performed. One of the application experiments was to complete the Ethernet interfacing and connecting the board to the outside world. This was done by invoking FTP and Telnet. Then, the Ethernet network support was activated during the *make menuconfig* command.

The Ethernet connection was tested using the *ifconfig* command. The *ifconfig* command allows the operating system to set up network interfaces and the user to view information about the conFigured network interfaces. A valid IP address is displayed after the label *inet addr* as shown in

Figure 4, which shows that the DE-2 board was successfully communicating on the network.

```

collisions:0 txqueuelen:0
RX bytes:0 <0.0 B> TX bytes:0 <0.0 B>

/> dhcpcd&
[22]
/>
/> ifconfig
eth0      Link encap:Ethernet HWaddr 00:07:ED:00:00:00
          inet addr:128.59.151.179 Bcast:128.59.151.255 Mask:255.255.248.0
          UP BROADCAST NOTRAILERS RUNNING MULTICAST MTU:1500 Metric:1
          RX packets:3374 errors:0 dropped:0 overruns:0 frame:0
          TX packets:7 errors:0 dropped:0 overruns:0 carrier:0
          collisions:0 txqueuelen:1000
          RX bytes:350749 (342.5 KiB) TX bytes:2832 (2.7 KiB)
          Interrupt:6 Base address:0x10f8

lo       Link encap:Local Loopback
          inet addr:127.0.0.1 Mask:255.0.0.0
          UP LOOPBACK RUNNING MTU:16436 Metric:1
          RX packets:0 errors:0 dropped:0 overruns:0 frame:0
          TX packets:0 errors:0 dropped:0 overruns:0 carrier:0
          collisions:0 txqueuelen:0
          RX bytes:0 <0.0 B> TX bytes:0 <0.0 B>

/>

```

Figure 4. ifconfig result

Furthermore, the Nios II processor developed was used to implement a variety of experiments. Examples are writing a device driver for the LCD controller interface and I/O and interrupt programming. Figure 5 shows the experience with the pulse-width modulation (PWD) of a specific duty-cycle to manipulate analog circuitry from a digital domain application.

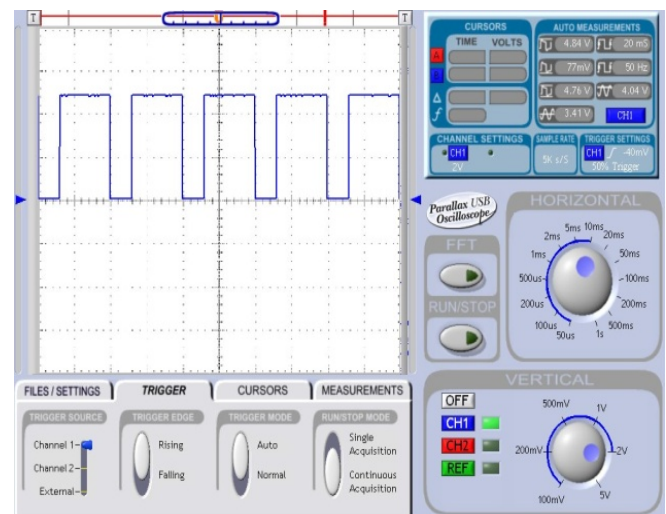


Figure 5. Pulse width modulation using Nios II

---

## Conclusion

As a result of this study, a new course, ECE 178 embedded systems, was developed. This course demonstrates how soft-core-processor embedded systems can be implemented on a real-time operating system on an FPGA. During this project, various applications in the Linux kernels were examined. The Ethernet-connection application and some other I/O and interrupt programming was implemented. Also, the Altera grant impacted three master-student projects, in-progress at the time of publication. Now, the platform to transcend graduate research and teaching this new approach for learning embedded-system concepts for the undergraduate students in the ECE 178 embedded-systems course is set. Overall, FPGA soft-core processors for learning and teaching will enable us to define a variety of laboratory experiments with different complexity in each design. Also, it provides students with a better learning experience by having their design components at-hand and be more economical by reusing the components for different design projects.

## References

- [1] Tyson S. Hall and James O. Hamblen, “Using an FPGA Processor Core and Embedded Linux for Senior Design Projects”, Proceedings of the IEEE International Conference on Microelectronics Systems Education, Issue. 3-4 pp. 33 – 34, June 2007.
- [2] “Embedded Design with FPGAs and ARM Cortex-M1”-Dominic Pajak, ARM, Jean Labrosse, Micrium and Mike Thompson, Actel from the April-2008 embedded systems conference.
- [3] Altera Homepage, [www.altera.com](http://www.altera.com)
- [4] Introduction to the Altera SOPC Builder- Quartus II Development Software Literature.
- [5] Zongqing Lu, Xiong Zhang, Chuihang Sun, “An Embedded System with uClinix based on FPGA”, IEEE Pacific-Asia Workshop on Computational Intelligence and Industrial Application, pp. 691-694, 2008.
- [6] Philipp Lutz , “Device drivers and Test application for a SOPC solution with Nios II soft-core processor and  $\mu$ Clinix” Masters Thesis, University of Applied Sciences, Augsberg, 2008.
- [7] J.O Hamblen, T.S Hall and M.D. Furman, “Rapid prototyping of digital systems”, Chapter 18 Springer Press, 2007.

## Biographies

**REZA RAEISI** is an Associate Professor in the Electrical and Computer Engineering Department at California State University, Fresno. He is also the Graduate Program Coordinator for the ECE department. His research interests include integrated circuits, embedded systems, and VLSI-CAD technology. He serves as Pacific Southwest regional director of American Society of Engineering Education. He is an entrepreneur with over 20 years of domestic and international experience and professional skills in both industry and academia. Dr. Raeisi may be reached at [raeisi@csufresno.edu](mailto:raeisi@csufresno.edu)

**SUDHANSU SINGH** is a graduate student in Electrical Engineering in the College of Engineering, at the California State University, Fresno. He received his bachelor's degree in Electrical Engineering from Gujarat University. His interests involve VLSI design, which includes the physical design and timing analysis, embedded systems. Mr Singh may be reached at [singh0601@csufresno.edu](mailto:singh0601@csufresno.edu)

# APPLICATION OF QFD INTO THE DESIGN PROCESS OF A SMALL JOB SHOP

M. Affan Badar, Indiana State University; Ming Zhou, Indiana State University; Benjamin A. Thomson, Reynolds & Co.

## Abstract

This was a case study involving the application of Quality Function Deployment (QFD) into the design process at Reynolds & Co., a small job shop in Terre Haute, IN, USA. The company's work is customer-oriented. The objectives of the research were to find the applicable QFD concepts and to reduce the average design time or number of design changes in the design process. The House of Quality (HoQ) was modified for organizational use in order to identify goals and priorities of the company. The case study was successful in providing research into the implementation of QFD concepts to improve the design process of a small job shop. However, the design time and the design changes were not decreased significantly. It was important to discover that job shops better understand their customers through direct interaction than do large consumer-based companies.

## Introduction

Quality Function Deployment (QFD) is a compilation of the product design and its manufacture, which includes the customer requirements as well as the design/engineering requirements. QFD is "a tool for collecting and organizing the required information needed to complete the operational quality planning process" [1]. Ternimko [2] stated that QFD is not a replacement for an existing design process. Instead, it would work with the design process in place and provide a more efficient system through the improvement of customer perceived quality. QFD was first developed in Japan [3]. QFD implementation generally results in significant improvements in both product design and the development process [4]. A variety of approaches to QFD have been implemented in the US with varying degrees of success [5].

The present work is a case study of implementing the necessary QFD concepts into the design process at Reynolds & Co., located in Terre Haute, IN, USA. A portion of this work was included in Thomson et al. [6]. Reynolds employs approximately 25 people, most of whom are machinists and fabricators by trade. This is a custom manufacturer of components and special machinery for the plastics industry as well as other types of industry around Indiana and the United States (business to business). Thus, this is a small "make-to-order" company, which is different from a typical high-volume "build-to-stock" or consumer-based company [7].

For purposes of this study, the phrase "design process" was used to describe the method of converting the customer requests into manufacturable products. The customer requests of the design process at Reynolds may include any of the following types. The first type of customer request is an outside customer order, where the customer provides the specifications, or prints, and details for the product/component. The second type of customer request is an outside customer order for a product/component, where Reynolds & Co. provides the specifications for the drawing design and the customer provides the requirements. The third type of customer request is where an outside customer provides a part or component to be reverse-engineereddesigned. The fourth type of customer request is the internal-customer type, where the products are manufactured after the design process is complete. These are all customers of the design process.

There exists an extensive amount of literature on QFD implementation in a high-volume or consumer-based manufacturing environment, but very little on job shops. This was the motivation behind this study. Specific objectives of the research were to 1) find the QFD concepts that apply to the improvement of this specific job-shop design process, 2) reduce the average design time, and 3) decrease the number of design changes. The design process was analyzed by averaging the design time and the number of design changes before and after the implementation of QFD strategies/concepts.

## Review of Related Literature

In this section, a review of related literature on Quality Function Deployment and job shops is presented.

In the late 1960's in Japan, Professors Mizuno and Akao [8] developed a quality-assurance concept of designing customer satisfaction into a product and called this Quality Function Deployment (QFD). QFD helps companies identify real customer requirements and translates these requirements into product features, engineering specifications, and manufacturing details. The product can then be produced to satisfy the customer. This means that the customer-perceived quality is present before the manufacturing even gets started. QFD is proactive since the vast majority of the design and marketing problems are handled before manufacturing begins; traditional quality control is reactive as it focuses on

---

fixing problems once production has begun. QFD was applied on its first large-scale application in 1966 at Bridgestone Tire in Japan by Oshiumi using fishbone diagrams to better accommodate customer needs into Bridgestone tires [8]. Mitsubishi Heavy Industry used QFD concepts to aid in the design of an oil tanker in 1972. In the following years, Toyota Motors used it to revolutionize the design process of new automotive vehicles [9]. Fishbone diagrams that were initially used were updated and transformed into a spreadsheet/matrix format to aid in the complexity of the Mitsubishi oil tanker design [8]. During the same period, Ishihara [8] introduced Value Engineering concepts to explain business functions necessary to ensure quality of the design process. As a result of the combination of these emerging concepts, QFD became the comprehensive quality-design system for both product and business process [8]. Jiang et al. [10] and Shiu et al. [11] modified QFD structure so that it can effectively be used in contract manufacturing and new-product development cycle, respectively.

QFD consists of two components: quality and function that are deployed into the design process [12]. Quality deployment brings the customer's voice into the design process, whereas function deployment brings functional specialists from different organizational functions and units into the design-to-manufacturing process. QFD process involves product planning, product design, process planning, and process control [13]. Akao [14] defines quality function deployment as converting the consumers' demands into 'quality characteristics' and developing a design quality for the finished product by systematically deploying the relationships between demands and characteristics, starting with the quality of each functional component and extending the deployment to the quality of each process. The overall quality of the product will be formed through this network of relationships. QFD is a compilation of planning and analyzing tools. Some of these tools are charts and graphs but the best known is the house of quality (HoQ). The HoQ chart [5], [15], [16] is used to analyze customer requirements and the engineering/design requirements and the relationships that exist between them. Akao and Oshiumi introduced the HoQ in the 1966 Bridgestone Tire project [8]. However, the HoQ is not a necessity for the implementation of QFD, particularly in technology-driven QFDs and cost-reduction-driven QFDs [2], [8], [16].

Another QFD documentation requirement deals with the organization and company goals. These can be broken into business or organizational goals, product goals, and project goals [17]. Goals are organized on a radar chart [1], [2]. The purpose of a radar chart is to list the company goals around the perimeter of the circle and compare the findings from before and after a change. The radar chart data is gathered by interviews with the organizational leaders or by customer

inputs. The metrics of the radar chart are that the closer the objective is to the outside of the chart the better the company is in this aspect [2]. The goal of the radar chart was to even out the goals with respect to one another. The radar chart should be round if the company's goals were met congruently [18]. The next form of documentation is in the form of questions that are geared to stimulate the customer's requirements during the review of the customer's requests, which may take place in the customer's plant [17].

The term "job shop" is used to refer to all types of custom manufacturing, make-to-order businesses—including machine shops—that meet the following criteria [7]: 1) Produce on an order-by-order basis to meet customers' specifications—order driven; 2) Secure work through a bidding process; 3) Serve other companies and/or distributors as opposed to customers or end-users; and 4) Serve as service companies. Job shops do not function like a typical high-volume build-to-stock company [7]. The job shop can be very diverse and can rapidly adapt to changes in production. A change can be made to a customer's order in a matter of minutes, typically, where a high-volume build-to-stock company thrives on stability. And should a change occur in a customer's order, the change may take days to weeks to be made. The job-shop process of design is focused on the following objectives: function, durability, appearance, and cost [19]. These design objectives are customer-driven. This means that the customer must approve, otherwise the design is not effective. Engineering objectives are requirements such as material strength, reliability, and design parameters. In addition, the designer has the job of designing with manufacturing in mind. This is achieved through simplicity of design, standard materials, and liberal tolerances [19]. Competition is similar between the consumer-based production manufacturer and the small job shop. The presentation of customer-perceived quality and the price of the product is subject to review by the customer. This review will influence the buying patterns of the customer.

Reinforcement for the rationale of this study includes the fact that United States companies are facing tough competition from overseas competitors [19]. Ternimko [2] states that QFD strategies aim at reducing cost by understanding the customer requirements better and therefore providing improved value to the customer. Improved value for the customer is a factor of achieving customer requirements such as cost, function and aesthetics.

## QFD Implementation at Reynolds

This case study was conducted from December 2004 through April 2005. An analysis of the Reynolds' design process was conducted in December 2004. There were four

types of customer requests for the design process at Reynolds as outlined in the introduction section. The average design time and the number of design changes for October and November of 2004 were measured.

Next was the QFD implementation phase, which was conducted during December 2004 and January 2005. Reynolds' goals were determined by interviews with the management and by research into the driving factors of the job-shop environment. Initial measurements of how the company was meeting its goals were obtained from interviews with the management. These measurements were compared with the measurements obtained from the customer surveys. The survey questions were prepared to capture customer perceptions of the Reynolds' goals and design process.

Customer	Description	Relationship Goals / Potential
Company 1	Blown film, printing, converting	1. Increase sales and design potential 2. Building improvement
Company 2	Blown film, cast film, printing, converting	1. Increase communication / design
Company 3	Closure Systems	1. Increase communication 2. Provide better service
Company 4	Cast Film	1. Design and build sheet dies
Company 5	Recycling plastics	1. Design and build blades 2. Design and build other auxiliary equipment
Company 6	Blown Film	1. Sales potential
Company 7	Aluminum Sheeting	1. Increase communication 2. Increase sales
Company 8	Steel Sheeting	1. Provide better service 2. Improve communication

Figure 1. Customer prioritization chart

QFD then required Reynolds to prioritize their customer list according to the value of the customer related to the company's goals. The customer-prioritization chart is shown in Figure 1. This prioritization was assembled through interviews with the management. The next form of documentation created was a list of questions that were designed to stimulate the customer's requirements during the review of the customer's requests, which could take place over the phone or face-to-face. The chart of customer requirements stimulating questions is shown in Figure 2. Understanding the customer requirements and stimulating these require-

ments may be a problem associated with the high-production consumer-based company. Small job shops, on the other hand, know exactly who their customers are because they are make-to-order companies.

#### Questions to Stimulate Customer Requirements:

JOB NUMBER: - DATE:

Question:	Answer:
1. Part / Mechanism description (part number, drawing number, physical size)	
2. Function (type of motion, how it works)	
3. Critical tolerances / fits	
4. Materials (Type & Hardness)	
5. Physical Size & Weight (Can we haul it & Machine it)	
6. Delivery (OT or Regular)	
7. Machining requirements (Type of machining)	
8. Contact name, phone, company	
9. Location of pickup / delivery	
10. Cost / pricing (P.O. Number)	

Figure 2. Chart to stimulate customer requirements

The next form of design-process documentation was to create a sheet or drawing to list the customer requirements as shown in Figure 3. This form of documentation was substantial in the form of time-savings during manufacturing and improved communication between the design department and the manufacturing department. This improved communication eliminated some rework time and additional design time that were not necessary to complete the job. An example of a communication error that occurred frequently because of lack of proper design documentation was when a part that was acceptable with saw-cut ends and a tolerance of plus or minus 1/32" was frequently machined to a tolerance of plus or minus five thousandths. The customer was not willing to pay extra for the time required to machine the part to this tighter tolerance; therefore, the profit margin was eroded.

Drawing / Manufacturing Information
Gibbs Cam (Name & Location)
Employee Number
Machine Number
Saw Cut Length Information
Machining Notes
Fixture Information

Figure 3. Drawing / manufacturing documentation

QFD breaks down customer requirements into different categories, each having a different expectation and satisfaction type. These requirements can be classified as the ex-

pected, normal, and exciting requirements [17], [20]. The customer requirements were brought to the manufacturing process by including them on the drawings/prints, according to the chart in Figure 3. The process of following customer requirements helped Reynolds to focus on customer-perceived quality and, therefore, provide better value to the customer.

According to QFD concepts, the customer requirements need to be evaluated in order to transform them into the design requirements and rank their importance. QFD recommends using the house of quality (HoQ) chart for product design. The HoQ was simplified for job-shop usage [20]. But, the HoQ was not helpful on the Reynolds' job because the amount of time required to construct a HoQ was substantially more than the entire job had initially required. Therefore, the HoQ was revised to make it an organizational improvement chart. The surveys were used to accomplish this objective. The revised HoQ chart is shown in Figure 4. The objective of using the HoQ for the organization was effective in understanding the customer requirements associated with the organizational standing of the job-shop environment. The design goals determined through interviews with the management of Reynolds were service, delivery, price, dimensional accuracy, and overall quality.

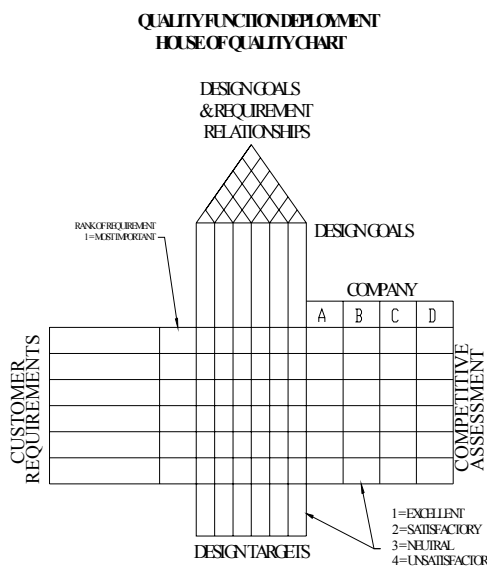


Figure 4. Organizational House of Quality chart

The progression of the implementation meant new ways of keeping track and documenting processes in order to save time and relieve confusion. In this regard, a document was created to list the common items ordered from certain vendors. The timeline for implementation of the QFD concepts (December 2004 through January 2005) was considered exempt from the before-and-after comparisons. The period before the QFD implementation was October and November

2004. The period of February and March 2005 was after the implementation. The data collection was focused on measuring the average design time and the number of design changes. Data was collected by searching Reynolds' job listings and collecting the design time out of the total time incurred by each job that started before or after this time period.

## Results

In this section, results of the QFD implementation are summarized.

Data for the time taken and the number of design changes for the design jobs that occurred during October through November 2004 were collected. Descriptive statistics for the design time and number of design changes are presented in Table 1 and Table 2, respectively. Raw data and other details are given by Thomson [20]. The total number of jobs with complete information was 337. The mean design time was 0.9325 hours with a median of 0.25 hours, and a standard deviation of 1.98 hours. The mean number of design changes that occurred was 0.1098, with a median of 0.0 (no design change required after the design), and a standard deviation of 0.683. The design-time and design-change data for the period February through March, 2005, as the post implementation stage of the study are given by Thomson [20]. There were 344 jobs in total. The mean design time was 0.843 hours, with a median of 0.25 hours, and a standard deviation of 1.91 hours. The mean number of design changes was 0.0727, with a median of 0.0, and a standard deviation of 0.4983. The data for design-time and design-change were found to be independent and random [20].

Table 1. Descriptive statistics for design time in hours from October through November, 2004

Statistics		
Design Time (October-November 2004)		
N	Valid	337
	Missing	7
Mean		.9325
Median		.2500
Mode		.25
Std. Deviation		1.98105
Variance		3.92456
Skewness		5.689
Std. Error of Skewness		.133
Kurtosis		45.343
Std. Error of Kurtosis		.265
Minimum		.00
Maximum		22.00

Dependant-sample T-Tests [21] were used to compare both the design-time and design-change data before and after the QFD implementation. The critical T value for a two-tailed test at a 95% confidence level and 336 degrees of freedom was 1.96 [21]. The T-Tests provided T values of 0.527 and 0.762 for the design time and design changes, respectively. Both were lower than 1.96. Therefore, the design time and number of design changes before and after the implementation were not statistically different.

**Table 2. Descriptive statistics for design changes from October through November, 2004**

Statistics		
Design Changes (October-November 2004)		
N	Valid	337
	Missing	7
Mean		.1098
Median		.0000
Mode		.00
Std. Deviation		.68343
Variance		.46708
Skewness		7.793
Std. Error of Skewness		.133
Kurtosis		69.812
Std. Error of Kurtosis		.265
Minimum		.00
Maximum		8.00

The next part of the study was to analyze the surveys sent to the customers to see how the customers viewed Reynolds in terms of service, delivery, price, dimensional accuracy, overall quality, and how well the company satisfied their goals and requirements. In order to satisfy the policies related to Research Involving Human Subjects, an exemption from the Institutional Review Board (IRB) was obtained. The IRB stated that in order to keep the survey anonymous, they must stay local so that the Post Office stamps on the return envelopes would not give away the location of the survey respondent. Therefore, only local companies were selected to represent Reynolds' customer base. Seventeen survey-responses were received. The mean values for all customer requirements were found to be between 4.65 and 4.82 on a scale of 5; the only exception was for price (3.94), which was considerably lower and had a higher standard deviation than the other customer requirements. However, this may be influenced by a bias in the respondents.

The management at Reynolds thought that they were satisfactory on price, service, delivery, and dimensional accuracy; and neutral on overall quality, as displayed in the radar chart of Figure 5. The customers, however, rated all factors as excellent and price as satisfactory, as depicted in the radar

chart of Figure 6. This, again, emphasizes the importance of the drawing or some kind of documentation, as shown in Figure 3, for manufacturing to avoid making a product more precise and, in turn, more expensive than what the customer wants. The findings from the survey were then analyzed in the form of the House of Quality, as shown in Figure 7. The HoQ was a means of discovering a relationship between the organizational goals and common customer requirements.

QUALITY FUNCTION DEPLOYMENT RADAR CHART

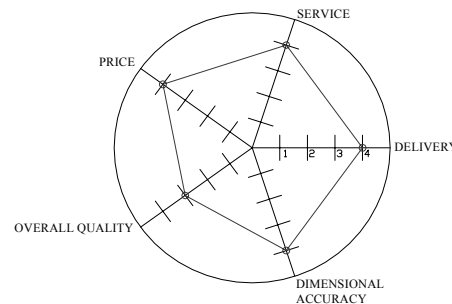


**Figure 5. Radar chart displaying the organizational goals based on the management interviews**

QUALITY FUNCTION DEPLOYMENT RADAR CHART

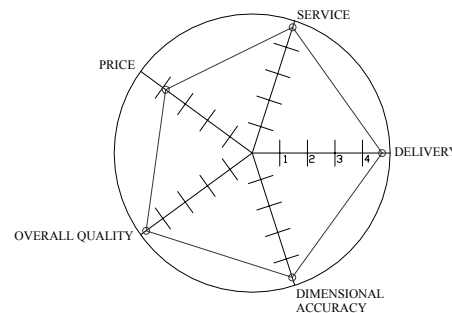


**Figure 6. Radar chart displaying the results of the survey**

The correlations section was deemed critical because this describes important areas that need attention when analyzing the customer requirements for individual jobs. The correlations that were important had to have a correlation of two or negative two. The rationale behind this decision—to focus on major issues and strong correlations—was that the job-shop environment is fast-paced and this study is short-term in nature. The first strong correlation was the delivery and delivery-time section. There was a strong positive correlation of two, and the design target was two; therefore, the total correlation was the correlation multiplied by the design target, which equaled four. Delivery is one aspect of a job shop that is extremely important; customers are demanding and may choose a competitor's quote over Reynolds' quote

based on the delivery time and not the price. The next strong correlation existed between delivery time and service. This was a strong negative correlation of negative two. As delivery time increases the customer perception of service decreases. The correlation between cost and price was two but the design target was zero, which produced an answer of zero. This correlation was not a priority, according to the management at Reynolds. The same relationship existed between delivery time and price. All of the other relationships were seen by the management to be secondary factors, equally important but not as important as delivery and service.

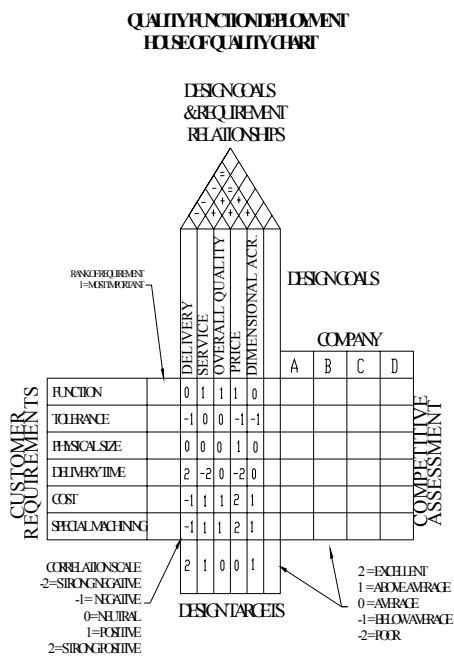


**Figure 7. The House of Quality chart for organizational goals and customer requirements (this was driven by the chart to stimulate customer requirements, shown in Figure 2)**

## Conclusions

This research could be generalized to other similar situations but is unique to the specific company where it was performed. The methodology used for the application of QFD into the design process at Reynolds was unique in that the majority of research involving QFD was focused on large consumer-based companies and not small job-shop business-to-business companies.

The progression of the implementation of QFD at Reynolds brought up other areas that were problems, such as communication and ordering. The communication gap was reduced by the drawing documentation that conveyed impor-

tant information to the manufacturing department after the design department had finished their part. The management at Reynolds saw processes that needed improvement that may not directly be influenced by QFD, but they were improvements that were needed in order to make the design department work more efficiently. One such example was the order list that was made to display commonly-ordered items with quantities to order and prices along with the supplier and contact name. This made it easier for whoever was ordering at that time to find the correct part numbers and quantities without wasting time. The quoting process was somewhat detailed, but as far as knowing the correct rates to charge—according to the type of work—was somewhat ambiguous. Thus, a quoting procedure was documented along with the best suppliers of materials for quoting purposes. This aided in finding the best sources as well as having a standardized method to follow while quoting. The purpose of this in terms of QFD was that this was a way to increase efficiency and to provide the best prices possible since, according to the survey, price was a controversial topic. The surveys aided Reynolds in discovering, on an organizational basis, where they stand with their customers.

The improvement at Reynolds came from closing the gaps in communication and understanding the customer better by knowing what is most important to them. One requirement that developed during the study was that the customers suggested that Reynolds' employees work Saturdays, because most of them are operating 24 hours per day seven days a week. The case study was successful in providing research into the implementation of QFD concepts to improve the design process, although the design time and the number of design changes were not significantly decreased. The discovery that job shops better understand their customers through direct interaction than do large consumer-based companies is a very important aspect of this case study.

## References

- [1] Juran, J.M. (Ed.), 1999, Juran's Quality Control Handbook, 5<sup>th</sup> ed., McGraw-Hill, New York, NY.
- [2] Ternimko J., 1997, Step-by-Step QFD Customer-Driven Product Design, 2<sup>nd</sup> ed., St. Lucie Press, Boca Raton, FL.
- [3] Cristiano, J.J., Liker, J.K., and White, C.C. III, 2001, "Key factors in the successful application of Quality function deployment (QFD)," *IEEE Transactions on Engineering Management*, 48, 1, 81-95.
- [4] Prasad, B., 1998, "Review of QFD and related deployment techniques," *Journal of Manufacturing Systems*, 17, 3, 221-234.
- [5] Sullivan, L.P., 1986, "Quality function deployment: A system to assure that customer needs drive the prod-

---

uct design and production process," *Quality Progress*, 19, 6, 39-50.

[6] Thomson, B.A., Badar, M.A., and Zhou, M., 2007, "Implementing QFD into a small job shop design process: a case study," *IIE Proceed. of the 2007 Industrial Engineering Research Conf.*, G. Bayraksan, W. Lin, Y. Son, and R. Wysk (eds.), 1126-1131, CD-ROM:IIE07/Research/IIE-202A.pdf, Nashville, TN, May 19-23.

[7] Bozzone, V., 2002, *Speed to Market: Lean Manufacturing for Job Shops*, 2<sup>nd</sup> ed., Amacom, New York, NY.

[8] QFD Institute, 2007, <http://www.qfdi.org>, retrieved on Jan 25, 2007.

[9] Hunt, R.A. and Xavier, F.B, 2003, "The leading edge in strategic QFD," *The Int. J. of Quality & Reliability Management*, 20, 1, 56-73.

[10] Jiang, J.-C., Shiu, M.-L., and Tu, M.-H., 2007, "Quality function deployment (QFD) technology designed for contract manufacturing," *The TQM Magazine*, 19, 4, 291-307.

[11] Shiu, M.-L., Jiang, J.-C., and Tu, M.-H., 2007, "Reconstruct QFD for integrated product and process development management," *The TQM Magazine*, 19, 5, 403-418.

[12] Lockamy, A. III, and Khurana, A., 1995, "Quality function deployment: Total quality management for new product design," *The Int. J. of Quality & Reliability Management*, 12, 6, 73-84.

[13] Bouchereau. V. & Rowlands, H., 2000, "Methods and techniques to help quality function deployment (QFD)," *Benchmarking*, 7, 1, 8-19.

[14] Akao, Y., 1990, *Quality Function Deployment: Integrating Customer Requirements into Product Design*, Productivity Press, Cambridge, MA.

[15] Hauser, J.R. and Clausing, D., 1988, "The house of quality," *Harvard Business Review*, 66, 3, 63-73.

[16] Hauser, J.R. and Katz, G.M., 1998, "Metrics: You are What You Measure?" *European Management Journal*, 16, 5, 517-528.

[17] Mazur, G., 2003, "Voice of the Customer (Define): QFD to Define Value," *ASQ Annual Quality Congress Proceedings*, USA, 57, 151-157.

[18] Conner, G., 2001, *Lean Manufacturing for the Small Shop*. Society of Manufacturing Engineers, Dearborn, MI.

[19] Bralla, J.G., 1999, *Design for Manufacturability Handbook*, 2<sup>nd</sup> ed., McGraw-Hill, New York, NY.

[20] Thomson, B.A., 2005, A case study on implementation of quality function deployment into the design process of a small job shop, MS thesis (Advisor: Dr. Badar), Indiana State University.

[21] Minium, E.W., Clarke, R.C., and Coladarci, T., 1999, *Elements of Statistical Reasoning*, 2<sup>nd</sup> ed., John Wiley & Sons, Inc., Hoboken, NJ.

## Biographies

**M. AFFAN BADAR** is an Associate Professor at Indiana State University (ISU). He has also been serving as the Assistant Director of the ISU Center for Systems Modeling and Simulation since 2004. He served the IIE Engineering Economy Division as the Director from 2005 through 2007. He received his Ph.D. in Industrial Engineering from the University of Oklahoma in 2002; M.S. in Mechanical Engineering from King Fahd University of Petroleum and Minerals in 1993; and M.Sc. in Industrial Engineering from Aligarh Muslim University in 1990. At ISU, he teaches courses for the BS in Mechanical Engineering Technology and MS/PhD in Technology Management programs. Dr. Badar has published more than 25 articles in refereed journals and proceedings in the areas of coordinate metrology, lean manufacturing, health care, design, QFD, stochastic modeling, reliability, and supply chain. Dr. Badar can be reached at [M.Affan.Badar@indstate.edu](mailto:M.Affan.Badar@indstate.edu).

**MING ZHOU** is a Professor and the ECMET Department Chairperson at the Indiana State University (ISU). He has been also serving as the Director of the ISU Center for Systems Modeling and Simulation since 2004. He received his Ph.D. degree in Systems and Industrial Engineering from the University of Arizona in 1995 and B.S. in Mechanical Engineering from Wuhan Institute of Technology in 1982. At ISU he teaches courses for the BS in Mechanical Engineering Technology and MS/PhD in Technology Management programs. Dr. Zhou can be reached at [Ming.Zhou@indstate.edu](mailto:Ming.Zhou@indstate.edu).

**BENJAMIN A. THOMSON** is a Design Engineer at Reynolds & Co. He received his MS degree from Indiana State University in 2005. Mr. Thomson can be reached at [benthomson81@yahoo.com](mailto:benthomson81@yahoo.com)

# USAGE OF AXIOMATIC DESIGN METHODOLOGY IN THE U.S. INDUSTRIES

Ali Alavizadeh, George Washington University; Sudershan Jetley, Bowling Green State University

## Abstract

Axiomatic Design, originally developed by Nam Suh [1], is a design methodology that attempts to systematize the design practices and to provide a basis on which design can be carried out and optimized. This case-study analysis was conducted to identify the extent to which Axiomatic Design is known to U.S. industries and to identify the factors influencing the use of the methodology. The results indicated that the methodology is not well known in the U.S., in particular in the automotive industries. Also, the methodology should first be applied to relatively small projects in order to realize its strengths and weaknesses. Plus, Axiomatic Design is not, and should not be regarded as, the only design methodology. It provides a framework within which one can use its axioms, as well as other various design methodologies.

**Keywords:** Axiomatic Design, Design, Design Methodologies

## Introduction

Design is one of the fundamental steps in product development. In this process, the designer defines and conceptualizes the purpose of the product, whether it is a component, software, product, or system. History evidences numerous scientific and technological advancements and innovations, yet failures often arise partially due to poor design. Poorly designed products are more difficult to manufacture and maintain [1].

Singh [2] states that several studies have suggested that most of a product's cost becomes fixed in its early life-cycle stage before the original design cycle is completed. A typical characteristic curve that indicates the cost incurred and committed during the product life cycle is shown in Figure 1. As seen in this figure, the majority of the product development cost occurs in the conceptual and detailed design phase. Also, the overall design change is easier in the earlier phases.

The design process can use different methodologies for product development and there are many such methodologies available in the market. One of these is the Axiomatic Design originally developed by Nam Suh [1].

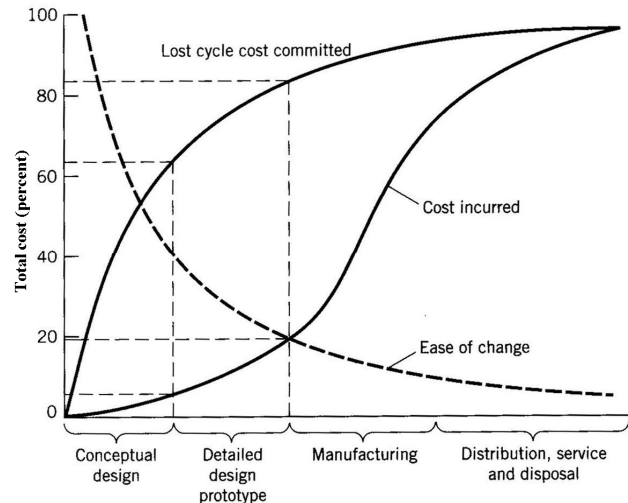


**Figure 1. The cost incurred and committed characteristics within the life cycle of a product [2]**

This study was conducted to identify the extent to which Axiomatic Design is known to U.S. industries and to identify the factors influencing the use of the methodology. The results indicated that the methodology is not well known in the U.S., in particular in the automotive industries. Also, the methodology should first be applied to relatively small projects to realize its strengths and weaknesses. Plus, Axiomatic Design is not, and should not be regarded as, the only design methodology. It provides a framework within which one can use its axioms, as well as other various design methodologies.

## Axiomatic Design

Professor Nam P. Suh at the Department of Mechanical Engineering at Massachusetts Institute of Technology (M.I.T.) developed Axiomatic Design (AD) as a design methodology to systematize the design process and to address the aforementioned weaknesses of traditional design practices. He defines design as an activity that involves the interplay between what the designer would like to achieve and how he/she satisfies this need.

In the Axiomatic Design methodology, there are four domains that drive the process including Customer domain, Functional domain, Physical domain, and Process domain, as shown in Figure 2 [1].

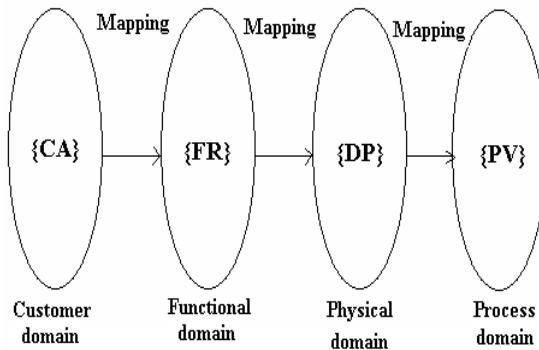


Figure 2. The four domains in AD

Customer's needs, called Customer Attributes (CA), are determined in the customer domain and then in the functional domain; these needs are specified as Functional Requirements (FRs) and Constraints (Cs). To satisfy the FRs, one needs to conceive Design Parameters (DPs) in the physical domain. Finally, Process Variables (PVs), describing the processes needed to fulfill the FRs, are developed in the process domain. Decisions regarding the appropriate design solution are made through a mapping process. These decisions are made on the premise that it should not violate the two fundamental axioms of AD, which are:

- The Independence Axiom: The independence of FRs must be maintained.
- The Information Axiom: The information content of the design must be minimized [1].

The first axiom maintains that the FRs must be set in such a way that each FR can be satisfied without affecting other FRs. The independence of FRs, however, does not necessarily mean physical independence.

The mapping process between the domains can be described mathematically. The functional requirements are considered as components of a vector that define the design goals, hence called a FR vector; similarly, DPs constitute the DP vector. The relationship between FR and DP vectors is shown in Equation 1:

$$\{FR\} = [A]\{DP\} \quad (1)$$

where, Matrix A is called the Design Matrix, whose elements are:

$$[A] = \begin{bmatrix} A_{11} & A_{12} & A_{13} \\ A_{21} & A_{22} & A_{23} \\ A_{31} & A_{32} & A_{33} \end{bmatrix} \quad (2)$$

Therefore, each FR is described in terms of the DPs as:

$$\begin{aligned} FR_1 &= A_{11}DP_1 + A_{12}DP_2 + A_{13}DP_3 \\ FR_2 &= A_{21}DP_1 + A_{22}DP_2 + A_{23}DP_3 \\ FR_3 &= A_{31}DP_1 + A_{32}DP_2 + A_{33}DP_3 \end{aligned} \quad (3)$$

The first axiom requires independence of the FRs. In order to satisfy this axiom, one should either have a diagonal or triangular design matrix as shown in Equations 4 and 5, respectively.

Diagonal matrix:

$$[A] = \begin{bmatrix} A_{11} & 0 & 0 \\ 0 & A_{22} & 0 \\ 0 & 0 & A_{33} \end{bmatrix} \quad (4)$$

Triangular Matrices:

$$[A] = \begin{bmatrix} A_{11} & 0 & 0 \\ A_{21} & A_{22} & 0 \\ A_{31} & A_{32} & A_{33} \end{bmatrix} \quad \text{or}$$

$$[A] = \begin{bmatrix} A_{11} & A_{12} & A_{13} \\ 0 & A_{22} & A_{23} \\ 0 & 0 & A_{33} \end{bmatrix} \quad (5)$$

If the design matrix is diagonal, the design is called uncoupled; if the design matrix is triangular, it is called decoupled. If the design matrix is none of these types, then the design is said to be coupled. In an ideal design, Suh [1] stated that, the design matrix is uncoupled, which means that each FR is satisfied independently from other FRs.

The information content is defined as the probability of satisfying a given FR; that is, the probability of satisfying FR<sub>i</sub> is P<sub>i</sub> [1]. Mathematically, this is defined by equations 6 and 7.

$$I_i = \log_2 \frac{1}{P_i} = -\log_2 P_i \quad (6)$$

The unit of the information content is a bit. If there are multiple FRs, then the total information content of the system, I<sub>sys</sub>, is:

$$I_{sys} = -\log_2 P_m \quad (m = \text{the number of FRs}) \quad (7)$$

where  $P_m$  indicates the joint probability that all FRs are satisfied when all of them are statistically independent:

$$P_m = \prod_{i=1}^m P_i \quad (8)$$

The second axiom implies that the design with the smallest information content is the best design because it requires the least amount of information to achieve the design goals.

Some scholars within academia have examined the application of AD and have reported its usefulness and impact on the understudied systems and designs in terms of cost and waste reduction [3]-[5]. However, there is a lack of formal study indicating the extent to which this methodology is used and practiced in industry. In addition, the literature review does not indicate existence of any study on what the AD users within the U.S. industry feel about this methodology.

## Literature Review

Axiomatic Design (AD) could be an appropriate tool to address the fast-changing nature of lean manufacturing systems [4]. According to Houshmand and Jamshidnezhad [4], identifying the factor(s) influencing implementing decisions of AD in industries would shed more light on the applicability of AD and/or identify technical problems and obstacles to implementing it in a particular industry.

AD has also been applied in the design of manufacturing systems [1], [4], integration of design-method software in Concurrent Engineering [6], developing e-commerce strategies [7], and machine control systems [8]. Moreover, AD has been implemented to provide a design method for lean production [5]. Nordlund, Tate, and Suh [3] stated that companies in Asia, Europe, and the U.S. have successfully trained their engineers in AD and started integrating AD into their product-development efforts. In their studies, they presented several case studies of applying AD in such areas as design process, business plan development, and analysis of reliability in wafer-processing equipment.

In the study conducted by Houshmand and Jamshidnezhad [4], an automotive body assembly was redesigned using AD methodology. Some of the improvements in the redesigned system reported were a 50% reduction in work-in-progress, decreased cycle time of the cell up to 20%, and increased flexibility.

Reynal and Cochran [5] studied assembly lines and machining of two manufacturing companies in order to implement the lean-manufacturing concept through the application

of AD. The first company, which was an assembly plant, was completely redesigned; of the results reported, there was more than a 50% reduction in cycle time of parts in the assembly process and space reduction of more than 40%. In the second company, the application of AD resulted in the reduction of the cycle time as well as cost-effective improvement.

Liu and Soderborg [9] presented the application of AD to a Noise, Vibration, and Harshness (NVH) problem in the automotive industry; a major attribute observed in a vehicle's design and analysis involved such quantities as sound pressure (noise), steering wheel vibration (vibration), and discomfort due to rough road conditions (harshness). They developed a design matrix to identify the relationship between FRs and DPs to rearrange the matrix with the aim of decoupling the matrix as much as possible. They concluded that the resulting matrix could provide a clear strategy for tuning the design to meet the intended FRs.

## The Study

Although the literature provided individual studies carried out using AD, the extent to which AD is used in industry was not fully evident. Neither was it clear which factors affect its implementation. Hence, the current case study was conducted with the intent of addressing the following questions:

1. To what extent is Axiomatic Design (AD) practiced in U.S. companies involved with engineering design practices?
2. What advantages/disadvantages have been realized through the use of AD?
3. What factors influenced the implementation/non-implementation of AD in these companies?
4. What inferences and recommendations can be identified for the implementation of AD?

This was accomplished by identifying and interviewing appropriate professionals in industry.

## Methodology

Initially, the U.S. automotive companies from which the sample would be drawn were chosen as the population, i.e., automotive companies involved with engineering design practices. This list of companies was obtained from the Automotive Engineering International's Worldwide Automotive Supplier Directory available to the members of the Society of Automotive Engineers (SAE) [10].

One of the categories in the directory is engineering design, which has two sub-categories including engineering design and engineering design services. A search in this category revealed a total of 93 companies in the U.S.

All of these companies were contacted to see whether they were familiar with AD. The result indicated that the majority were unaware of AD. Therefore, it was decided to broaden the scope of the study to include non-automotive, yet transportation-related companies, and to conduct the study in those companies that utilized AD in their practices. The method used to identify companies that possibly used AD was to look at the clients of the AD software provider, Axiomatic Design, Inc. This resulted in identifying five companies of which four were willing to participate in the study. Three of these companies were large corporations and one company provided consulting in engineering designs to large companies.

Per contact with these companies, hereafter referred to as companies A, B, C, and D, five individuals, who held either managerial or design supervisory positions in these companies, were identified. The initial contacts with each of the interviewees indicated that they were aware of the current design practices and methodologies performed and used by their engineers in their departments. These individuals are hereafter referred to as *P1*, *P2*, *P3*, *P4*, and *P5*. A questionnaire, shown in Appendix A, was then designed to elicit the desired information. Using this questionnaire, these individuals were interviewed by telephone, the duration of which ranged from 45 minutes to 2 hours. Although the questions on the questionnaire were asked, the interview was conducted in a conversational mode so that additional questions could be asked depending upon the answers given. This was done to gain a deeper understanding of the situation in that company. All conversations were recorded.

Participants *P2* and *P3* both belonged to Company B. Figure 3 includes the types of the selected companies and the interviewees' job titles.

## Results and discussion

An example of the responses to the survey questions is shown, in summary form, in Appendix B. The analysis of the conversations indicated that AD had been introduced and used only partially in the companies under study. It had not been fully used in any of the companies. In most cases, AD had been used just as a tool that was suggested to the designers along with other methodologies.

Company		Interviewee	
Label	Types of Business	Label	Position
A	Aerospace	P1	Program Director
B	Automotive	P2	Reliability Engineer
		P3	Researcher
C	Electronics, Transportation components	P4	Manager
D	Supplier training	P5	Consultant

**Figure 3. The backgrounds of the companies and the interviewees**

Hence, the designers were free to use any methodology they deemed appropriate. All five participants mentioned that the application of AD had been case-based. They started implementing AD, in the words of one of the respondents, in some 'toy' projects for initial learning and later on, in a few cases, they began using the methodology. Nonetheless, the results show that overall AD is not fully implemented in any of these companies.

The results also show that one of the major advantages of AD is that it provides a theoretical base for design. Therefore, it helps to have the designers think objectively about their designs. Even when not used fully, evidence suggests that AD was recognized as a powerful evaluation tool for existing designs. Designers can diagnose the coupled designs and decouple them. The design-matrix notion was found to be a useful tool in this regard.

It seems that AD is more useful to a company that designs components than to a company that designs systems due to the inherent project complexity. Moreover, if there are products being developed from scratch, their use would be beneficial. Evidence suggests that the major disadvantages of AD are difficulties in its usage, especially for complex systems and its inability to provide examples of solutions, as mentioned by *P5* at Company D.

Almost all of the participants agreed that AD is a useful methodology to be used by the designers regardless of the size of the design project. They supported the implementation and/or the introduction of the methodology in design activities. Nonetheless, based on the data obtained from the interviews, the following are among the most referred issues brought up by the interviewees in regard to implementing AD:

- Cultural change in organizations
- Training costs
- Difficulty in implementation of the methodology where there are multi-FR projects
- Size of the design project in terms of the number of FRs and complexity
- The opinions of the customers involved in the projects

One of the main reasons for paucity of use of AD in industry is the sheer difficulty of the methodology. It is a theoretical technique and there is some evidence that it is difficult for most designers to fully comprehend. Also, learning the methodology is very time-consuming and it may not be possible for companies to invest time to train their designers.

The most important obstacle in implementation of any new methodology is the cultural resistance of the organization. The organizations contacted as well as their customers were familiar with and used traditional methodologies such as Design for Manufacturing and Assembly (DFMA), Robust Design, etc. As indicated by some of the interviewees, people who are not used to the new methodology are more likely to resist. This was also found to be true in this case, i.e., resistance to change, especially with AD, which is not widely known in industry. One can speculate that a reason for the unfamiliarity may be due to its absence in colleges' design curricula, as mentioned by one of the interviewees.

The methodology also does not provide examples or mechanisms to find innovative solutions, such those found in the Theory of Inventive Problem Solving (TRIZ) methodology. It is also cumbersome to use, especially for large complex projects. Hence, in the words of one of the interviewees, it does not become a "winner" when competing for its use with other methodologies in the environment, as stated earlier, where designers are free to select any methodology. On the positive side, evidence shows that the methodology being theoretical is useful in design evaluation. Hence, results show that individual designers use it for this purpose.

The organizational factors also influence the lack of acceptance of AD methodology. Contemporary industry uses the culture of collaboration among teams and supply chain members, i.e., the vendors and customers in all phases of design and manufacture. So, as mentioned above, in some cases it becomes difficult to implement new theoretic methodologies such as AD.

The results of the study also showed that Axiomatic Design is a methodology that is recommended to be used along with other methodologies. For example, a combination of AD and Robust Design is useful, as mentioned by one of the interviewees. The application of AD depends on the com-

plexity of the design project or, more specifically, the number of FRs. The company should not mandate or emphasize any one design methodology, AD included.

The first question in implementing the methodology is how and to what degree AD would help the company in its product-design endeavor. There must be a clear understanding of the company's customers, marketplace, and resources available to invest. It is recommended that companies first start implementing AD in simple projects, i.e., with few FRs, to see whether any quality improvement and time and cost reduction would be realized. Then, based on the available budget, they should select the appropriate training to introduce AD. As the results of the study indicate, if there are several design groups and/or too many designers need to be trained, the recommended training method would be in-house workshops. Regardless, the training cost is an important factor and its choice depends on a company's budget and available resources.

The collaboration among various companies and their individual preferences in terms of the methodology can be a problem. In such cases, it is critical to have an agreement on the design methodologies used. Selecting a design methodology that may not be familiar to other companies can cause misunderstanding and miscommunication, which could increase cost, as was mentioned by P1 at Company A.

The role of management in supporting the methodology's implementation is crucial. One needs to obtain their support to introduce the methodology. As one of the interviewees mentioned, "I think you need a management champion who believes strongly in the methodology." Another participant stated that the managers would be interested in seeing what improvements in terms of cost and cycle time one can achieve by implementing any methodology. He believed that the managers would not care what methodology one may use as long as the methodology is cost-effective and beneficial. However, the designers should be interested in trying and/or using the new methodology.

## Further Discussion

Often there is commercial software available for implementing different design methodologies. AD is no exception. As stated earlier, Axiomatic Design, Inc. is a provider of the software, called Acclaro. All interviewees were either familiar with this Axiomatic Design software or had used it at some point. Yet, they had used other software such as MS Excel and MATLAB. The interviewees believed that Acclaro was helpful in implementing AD; yet, the version of the software the interviewees were familiar with was not fully capable of handling designs with many FRs. They be-

lieved, however, that recent versions of the software would perhaps address this issue. The website of Axiomatic Design claims that one of their software packages, called Acclaro DFSS, is capable of “Implementing Axiomatic Design Quality framework with the DFSS quality processes of VOC, QFD, FMEA, TRIZ, DSM, Pugh concept analysis, and more” [11]. Therefore, it seems that the new version of the software includes more features and design tools and one can use it to help with design projects. Nonetheless, one still needs to examine this new version to assess its capabilities in handling multi-FR designs as claimed by the software company.

## Concluding Remarks

In summary, by definition, Axiomatic Design provides guidelines for designers to ensure that the design contents would meet design requirements. The designer can gauge the design in hopes of meeting the functional requirements using various axioms and corollaries, particularly the Independence and the Information axioms. AD encompasses any design activity in any context such as manufacturing, software development, and so on. Nonetheless, it seems that AD is not known widely in the U.S. Industrial sectors studied here, although the literature review indicated the implementation of the methodology in a few industries.

Some of the interviewees mentioned that the designers did not seem to learn about AD as a part of their educational background. This would result in lack of familiarity with AD and so could be one reason for its limited use in industry. Yet, the impact of the designer’s educational background on the expansion of AD in industry seems to be unknown and was not within the scope of the current study. Perhaps a combination of AD and TRIZ might provide a broader framework for design practices; however, one needs to study how these methodologies can be used together to provide such a framework. The other main reason for the lack of widespread use of AD is the organizational and cultural factors.

## Appendix A

1. Please explain about your position and the number of years that you have with your company, and your work experience in the current and previous company (ies). What other positions/jobs have you held with current and prior company (ies)?
2. In what context do you use AD? (I.e. product design and development, process design, product/process redesign, mechanical design process, etc.).

3. Do you utilize any other design methodologies?
4. How did you initially learn about AD?
5. Were you involved with the introduction of AD in your workplace(s) (i.e. departments, divisions)?
6. What was the strategy that you used to introduce and implement AD? How long did it take?
7. What is your perception of what the AD users think about utilizing it at your company?
8. Has the number of the AD users in your organization increased/decreased? Why?
9. Was the decision on implementing AD an internal decision (by you or your department) or by the top management? In either case, what do you think about the management support in this regard?
10. In terms of the method of implementation, what methodology and/or strategy do you recommend to introduce AD in an organization?
11. Do you recommend AD to be used?
12. If so, do you recommend to use only AD or in combination with other methodologies?
13. To whom and for what type of design do you recommend AD? What about cost or ROI?
14. Do you implement any AD software? If so, is it commercial?
15. In your opinion, what are the positive and negative aspects of AD, in terms of
  - Methodology?
  - Implementation?
16. Overall, please describe your experience and perspective regarding AD and its implementation, advantages, and disadvantages.

## Appendix B

Some example responses from the Interview with P4 of Company C:

### Questions and responses regarding the extent to which Axiomatic Design practiced in the U.S.

#### **In what context do you use AD?**

It is a part of DFSS curriculum at the company. AD is used in the concept development phase within DFSS. It is used in product design to realize where coupling occurs.

#### **Do you utilize any other design methodologies?**

DFSS, Pugh analysis, Taguchi method.

---

**Has the number of the AD users in your organization increased/decreased? Why?**

AD is used in the division but not in all others. Nothing specific observed, though there would be a resistance when introducing a new idea/concept but when people see the benefit, they would not object.

**Questions related to advantages/disadvantages that have been realized through the usage of AD.**

**In your opinion, what are the positive and negative aspects of AD, in terms of: Methodology and Implementation?**

If one tries to improve design without fundamentally changing the concept, then AD is a difficult tool to use. However, if there is room for innovation and concept modification, then AD is very powerful.

**Overall, please describe your experience and perspective regarding Axiomatic Design and its implementation, advantages, and disadvantages.**

When developing highest FR, one should not have more than five or six FRs. Sometimes designers confuse FRs with constraints. Also, for the implementation of AD, one needs to have a person with authority.

**Questions and responses related to factors influencing the implementation/non-implementation of AD.**

**What is your perception of what the AD users think about utilizing it at your company?**

There were almost no complaints about the methodology at the division. The implementation was successful.

**Do you implement any AD software? If so, is it commercial?**

Yes, Acclaro is the software used.

**How did you initially learn about AD?**

Through self-inquiry and workshop.

**Were you involved with the introduction of AD in your workplace?**

Yes

**Questions related to inferences and recommendations for implementation of AD.**

**What was the strategy that you used to introduce and implement AD?**

Nam Suh was invited to give a talk to chief engineers. Then, an in-house workshop was conducted to introduce AD to the engineers.

**Was the decision on implementing AD an internal decision (by you or your department) or by the top management?**

Yes, it was an internal decision.

**What methodology and/or strategy do you recommend to introduce AD in an organization?**

In-house workshop.

## References

- [1] Suh, N. P. (2001). *Axiomatic design: Advances and applications*. Oxford, NY: Oxford University Press.
- [2] Singh, N. (1996). *Systems approach to computer-integrated design and manufacturing*. New York: John Wiley & Sons.
- [3] Nordlund, M., Tate, D., & Suh, N. P. (1996). Growth of axiomatic design through industrial practices. *3<sup>rd</sup> CIRP Workshop on Design and the Implementation of Intelligent Manufacturing Systems*. Tokyo, Japan, June 19-21. pp. 77-83.
- [4] Houshmand, M., & Jamshidnezhad, B. (n.d.). *Redesigning of an automotive body assembly line through an axiomatic design approach*. Retrieved February 28, 2005, from [http://www.mmd.eng.cam.ac.uk/mcn/pdf\\_files/part8\\_2.pdf](http://www.mmd.eng.cam.ac.uk/mcn/pdf_files/part8_2.pdf).
- [5] Reynal, V. A., & Cochran, D. S. (1996). *Understanding lean manufacturing according to axiomatic design principles*. Retrieved February 28, 2005, from [https://hpds1.mit.edu/retrieve/952/RP960728Reynal\\_Cochran.pdf](https://hpds1.mit.edu/retrieve/952/RP960728Reynal_Cochran.pdf).
- [6] Chen, K. (1998). Integration of design method software for concurrent engineering using axiomatic design. *Integrated Manufacturing Systems*, 9(4). 242-252.
- [7] Martin, S. B., & Kar, A. K. (2001). *Developing e-commerce strategies based on axiomatic design*. Retrieved February 10, 2005, from <http://ecommerce.mit.edu/papers/ERF/ERF140.pdf#search=axiomatic%20design%20advantages>.
- [8] Lee, K.D., Suh, N.P., Oh, J-H. (2001), "Axiomatic design of machine control system", *Annals of the CIRP*, 50 (1), pp.109-114Liu, X., & Soderborg, N.

---

(2000). *Improving an existing design based on axiomatic design principles*. Proceedings of ICAD 2000Liu, X., & Soderborg, N. (2000). *Improving an existing design based on axiomatic design principles*. Proceedings of ICAD 2000.

[9] Liu, X., & Soderborg, N. (2000). *Improving an existing design based on axiomatic design principles*. Proceedings of ICAD 2000.

[10] SAE International (2005). *Worldwide automotive supplier directory online*. Retrieved June 5, 2005 , from <http://www.sae.org/wwsd/>.

[11] Acclaro DFSS Overview (n.d.). Retrieved March 10, 2005, from <http://www.dfss-software.com/default.asp>.

## Biographies

**DR. ALI ALAVIZADEH** received his Ph.D. from Indiana State University in Technology Management. He has worked in various domestic and international companies, holding positions including software system developer, and systems coordinator. He is currently teaching at The George Washington University in the Department of Engineering Management and Systems Engineering. His areas of expertise include engineering design methodologies, systems engineering, enterprise architecture and integration, and systems modeling and simulation. Dr. Alavizadeh may be reached at ali.r.alavi@gmail.com.

**DR. SUDERSHAN JETLEY** is an Associate Professor in the College of Technology at Bowling Green State University. He received his Ph.D. from the University of Birmingham. He has taught and supervised graduate and undergraduate students in the areas of statics, materials, automation, quality, GD & T, research methods, and manufacturing processes. Author of numerous articles, his research interests include rapid prototyping, machining, neural network applications, and machine vision. Dr. Sudershan Jetley may be reached at [sjetley@bgsu.edu](mailto:sjetley@bgsu.edu)

## Acknowledgments

The Authors are thankful to Bowling Green State University for the support provided for this study and its publication. The authors are also thankful to IJME for support in the development of this document.

# FEASIBILITY STUDY FOR REPLACING ASYNCHRONOUS GENERATORS WITH SYNCHRONOUS GENERATORS IN WIND-FARM POWER STATIONS

Mohammad Taghi Ameli, Power and Water University of Technology (PWUT);  
Amin Mirzaie, Power and Water University of Technology (PWUT); Saeid Moslehpoour, University of Hartford

## Abstract

Because of the global energy crisis, the unpredictability of the non-ending price fluctuations of fossil fuels and the complexities of construction and maintenance of nuclear power plants, wind energy and utilization of wind farms has gained an increasing importance and interest. Several wind farms are being utilized, the most important of which is the example farm power-station. In this power station, all units have induction generators with gearboxes of various power capacities. In this study, the authors

1. compared synchronous and asynchronous generators of wind farms from the viewpoints of capacity, speed, excitation, independent operation, voltage regulation, power coefficient control, paralleling with electrical power network, impact on the electrical power network during paralleling, cost and power coefficient; and,
2. studied the feasibility of replacing synchronous generators with synchronous generators, particularly the ones with no gearbox, on a test farm.

Of the four generator types—squirrel-cage induction, synchronous with permanent magnet, induction with wound rotor, and synchronous with wired field—the squirrel-cage induction and synchronous with permanent magnet types offer the best advantages to wind-farm power plants. Comparing these two, the synchronous generator with permanent magnet was found to be significantly superior to the squirrel-cage induction generator in terms of higher power coefficient and higher efficiency. Furthermore, it does not require power storage. This study evaluated the replacement options for a test farm as a model power station and reviewed the various major brands of equipment on the global market.

## Introduction

A wind-farm power plant generally includes the following:

1. Wind turbine and subassemblies
2. Generators of electrical power
3. Transformers
4. Load regulators for the power plant, independent of the power network

5. Other components such as voltage and frequency regulators, and regulators of mechanical components (brake, direction etc.)

Wind turbines that were originally designed for use in rural areas were directly connected to generators; that is, the generator and turbine had the same revolutions per minute (RPM). In modern systems, the turbine is connected to the generator via a gearbox that allows variable generator speeds, up to four or five times the speed of the turbine, or more in some cases. For example, if the turbine rotates at 100rpm, the generator can have a speed of 400rpm. While this reduces the generating cost, it increases the weight (and costs) of the wind converter and its tower, and has one-time procurement and annual maintenance costs associated with the gearbox. In comparison to light-weight systems, heavier wind converters cause further difficulties in crane hauling and installation on the tower top. One of the advantages of direct connection of the turbine and the generator is elimination of the gearbox and its maintenance requirements.

In wind turbines, its blades and the generator are generally designed for mounting on top of the tower. A power transmission shaft can be used to have the generator installed at ground level. Wind-farm generators can produce direct or alternating currents. The frequency of the alternating current produced by AC generators is directly proportional to the rotational speed (RPM) of the turbine, and is required to be fixed at 60Hz in the U.S. and 50Hz elsewhere.

For small wind-farm power stations, the cost of a mechanism for keeping the RPMs at a constant level may be prohibitive. Synchronous generators output AC power but are required to meet voltage and frequency standards. This requirement further complicates the design of the turbine blades to operate under varying wind velocities. Today's technology provides generators that are electronically regulated to produce electricity with a constant frequency under variable wind conditions. Through a different method, the generator produces DC current that an inverter converts to AC. In a widely-used method, the generator's DC output is extracted via brushes that contact the commutator of the generator. In yet another method, the generator's AC output is converted to DC via a diode, hence brushes and commutator rings are not used.

---

## Characteristics of an Optimal Generator for Wind-Farm Power Plants

In a wind-farm power plant, the input energy has no sustainable trend, and its variation is dependent on the wind velocity, that is, both direction and speed of the wind. The regulation of these variations for optimizing the power generator's input couple is achieved by changing the blades' pitch angle, gearbox, etc. Therefore, additional equipment is needed to ensure the constancy of the desired characteristics of the output power in changing wind velocities, adding to the weight of the cost factor. In other words, the generator's higher sensitivity to wind variations and resulting effects (tensions) add to the overall cost of the system. Selection of an optimal wind-farm generator requires the following considerations:

1. The generator should be as simple as possible, while tolerating the electromechanical tensions;
2. It should be capable of operating within a wider range of variations;
3. Maximum controllability of the voltage and frequency should be a built-in characteristic of the generator itself;
4. Control systems should be minimally necessary and sufficient and economically justifiable;
5. Minimum requirements for maintenance are needed to be installed at a high altitude; and,
6. Maximum generating power [1].

Based on the previous studies on induction and synchronous AC generators, these kinds of generators are highly suitable for wind-farm power plants.

## Comparison of Characteristics of Synchronous and Asynchronous Generators

Both synchronous and asynchronous generators are suitable for wind-farm power plants. However, before selecting a generator, it is mandatory to study the operation of the generator and the status of the host power network of which the generator will be a component. Following is a comparison of the characteristics of each type of generator, with a view of the case that the asynchronous generator is connected to the power network [2].

- Capacity: Synchronous generators are suitable for high capacities, while asynchronous ones that consume more reactive power are suitable for smaller capacities.

- Speed: Higher speeds create no problems other than difficulties in manufacturing synchronous generators with large capacities.
- Excitation: Electrical excitation of synchronous generators requires coils for exciting field, whereas asynchronous ones do not need any coils for excitation because the necessary power for excitation of the armature coils can be drawn from the power network. Synchronous generators with permanent magnets are also free from exciting coils.
- Independent Operation: Synchronous generators can be utilized independently, while the operations of asynchronous ones need to be fed with an exciting current from the power network.
- Voltage Regulation: The output voltage of synchronous generator terminals can be regulated but the voltage of asynchronous generators is always the same as the voltage of the power network.
- Power Factor Control: In synchronous generators, the power factor of the front and rear phases and the reactive power can be controlled. Asynchronous generators work with the power factor of the rear phase and a condenser is required for any correction of the power factor.
- Paralleling With The Power Network: For synchronous generators, this is a complex control that requires regulation of the voltage, frequency and phase. For asynchronous generators, however, the control is simpler as paralleling is done only at the synch speed.
- Impact on the Power Network during Paralleling: For synchronous generators, no impact is generated during connection to the network, but some additional currents will flow in asynchronous generators that produce no voltage before connection to the network necessitating consideration of any drop in the network.
- Cost: The Synchronous generators with an electrical exciter are more expensive than asynchronous ones, but below 750kw, synchronous generators with permanent magnets are less expensive than their asynchronous equivalents. For systems above 750kw, the price is slightly higher but, with respect to other advantages, their use may find long-term economical justification. Another point to be considered is that low-speed asynchronous generators are generally expensive.
- Power Coefficient: The standard power factor of synchronous generators is 90% of the front phase; for induction generators, the power factor is determined by the wind within 5% to 90% of the rear phase.

Winds can be classified into regular and seasonal types [3]. On our test farm, the wind is a local, strong wind that blows southward from noon to midnight. In this paper, the test wind-power plant was used for comparison and a test case for evaluation of the advantages of synchronous generators over asynchronous ones. The first wind turbines with 500kw power and 37m rotor diameter were installed and commissioned in December, 1994. After ten years, the number of units rose to 50. A new contract has recently been signed for installation of twenty, 660kw units. Specifications of the units are presented in Table 1.

**Table 1. Technical Specifications of the New Units**

Generator Type	Asynchronous. With Gearbox
Rotor Diameter	4 m
Lower Cutting Speed of the Wind	4 m/s
Upper Cutting Speed of the Wind	25 m/s
Nominal Speed of the Wind	15 m/s
Nominal Power of the Generator	660 kw
Number of Blades	3

Figures 1 and 2 show the trend for installation and capacity expansion from 1995 to 2004.

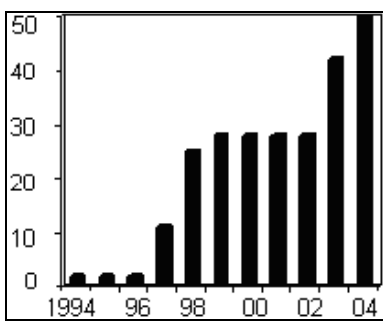


**Figure 1. Installed units**

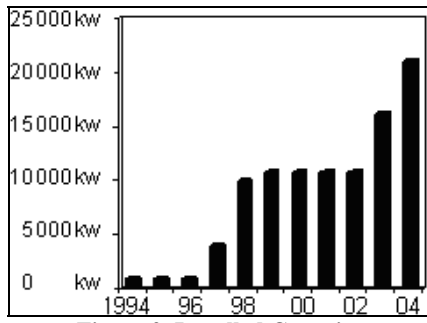


**Figure 2. Installed Capacity**

On the basis of the above discussion and the general global trend toward synchronous generators, it seems that for wind-farm power plants, synchronous generators with permanent magnets are superior to electrically excited asynchronous ones. This idea is verified by analyzing global

trends. All of the existing 50 generators, and even the 20 new ones, are of the induction type and have gearboxes. A survey of maintenance reports clearly indicates that a major part of the maintenance work-load is attributable to breakdowns and faults of the gearboxes.

A comparison of the generators with and without gearboxes shows that those with no gearbox have a larger diameter, shorter length, are approximately of equal weight, and slightly higher price [4]. Currently, the 1,000kw and 3,000kw generators with permanent magnets are available on the international market. In July, 2004, Mitsubishi started operation of the first unit of its wind-farm power plant that utilized a synchronous generator with permanent magnets and no gearbox. It is interesting to note that it has a higher reliability and a lower initial cost. It is also significant that both the technical specifications of this generator and the wind characteristics suitably correspond to requirements and climatic conditions. Besides, the lower cutting speed of the wind for this generator is 2.5m/s, while the existing ones have a lower cutting speed of 4m/s. Table 2 summaries the characteristics of this generator.

**Table 2. Specifications of Mitsubishi Generator in Japan**

Generator Type	Synchronous Permanent Magnet without Gearbox
Nominal Power	300 kw
Rotor Diameter	30 m
Lower Cutting Speed of Wind	2.5 m/s
Nominal Speed of the Wind	14 m/s
Upper Cutting Speed of Wind	25 m/s

Obviously, this is only one of many choices. Previously, the synchronous generators were disadvantaged in economic terms and initial costs. Today, the permanent magnet synchronous generators with no gearbox in the capacity range of 300-600kw and above 750kw have an initial cost that is only slightly more than the cost of induction generators. In the following, the feasibility of replacing induction generators with multi-pole permanent-magnet synchronous generators is discussed from six different aspects, the first five of which are related to the 20 new generators that are going to be installed in the near future.

- A. Initial Cost
- B. Efficiency
- C. Required surface area
- D. Maintenance cost
- E. Savings in generating power

## A – Initial Cost

The initial cost of a 600kw induction generator with gearbox (Table 2 above) is \$263,000 compared to \$223,000 for Model A of a permanent-magnet synchronous generator with a nominal power of 750kw. The price of a 1.5Mw Enercon Wind synchronous generator with a permanent magnet was quoted at \$577,000. At first glance, this initial cost is twice that of the currently-selected generators, but any comprehensive analysis and comparison needs to consider other factors like efficiency, maintenance costs, reliability, costs of reactive power and, last but not least, the step size for expansion of the total output power. Therefore, in order to upgrade reliability and full utilization of wind energy, the above comparisons are no more than an illustrative example. Despite differences in the price of the gearbox or generator from one vendor to another, one can reliably assume that, currently, the price of any permanent-magnet synchronous generator with up to 750kw of power is below the price of an equivalent asynchronous generator. Figure 3 is a chart of the initial cost [5]-[7].

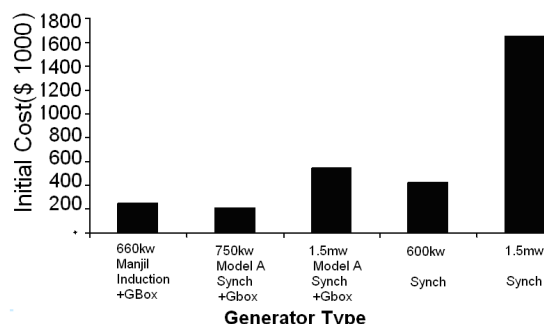


Figure 3. Initial Cost Comparison

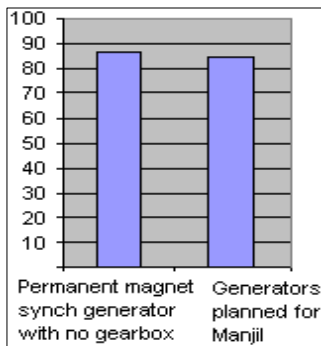


Figure 4. Efficiency

## B – Efficiency

The efficiency of an average permanent-magnet synchronous generator with no gearbox is 86.6%, while the effi-

ciency of the 20 variable-speed generators with gearbox induction (planned) is 84.3% (see Figure 4).

## C – Maintenance Cost

A major component of maintenance costs comes from the gearboxes. All 20 planned generators will have a gearbox, while a quick review of the product catalogs of various international manufacturers and vendors indicates that the maintenance cost of permanent-magnet synchronous generators with no gearbox is half the cost of equivalent induction generators that include gearboxes; this amounts to a large savings in maintenance costs and another considerable saving by elimination of costly shut-downs due to gearbox breakdown [6].

## D – Gain of Generating Power

The following discussion is based on the generator's efficiency. Since 20 units of 660kw will be installed, the total output power will be 13,200kw. Due to the efficiency of the variable-speed gearbox-type induction generators, the effective output of these 20 units will be 11,127.6kw. Permanent-magnet synchronous generators with no gearbox, with equal nominal output power, will yield 11,431.2kw; thus, a gain of 300kw is within reach. If all units are replaced, the gain will be considerable.

## E – Surface Area

Following is a discussion of replacing generators with respect to surface area. The diameter of the rotor determines the distance between wind units. Assuming that the 20 units with 4-meter rotor diameters are installed in four rows and five columns, the allowable distance between units, then, is 150 meters. Table 3 shows the technical specifications of an 800kw generator, model E-48.

Table 3. Specifications of an 800kw Generator, model E-48

Generator Type	Synchronous no gearbox
Nominal Power	800 kw
Rotor Diameter	48 meter
Lower Cutting Speed of the wind	3 m/s
Nominal Wind Speed	13 m/s
Upper Cutting Speed of the Wind	28 m/s

A quick calculation indicates that the surface area for the above installation is 675,000m<sup>2</sup>. Since the rotor diameter for 800kw generators is approximately equal to 1 rotor diameter

of the units, then in the same area of  $675,000\text{m}^2$ , 20 units of 800kw generators can be installed that will result in several advantages:

- The initial costs of the new units would be approximately equal to that of the planned ones.
- The total output power will increase from 13.2Mw to 16Mw, a gain of 2.8Mw.
- The new synchronous generators will be free from gearbox maintenance costs, provide higher efficiency and higher reliability, generate no reactive power, and allow larger expansion steps, as discussed earlier.

The replacement of the planned generators with the 2Mw ones will further accentuate the gains (see Table 4) [8].

## F – Analysis of Replacement with Identical Output Power

If the 20 units are replaced with units that have power outputs of 2Mw, then only 10 units need to be installed; whereas, if replacement is made with 660kw units, 30 units would need to be installed. Thus, there will be no significant advantages and plenty of disadvantages in terms of maintenance cost, reliability, efficiency and output power index. Besides, the use of induction generators would require capacitors for reactive power, further increasing costs.

**Table 4. Technical Specifications of the 2Mw Generator**

Nominal Power	2,000 kw
Lower Cutting Speed of the Wind	2.5 m/s
Nominal Wind Speed	13 m/s
Upper Cutting Speed of the wind	20-25 m/s
Generator Type	Synchronous Permanent Magnet without gearbox
Tower Height	60 meters

On January 24th, 2004, this generator began its operation in Japan. Despite the slightly higher initial cost of a permanent-magnet synchronous generator with no gearbox, its numerous advantages make it economically advantageous. Currently, the total installed capacity of the farm, excluding the 20 units that are planned and other expansion plans, is 20,980kw or approximately 21Mw. This consists of 18 units of 550kw, two units of 500kw, 27 units of 300kw, and three units of 6,660kw. Only ten units of the proposed generator can replace the existing 50 units. One proposed unit can replace seven units of 300kw, thereby reducing the maintenance costs.

The present configuration has an output power of 17,203.6kw at an optimistic efficiency of 82%. Using the permanent-magnet synchronous generators that have an efficiency of 86.6%, the output power will increase to 18,168.7kw, yielding a gain of 965kw, nearly a 1Mw increase in capacity. Additionally, the system will be reactive-power-free and not have related capacitor banks. The squirrel-cage generators, with connection to the power network, have a lower power index. Their maintenance costs is  $t$  times that of the generators with no gearbox. In summary, the use of permanent-magnet synchronous generators of 1Mw and above is both economically and operationally advantageous, and also why global trends support their use.

## Summary and Proposals

This paper considered the power generation of a test farm as a case study, but its conclusions seem to be valid for all wind farm-power stations around the world. Among the squirrel-cage induction generators, induction generators with a coiled rotor, synchronous with a coiled field and synchronous with a permanent magnet, two types are more advantageous for wind farms: the squirrel-cage and permanent-magnet types. The test farm utilized the squirrel-cage type, while the permanent-magnet type had higher advantages, including a higher-power coefficient and efficiency, and elimination of capacitor banks.

Table 5 summarizes the previous discussions about the various generators in the wind farms. Consequently, the following proposals are presented:

- For capacities of up to 750kw, due to lower initial costs, replacement of the induction generators with synchronous generators seems logical.
- Above 1Mw, despite the slightly higher initial costs, the use of synchronous generators seems economically justifiable.
- Since the wind turbines have a 20-year life, it seems advisable to replace the units that are older than ten years, and consider synchronous generators for new installations.

## References

- [1] Khosh Sowlat, A.H.; "Optimal Selection of Wind Farm Power Generators"; Power and Water University of Technology, May 1997.
- [2] J. Kean; "Electrical Aspects of Wind Turbines". March 1998.

**Table 5. Comparison of the Various Generators for Variable Speed Turbines** ✓: Advantage ✗: Disadvantage

Squirrel-cage Induction	Induction with coiled rotor	Synchronous with coiled field	Synchronous with Per- manent Magnet
✓ Simple and Robust	✗ Complex Structure	✗ Complex Structure	✓ Simple and Robust
✓ Reliable	✗ Slipping rings for DFIG	✗ Slipping Rings	✓ Reliable
✓ No Slipping Rings	✓ No Slipping Rings for BDFG	✗ Regular Maintenance	✓ No Slipping Rings
✓ Low Maintenance	High Cost	✗ High Cost	✓ Low Maintenance
✓ Low Cost	✗ Large and Heavy	✗ Large and Heavy	✓ Low Cost
✗ Low efficiency	✓ High efficiency with DFIG	✓ High efficiency in a wide range of load	✓ Small and lightweight
✗ Low power coefficient	✗ Low power coefficient	✓ High power coefficient	✓ High power coefficient
✗ Narrow speed range	✓ wide speed range	✓ wide speed range	✗ Narrow speed range
✓ Flat Torque	✗ Wavy Torque	✓ Wide-range torque	
		✓ Flat Torque	
Control and Regulation			
		✓ No need for Capacitors	
✗ Needs Capacitors	✗ Needs Capacitors	✓ Ease of Voltage Control	✓ No need for Capacitors
✗ Complex Voltage Con- trol with static generator	✗ Complex Voltage Con- trol with static generator	✓ Quick Torque Control	
✗ VAR or Capacitor	✗ VAR or Capacitor	✓ Easy control of Power Coefficient and reactive power	
✓ Stable operation in Unstable conditions	✓ Can be used as starter Motor		
✓ Can be used as starter Motor		✓ Can be used as recovery break	
Inverter Requirements			
✗ Large Scale Inverter	✓ Inverters for 25% to 50% of nominal power	✗ Large Scale Inverter	✗ Large Scale Inverter
✓ One controlling inverter	✗ Two controlling invert- ers	✓ One controlling inverter	✓ One controlling inverter
✓ Simple inverter control	✗ Complex inverter con- trol	✓ Simple inverter control	✓ Simple inverter control
1 rectifier + 1 inverter		1 field controller + 1 inverter	1 Rectifier + 1 inverter

---

- [3] Aminian, H. and Rezaei, M.H.; *"A Survey of Using New Energies in Iran"*; Power and Water University of Technology March 1993.
- [4] Fathiyah, Mellott, Panagoda; *"Windmill Design Optimization Through Component Costing"*; IEEE Seminar London July 2000.
- [5] E. Spooner; *"Case study-Direct Drive Wind Turbine Generators"*; IEEE seminar London, July 2000.
- [6] Winwind catalogue
- [7] C.Veganzones N.Fransisco Blazquez, D.Ramirez; *"Guidelines for the Design and Control of Electrical Generator System for new Grid Connected Wind Turbine Generators"*, E.T.S Engineers Industrials. June 2004.
- [8] [www.enercon.de](http://www.enercon.de)

## Biographies

**MOHAMMAD T. AMELI** received his BS in Electrical Engineering from the Technical College of Osnabrueck in Germany 1988. His Msc & PhD from Technical University of Berlin in Germany 1992 &1997. Since then he taught and conducted research as an Assistant Professor in the EE Dept of Power & Water University of Technology. He was general director of areas of research: Power system Simulation, Operation, Planning & Control of power system.

**SAEID MOSLEHPOUR** is an Assistant Professor in the Electrical and Computer Engineering Department in the College of Engineering, Technology, and Architecture at the University of Hartford. He holds his PhD (1993) from Iowa State University and Bachelor of Science, Master of Science (1990), and Education Specialist (1992) degrees from the University of Central Missouri. His research interests include logic design, CPLDs, FPGAs, electronic system testing and distance learning.

**AMIN MIRZAIE** received his Master of Science in Electrical Engineering from The Power & Water University of Technology.

# A SURVEY ON ADMISSION-CONTROL SCHEMES AND SCHEDULING ALGORITHMS

Masaru Okuda, Murray State University

## Abstract

There has been a sustained interest among researchers and network operators in providing quality of service (QoS) over the Internet. As an essential tool for supporting QoS, development of effective and scalable admission control is an important topic of research. Over the years, various admission-control schemes have been proposed that claim to scale well in a network environment where the network core is kept relatively simple and processing burdens are pushed to the edges of the network. This study surveyed selected admission-control schemes of this type. The contribution of this study is an introduction of new classifications of admission-control schemes, which is based on locations where the key admission-control mechanisms are implemented in a network. The survey of the literature was conducted in light of location-based classification of admission controls and details the workings of schemes, discusses their contributions, and identifies areas of further development.

## Introduction

Admission control is a process through which a network node determines whether to accept a new flow request or deny it. It is a traffic management tool through which the load on a network is controlled. The admission decision is made based on several criteria: 1) the current and future availability of network resources, 2) the impact of admission decisions on the existing flows, and 3) the policy control implemented by the network administrator.

Admission control is essential when the network promises service guarantees or levels of service assurances. The goals of the admission control are to protect the performance objectives of the existing flows, deny any requests the network is unable to provide for, and accept as many new flows as the network can commit to.

## A. Classical Admission Control

Admission control has been a topic of strong interest among researchers for many years. Research activities were particularly active when ATM standards were emerging. ATM employs a connection-oriented, hop-by-hop admission-control scheme as follows: A call is requested from a user to the network by means of signaling. The signaling message carries a profile of the requested call, referred to as

a traffic descriptor, which details the characteristics of the generated traffic such as peak rate and delay requirement. Upon receiving the call request, the network node executes an admission test by examining the traffic descriptor against the current state of the node. If enough resource is available, the node admits the new call and forwards the request to the downstream node. The downstream node, in turn, executes an admission test and decides whether to admit the requested call or not. This process is repeated until the call request reaches the destination.

In order to make a sound admission decision, each node maintains the state of all calls established through the node. This information is updated every time a new call is added or an existing call is terminated. Due to a large amount of state information required at each node, concerns have been raised regarding resource usage efficiency and the scalability of such admission processes.

## B. Integrated Services and RSVP

Successful deployment of ATM networks inspired researchers and engineers to build IP networks capable of QoS support, similar to that of ATM. Much of the knowledge and experience gained from ATM has been incorporated into the design of new IP networks. Integrated Services [1] and RSVP [2] are the outcomes of their effort and define the core specifications for QoS-enabled IP networks. The combination of IntServ and RSVP gave hope for the QoS support on IP networks. As with ATM, IntServ architecture aims to provide service guarantees through resource reservation. Through RSVP, it employs end-to-end signalling to communicate QoS parameters for the reservation of resources. However, on this type of architecture, each reservation of resource requires a state to be maintained at every node along the path of an end-to-end flow. It has been said that such architectures may not scale well due to heavy processing overhead and large memory consumption required to maintain those flow states. Considering the rate at which the size of Internet is growing and the number of hosts being added, the concentration of flows within the core routers can be a real issue and the management of individual flow states will become increasingly difficult. A mechanism that simplifies the operations of the network core is desired.

---

## C. Differentiated Services Architecture

To remedy the scalability problem of IntServ with an RSVP approach, differentiated services [3] have been proposed. DiffServ achieves the scalability by relieving the network core from resource-intensive operations and placing the complexity at the edge routers. Specifically, classification and conditioning of packets is performed only at the edges of the network. DiffServ does not employ hop-by-hop signaling in order to avoid the maintenance of per-flow state within the core of the network. Instead, flows with similar profiles are aggregated at the edge routers so that the core routers only need to handle bundles of flows.

DiffServ supports class-of-service differentiations. In order to maintain the promised level of service, the amount of traffic accepted at each class, especially at higher levels of classes, must be limited. Otherwise, the Service Level Agreement between the user and the network will be violated [4]. Thus, there is a need for admission control. In order for the edge nodes to make sound admission decisions, they must receive feedback from other parts of the network. DiffServ specification makes no mention of how this is to be done.

## D. Multiprotocol Label Switching

Multiprotocol Label Switching (MPLS) [5] is an evolving and expanding set of protocols developed by IETF. MPLS can be seen as a combination of different feature sets from ATM, IntServ, and DiffServ. This is achieved through the creation of a unidirectional signaled path, known as Label Switched Path. Label Switched Path is established by RSVP-based call control, known as RSVP-TE. MPLS aims to provide QoS-enabled transmission paths over the Internet. MPLS employs encapsulation of packets with short descriptors known as labels at the entry nodes of the MPLS network. The label determines which QoS class the packet belongs to and where it will be forwarded to. The same label will be placed on all packets that belong to the same QoS class and the same forwarding destination.

MPLS is gaining wide acceptance as a WAN protocol-of-choice and replacing Frame Relay and ATM-based WANs. It is used to transport Voice Over IP (VOIP) traffic and extend Ethernet LANs over the Internet. The strengths of MPLS include the seamless support of IP packets with QoS support, ability to operate through segments of network that do not support MPLS, and scalability afforded by the implementation of labels and simple operations at the core of the network. MPLS is protocol agnostic in that the payload of the labeled packets may be of any type, such as Ethernet frames or ATM cells. MPLS is designed specifically for

those protocols that do not support QoS natively, such as IP. MPLS allows multiple layers of label encapsulations to allow tunneling through different administrative MPLS domains. Because MPLS uses RSVP-based call control, it inherits the same strengths and weaknesses of RSVP.

There is a need for admission control that scales well in an environment where core routers are kept relatively simple and processing burdens are pushed to the edges of the network. This study surveyed admission-control schemes recently proposed, all of which claim to offer some level of scalability. The remaining sections of this paper are organized as follows: Section 2 classifies the admission-control schemes and scheduling algorithms in several categories. Section 3 surveys the admission-control schemes being proposed in recent years and describes the goals, approaches, contributions, and shortcomings of each scheme; Section 4 concludes the survey.

## Classifications of Admission Control and Scheduling Algorithms

This section describes the classifications of admission-control schemes and scheduling algorithms.

### A. Parameter-Based vs. Measurement-Based Admission Control

Admission-control schemes are generally classified as either parameter-based or measurement-based approaches. In either case, users request service from the network by sending flow specifications. Flow specifications describe the nature of packet flows (e.g. peak rate) and requirements for packet handling within the network (e.g. loss rate). The network uses parameters specified in the flow specifications to compute how much resource it must set aside in order to support the requested flow. The admission decision will be made by comparing the required resource against what is available on a node.

The differences between the two approaches exist in the way the allocated resource on a node is being estimated. In parameter-based admission control, the node computes its reserved resource by keeping track of parameter values in flow specifications at each flow establishment and termination. With this approach, the amount of allocated resource is a discrete function and the network node knows exactly how much resource is used or reserved at any given time. The strength of this approach lies in its ability to provide hard guarantees to each flow being accepted. One of the shortcomings is that it does not use the resource efficiently. The worst-case scenario is typically used to compute the resource

---

reservation requirements to assure hard guarantees. Once the resource is marked as reserved, it is no longer available for new flows that request guaranteed service.

Under the measurement-based approach, the resource consumed by existing flows on a network is estimated by measuring the actual traffic flow. It applies statistical principles to assess the current and very-near-future state of the network. Expressed by way of confidence level, it can predict a likelihood of being able to support a requested level of service based on the traffic pattern of the past. Using this information, a network node decides whether to admit a flow or reject it. This approach is shown to have much better utilization of network resources than the parameter-based one. However, measurement-based admission control does not provide hard guarantees.

The level of assurance this approach gives is based on the past history; the applicability of confidence level depends on whether the traffic pattern will remain similar to that of the past. Since the network is not immune to sudden changes in its environment (e.g. traffic pattern changes, link failures), the measurement-based approach may be effective only on stable networks. Another shortcoming of this approach is that it requires an accumulation of a long history. In order to yield a high utilization, the confidence interval at a given confidence level must be kept short. This requires many samples. Without a long history, admission decisions must be made with a very conservative view of the unused resources.

In recent years, admission-control schemes that are hybrid between parameter-based and measurement-based approaches have been investigated [4], [6], [12], [14]. They incorporate past history (i.e., measurements) to adjust the reserved bandwidth (i.e., parameters) of flows. Due to their duality, the strengths of either approach may mitigate the weaknesses of the other. Because of this unique property, a hybrid approach to admission control is gaining interest.

## B. Stateful vs. Stateless Scheduling Algorithms

The manner in which the arriving packets are queued and processed at each network node, referred to as scheduling, can have a significant impact on the way the admission control is carried out. Scheduling algorithms are generally classified as stateful or stateless for the purpose of scalability discussion. Stateful algorithms require maintenance of individual flow state at every node along the path of a flow. Examples of stateful-scheduling algorithms include Fair Queueing [7], [8], Virtual Clock [9], and their variants such as Weighted Fair Queueing [8] and Jitter-Virtual Clock [4].

These algorithms have been developed for the support of guaranteed service as their primary objective. They give precise control over the treatment of individual flow and can provide bounds on bandwidth allocation and end-to-end delay. The major drawback of stateful schedulers is that they require maintenance of per flow QoS state of all flows at each network node. Due to the size of and the complexity involved in the management of QoS state information, the scalability of this approach has been challenged. When a stateful scheduler is deployed in a network, admission control makes use of individual QoS state maintained at each node and determines whether the node has sufficient resources to meet the demands of the newly-requested flow.

Stateless-scheduling algorithms, on the other hand, maintain no QoS state at any part of the network. FIFO and LIFO queueing are examples of stateless algorithms. Since it requires no state maintenance, it is scalable. However, it does not provide the control necessary to support various QoS requirements. The Internet, for the most part, is composed of network nodes supporting stateless-queueing algorithms.

In recent years, a new type of scheduler has been added to the above. It is called core-stateless scheduling. Core-stateless scheduling aims to provide a similar level of QoS control offered by stateful algorithms, yet tries to achieve network scalability comparable to one offered by stateless algorithms. In core-stateless algorithms, the edge nodes maintain QoS states of individual flows, but the core routers do not. The core routers may maintain aggregate-level information that assists in controlling flows, depending on the implementation. The elimination of individual flow states from the core routers is made possible by embedding the QoS states in each packet header. There have been some novel ideas proposed using this scheduling mechanism. Core-Stateless Fair Queueing [10], Core-Jitter VC [4], and Virtual Time Reference System [11] are examples of core-stateless algorithms. They are further explained later in the survey section of this paper.

## C. Location Based Classification of Admission Control

A contribution of this study is the introduction of location-based classification of admission-control schemes. It is a new classification based on locations at which the key admission-control algorithms are applied. According to location-based classification, admission-control algorithms proposed in recent years are classified into the following five categories: admission control at 1) edge nodes (Edges), 2) central node (Central), 3) ingress node (Ingress), 4) egress node (Egress), and 5) end-user station (End-to-End). The taxonomy of admission-control schemes is given in Figure 1.

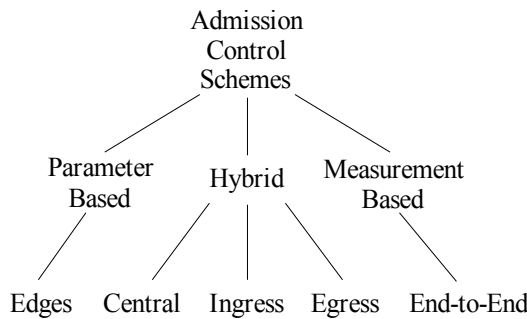


**Figure 1. Taxonomy of admission-control schemes**

Admission control at edge nodes (i.e., Edges) lessens the processing requirements of core routers through flow aggregation at network edges. Core routers process and maintain only the aggregate flow reservation information. Through aggregation, overhead reduction is made possible by fewer signaling-message exchanges and less call-state maintenance. Aggregation of RSVP [13] belongs to this category.

Admission control at central node (i.e., Central) employs a master server that performs admission-control functions on behalf of all routers in a network. By off-loading resource-intensive services, core routers become lightweight. Bandwidth Broker [12] uses this approach.

Admission control at ingress node (i.e., Ingress) enables core routers to make admission decisions without needing to maintain individual flow states. Ingress node measures the rate of packet arrivals for each individual flow and inserts this information in each packet header. Core routers read this information and accumulate them per aggregate flow. Thus, the core routers only maintain aggregate flow states and are able to make admission decisions at an individual flow basis. Dynamic Packet State (DPS) [4] uses this approach.

Admission control at egress node (i.e., Egress) pushes the complexity to the egress routers so that no per-flow states need to be maintained in the core of the network. Egress routers construct profiles of flows by monitoring the packet arrivals and departures. By measuring delay experienced by each packet, egress routers estimate the dynamically changing network load. Based on this information, the egress routers make admission decisions. Egress admission control [14] belongs to this category.

Admission control at the end-user station (i.e., End-to-End) uses a form of in-band signaling to estimate the availability of network resources. The admission decision is typically made by end users, rather than the network. Prior to sending data traffic, an originating end user sends a stream of packets at a constant rate for a short period of time. The

receiver measures the arrival pattern of probing packets and returns the summary statistics. Upon receiving the summary information, the sender decides whether the network is capable of carrying the requested load. Scalable Reservation Protocol [15] and others [16]–[18] belong to this category.

## Survey of Admission-Control Schemes

In light of location-based classifications of admission-control schemes described above, this section surveys selected admission-control schemes.

### A. Admission Control at Ingress Node

Dynamic Packet State (DPS) [4] is an ingress-node based admission-control scheme and employs a core-stateless scheduler. Its goal is to make admission decisions for new flows without maintaining individual flow states in the core of the network. DPS also aims to achieve end-to-end per-flow delay and bandwidth guarantees on a network, where only the edge routers perform per-flow management. To meet these goals, DPS uses a packet-header marking technique, where the ingress node encodes state information on the header of each packet. The core nodes apply control to packets according to their header markings. DPS proposes two innovative schemes, one in admission control and the other in scheduling. How these schemes work is described in subsequent sections.

DPS's admission-control scheme is comprised of two algorithms: 1) per-hop admission control and 2) aggregate reservation estimation. The former is parameter-based, while the latter is measurement-based. Each algorithm independently computes an estimated reserved bandwidth of aggregated flows. These estimates should be very close, if not the same. However, under certain conditions, deviations from the true reserved bandwidth are observed on each of the two algorithms in opposite directions. One algorithm estimates at a higher rate than the true reserved bandwidth and the other estimates at a lower rate. The first algorithm does not account for the duplicate reservation requests. This can lead to an under-utilization of a link due to inflated estimation of the reserved bandwidth.

The second algorithm does not include the effects of new calls being admitted in the middle of an estimate cycle. This results in estimating the reserved bandwidth at a lower rate than the actual rate. The results from these two algorithms are reconciled at the end of a fixed interval and arrive at one value that better reflects the true reserved bandwidth. The goal of admission control in DPS is to estimate a close upper

bound on a reserved aggregate rate so that a deterministic guarantee can be made to those calls being accepted, while minimizing over-reservation. DPS proposes a scheduling algorithm that provides service guarantees at levels comparable to IntServ on DiffServ-like environments. This scheduling algorithm is called Core-Jitter Virtual Clock (Core-Jitter VC). It is a non-work conserving scheduling algorithm.

Core-Jitter Virtual Clock is a variant of Jitter Virtual Clock (Jitter VC). The primary difference between the two algorithms is that Core-Jitter VC is a core-stateless-based scheduler, while Jitter VC is a stateful scheduler. Core-Jitter VC provides the same delay guarantee as Jitter VC at an end-to-end path, but not at intermediate routers. Jitter VC has been proven to provide the same level of guarantee as Weighted Fair Queueing (WFQ) [19]. Thus, Core-Jitter VC also provides the same guarantee as WFQ at the end-to-end path.

Jitter VC and Core-Jitter VC, are based on a packet-header marking and queueing architecture, where each router in a path of a flow reads and re-marks packet-header information for queueing and scheduling purposes. They employ a delay-jitter-rate-controller unit [20] for queueing purposes and a Virtual-Clock scheduler for scheduling purposes. A packet entering into a Jitter-VC router or a Core-Jitter-VC router will be held in a waiting room by the delay-jitter-rate-controller until it becomes eligible for transmission. Once the packet is released from the waiting room, Virtual-Clock scheduler services them in order of their earliest deadline. Each packet is given a deadline by which it must leave the Jitter-VC server or the Core-Jitter-VC server.

In order to better explain the workings of Core-Jitter VC, Jitter VC is described first. For the  $k^{th}$  packet of flow  $i$ , its eligible time  $e_{i,j}^k$  and deadline  $d_{i,j}^k$  at the  $j^{th}$  node on its path under the Jitter-VC algorithm are computed as follows:

$$e_{i,j}^1 = a_{i,j}^1, \quad e_{i,j}^k = \max(a_{i,j}^k + g_{i,j-1}^k, d_{i,j}^{k-1}) \quad i, j \geq 1, \quad k > 1 \quad (4)$$

$$d_{i,j}^k = e_{i,j}^k + \frac{l_i^k}{r_i}, \quad i, j, k \geq 1 \quad (5)$$

where  $a_{i,j}^k$  is the arrival time,  $l_i^k$  is the packet length, and  $g_{i,j-1}^k$  is the amount of time between the packet's deadline and the actual departure time. At every packet departure at every router, this  $g$  value is computed and recorded in its packet header and read at the subsequent router. A sample time diagram of packets going through a series of Jitter-VC servers is depicted in Figure 2(a). The shaded area depicts delays experienced by the second packet at each node.

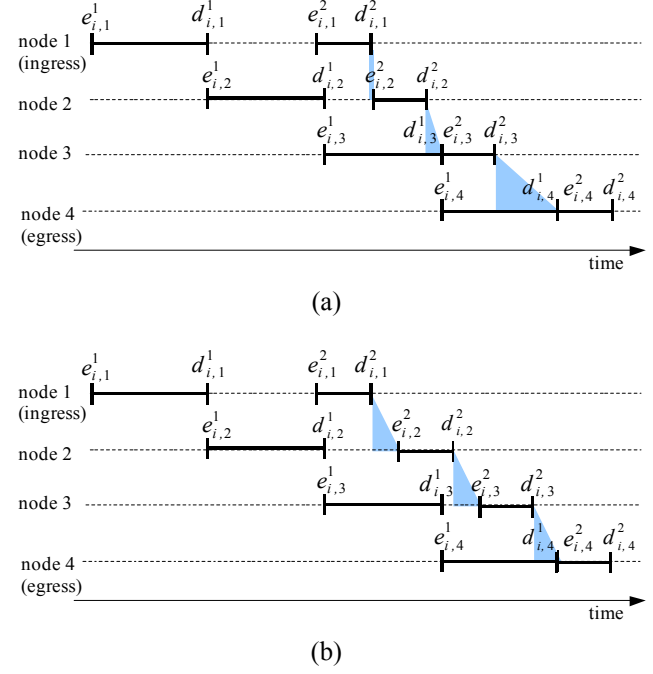


**Figure 2. The time diagram of packets through (a) Jitter-VC servers and (b) Core-Jitter-VC servers**

Jitter VC is a stateful service because, by equation (4), each router must maintain the deadline,  $d_{i,j}^{k-1}$ , of a previously received packet when it computes the eligibility time,  $e_{i,j}^k$ , of an arriving packet from the same flow.

Core-Jitter VC improves upon Jitter VC and makes the scheme stateless. It does so by removing the term  $d_{i,j}^{k-1}$  from the equation (4) and introducing a new term,  $\delta_i^k$ , a slack variable, instead, which holds the following property:

$$d_{i,j}^k + g_{i,j-1}^k + \delta_i^k \geq g_{i,j}^{k-1}, \quad j > 1 \quad (6)$$

With the above definition, the eligibility time of a packet at the  $j^{th}$  node can be computed as follows—compare it to equation (4):

$$e_{i,j}^k = a_{i,j}^k + g_{i,j-1}^k + \delta_i^k, \quad j > 1 \quad (7)$$

The details of how the actual value for the slack variable  $\delta_i^k$  is determined are given by Stoica and Zhang [4]. A sample time diagram of packets going through a series of Core-Jitter-VC servers is depicted in Figure 2(b). Observe

---

that the slack time,  $\delta$ , is a fixed value for all participating nodes in flow  $i$  for the  $k^{th}$  packet.

The strengths of DPS include its ability to guarantee bandwidth and delay bound-through Core-Jitter VC. The proposed admission-control algorithm is robust in the presence of network failures and partial reservation since the algorithm to estimate the reservation rate does not remember the past beyond the period,  $T_W$ . DPS's largest contribution is that it is the first of its kind to demonstrate that there is a way to provide a hard guarantee on bandwidth and delay requirements without maintaining individual flow states in the core of the network. DPS proposed a noble idea of inserting individual flow states in the header of packets so that the core nodes don't have to maintain them. DPS inspired others in developing new schemes based on this premise [11], [21].

While DPS offers guaranteed services without individual flow-state maintenance at core routers, the overall scalability gained from this architecture remains a question. Insertion and interpretation of state information in every data packet can be an expensive operation. Indeed, there is a concern that DPS may be transforming all data packets into control packets such that core nodes must pay extra attention to every packet they receive regardless of its type. Core-Jitter Virtual Clock scheduler requires both ingress and core nodes to monitor and alter the header of every data packet that travels through. For admission control, only the ingress router writes to the packet header, yet core routers must read and process every data packet. Since the control information is embedded in the data packet headers, all packets become essential to the healthy operation of the network. Considering the parameter-based QoS model, where only the control packets need extra attention from the routers, DPS's new approach could potentially add higher processing demands on network routers.

Another drawback of DPS's admission control is that it requires insertion of dummy packets at the ingress router when there is no data flow. Dummy packets must be injected in the network every time there is a gap between data packets, which is larger than the maximum inter-packet arrival time  $T_I$ .  $T_I$  is typically a small window compared to the period  $T_W$  used to compute the aggregate reserved rate. This type of approach works well for those applications that generate traffic at a constant bit rate and always terminate the reservation as soon as the transmission is over, such as telephony. DPS's admission-control scheme may not appeal strongly to other types of network applications. If the source is silent for an extended period of time, constant bit-rate dummy packets must be inserted into a network at  $1/T_I$  rate. This could result in wasted bandwidth because even the best-

effort traffic cannot take full advantage of unused bandwidth.

## B. Admission Control at Central Node

Bandwidth Broker (BB) [12] belongs to the centrally-controlled admission-control approach that aims to provide scalability in the network by off-loading the routers' control-plane functionalities to a master server known as a Bandwidth Broker. Bandwidth Broker maintains QoS-state information for all flows of every router within a designated domain. Network routers perform only the data-plane functionalities (i.e., packet forwarding), in addition to the exchange of QoS-related information of each flow with Bandwidth Broker.

Bandwidth-Broker architecture is built upon the Virtual Time Reference System (VTRS) [11]. It is classified as a core-stateless scheduling scheme, where the core routers in the network do not maintain individual flow states. VTRS is a framework on which guaranteed services can be offered in a network without mandating that a specific scheduling algorithm (e.g., Core-Jitter VC) be employed. It consists of three logical components: a packet state carried by packets, edge-traffic conditioning at the network edge, and a per-hop virtual-time reference and update mechanism at the core routers.

VTRS was inspired by the work presented in Dynamic Packet State (DPS) [4], where the core-stateless approach was first introduced. VTRS is an extension to DPS; however, VTRS has unique and significant contributions beyond what DPS proposed. First, it established generalized mathematical expressions that bound end-to-end delay and bandwidth requirement for the support of flows that travel through core-stateless routers. Second, framework defined in VTRS is generic enough that it not only expresses delay bounds and sustainable rates of a flow through core-stateless schedulers, but also through stateful schedulers (e.g., WFQ) as well as stateless (e.g., FIFO) schedulers. Third, the framework allows mixing of rate-based and delay-based schedulers in the path of a flow. Fourth, it introduced two new work-conserving core-stateless scheduling algorithms: Core Stateless Virtual Clock (CSVC), which is rate-based and Virtual Time Earliest Deadline First (VT-EDF), which is delay-based.

Consider the path of a flow  $j$  on a network, traversing  $h$  hops of routers. Suppose that  $q$  routers execute rate-based scheduling and  $h - q$  routers employ delay-based schedulers. Packets entering the network will be shaped at the edge node and move through a series of core nodes. Delays that the packets experience will be at the shaper and at each core

node. Then, the total delay of end-to-end path of flow  $j$ ,  $d_{e2e}^j$ , is

$$d_{e2e}^j = d_{shaper}^j + d_{core}^j \quad (8)$$

For simplicity, we do not consider the delay experienced at the shaper in this paper. It suffices to say that  $d_{shaper}^j$  varies by the type of shaper being used and the maximum delay that can be bounded. Zhang gives an example of delay experienced at the shaper using a dual token-bucket regulator [12].

The delay experienced at core nodes is bounded by

$$d_{e2e}^j = q \frac{L^{j,\max}}{r^j} + (h-1)q d^j + \sum_{i=1}^{h-1} \pi_i + \sum_{i=1}^h \psi_i \quad (9)$$

The term  $q \frac{L^{j,\max}}{r^j}$  represents the delay experienced at rate-based routers and  $(h-1)q d^j$  represents the delay observed at delay-based routers.  $\sum_{i=1}^{h-1} \pi_i$  is the total propagation delay and  $\psi_i$  is the error term of node  $i$ , which has the following property:

$$\hat{f}_i^{j,k} \leq \hat{v}_i^{j,k} + \psi_i \quad (10)$$

where  $\hat{f}_i^{j,k}$  is the virtual finish time of packet  $k$  in flow  $j$  at node  $i$ . It means that the targeted packet-departure time in a virtual time line is the latest time the packet may leave the node and still meet the delay requirement.  $\hat{v}_i^{j,k}$  is the actual finish time (i.e., actual packet departure time) of packet  $k$  in flow  $j$  at node  $i$ .

Having achieved the bandwidth and delay guarantees through VTRS on core-stateless network, the designers of VTRS enhanced its scalability further by moving the QoS-related control functions out of core routers to a master server known as a Bandwidth Broker. Bandwidth Broker is composed of three service components: policy control, QoS routing, and admission control. Policy control determines which hosts and applications are allowed to access the network. QoS routing selects a path that fulfills the requirements of a requested flow. Admission control determines the eligibility and feasibility of the requested flow by consulting the policy control and QoS routing control.

Bandwidth Broker (BB) suggests that by moving the admission-control function from the core routers to a central server, several positive outcomes can be expected. First, it further alleviates the core routers from burdensome processing and making them potentially more efficient. Second, service guarantees can be made for both per-flow and aggregate flows. Third, by decoupling the QoS-related functionalities of control plane from core routers, it may be possible to introduce new guaranteed services without requiring software or hardware upgrades at core routers. Fourth, it allows the execution of sophisticated and optimized admission control for the entire network, which might have been difficult under the hop-by-hop admission control. Fifth, the problem of inconsistent QoS states observed in the hop-by-hop reservation mechanism can be lessened. Sixth, through the physical separation of control- and data-plane functionalities, issues in control plane (e.g., scalability of Bandwidth Broker) can be dealt separately from the issues in data plane. Seventh, admission control can be performed at an entire path level, as opposed to a local level as done by the hop-by-hop approach, and could reduce the complexity of admission-control algorithms. Finally, BB addresses the effects of dynamic join and leave of individual flows to and from an aggregate flow and incorporates such effects into the admission-control algorithm.

There are several open issues with the design of Bandwidth Broker. While it addresses the core routers' scalability issues well, it does not elaborate much on the Bandwidth Broker's scalability issues. The amount of flow state information the Bandwidth Broker must manage could increase dramatically as the size of the network grows. There is a mention [12] that this problem can be alleviated by employing multiple Bandwidth Brokers in distributed fashion. This is contrary to one of the original motives of BB, where it tries to avoid the problem of inconsistent network view, which is often introduced by the distributed approach.

There also may be a potential delay incurred when the concentration of communications to and from the Bandwidth Broker becomes severe. Though it is convenient to have policy and QoS-routing information on-hand for admission decisions, performing all three tasks for the entire network can be demanding and it warrants a careful feasibility study. Finally, there is always a danger of a single point of failure, which results not only in an inability to make admission decisions, but also in loss of all QoS-related control-plane functionalities, which Bandwidth Broker provides.

### C. Admission Control at Edge Nodes

Aggregation of RSVP reservations [13] belongs to the edges-based admission-control approach and it aims to pro-

---

vide scalability in the network core by aggregating reservation requests of individual flows at the edge nodes. Individual flows between the same pair of source and destination nodes can form an aggregate. It is an extension to RSVP specifications. The primary focus of this approach is on the reduction of RSVP message exchanges, which leads to conservation of memory and processing power at those locations where the volume of individual flows may be heaviest.

The scheme employs two techniques to achieve its goals: suppression and aggregation of reservation messages. Individual-flow RSVP requests are suppressed at the ingress node by altering their protocol ID. The subsequent nodes in the routing path will not see these packets as reservation messages, except at the egress node. When the packets reach the egress node, they will be restored to their original IDs. As the egress node alters the protocol ID of reservation packets for individual flow, it computes the total bandwidth requested from each flow. Once the requests reach a certain total bandwidth, the ingress node initiates an aggregation and sends an AGGREGATE PATH message to downstream nodes. Upon receiving this message, the egress node returns an AGGREGATE RESERVE message and nodes in the path commit the reserved resource for the aggregate flow. Each node in the downstream path marks an appropriate amount of resources for reservation.

RSVP Reservation Aggregation is a logical and natural extension to the existing RSVP. The main contribution is that RSVP will be able to signal AGGREGATE PATH and RESERVE messages and that the core routers need not maintain per-flow states any longer.

Anticipated resource savings can be large when the number of aggregated flows is substantially fewer than the individual flows. It will work well in an environment where there are many end stations that are networked together with a few edge routers, such as VPN. On the other hand, when the scheme is applied to a network, where the number of edge routers is large and the distribution of flows is evenly spread among all edges, resource savings may not be as large as the previously-described environment due to lack of concentrations. Service-provider networks typically belong to the latter type. Furthermore, when the number of aggregate flows increases to a substantial volume, they face similar problems to having many individual flows.

The scheme presented in RFC 3175 allows only those individual flows with the same source and destination pair to form an RSVP aggregate. This is different from DiffServ aggregation, where any flow can form an aggregate, regardless of addresses, so long as they are marked with the same DS Code Point.

RFC 3175 points out that frequent modifications to the bandwidth reservation of aggregate flows due to additions and terminations of individual flow can lead to a large number of reservation updates. This is contrary to the base assumption that fewer reservation messages are generated when individual flow requests are aggregated. On the other hand, infrequent updates to the reserved bandwidth of an aggregate flow can result in wasted bandwidth, since a large block of resources will need to be reserved to absorb temporal bandwidth fluctuations. Thus, there is a trade-off between scalability of the scheme and efficient use of bandwidth.

## D. Admission Control at Egress Node

Egress Admission Control [14] performs data collection and admission decisions at the egress router. It processes reservation messages only at the network edge (egress router) and uses continual passive monitoring of a path to assess its available resources. It models the network as a black-box system, where a flow of packets arrives at one end of the box (ingress node), goes through the box (core nodes), and comes out at the other side of the box (egress node). All other flows on the network are modeled as interfering cross-traffic of the measured flow. Using this block-box model, Egress Admission Control aims to develop envelopes that accurately characterize the upper bounds on arrival and service processes through measurement at the egress node. A unique characteristic of these envelopes is that they implicitly include the effects of cross traffic that are not directly measured at the egress point and implicitly prevent other egress points from admitting flows beyond an acceptable range. By applying the extreme theory [22] to the measured envelopes, it estimates the end-to-end service availability of a certain traffic class. This estimate is used for making admission decisions.

Egress Admission Control constructs envelopes for arrival process and service process. All edge nodes are synchronized with each other using Network Time Protocol [23] and they time stamp every packet entering the network. When packets reach the egress node, the time stamp in the packet header is read and an arrival envelope, known as peak rate envelope [24], which captures the behavior of the peak rate of the arrival process, is constructed. The peak rate envelope is constantly updated at a short fixed interval. At a longer time scale, changes in the envelope are measured, expressed as variance, and used to compute the confidence interval of the peak-rate envelope.

The service envelope describes the behavior of the worst rate of service process. When packets arrive at an egress node, it examines each packet's header and computes the delay it experienced. Using this information, the egress node constructs the trace of maximum time required to service a

certain number of bits, called minimum service envelope. The variance observed by the changes in the service envelop in a longer time scale is used to compute the confidence interval.

When a new flow is requested, using its declared peak rate and delay bound, adding it to the measured peak rate arrival envelope, the admission test will compare this value against the measured service envelop, taking into account variances, and determine if statistically enough bandwidth exists through the network.

Consider a black-box system that has a measured peak arrival envelope with mean  $\bar{R}(t)$  and variance  $\sigma^2(t)$ . Assume it has a minimum service envelope with mean  $\bar{S}(t)$  and variance  $\psi^2(t)$ . Suppose a new flow request arrives with the peak-rate envelope  $r(t)$ . Then, through the extreme theory [14],  $\bar{R}(t)$  and  $\bar{S}(t)$  are Gumbel distributed and the flow can be admitted with delay bound  $D$  at confidence level of  $\Phi(\alpha)$ , if

$$t\bar{R}(t) + tr(t) - \bar{S}(t + D) + a\sqrt{t^2\sigma^2(t) + \psi^2(t + D)} < 0 \quad 0 \leq t \leq T \quad (17)$$

$$\lim_{t \rightarrow \infty} \bar{R}(t) + r(t) \leq \lim_{t \rightarrow \infty} \frac{S(t)}{t} \quad (18)$$

Egress Admission Control has several noteworthy properties. First, since it employs a measurement-based algorithm, there is a potential for an efficient use of network bandwidth. Second, it does not require core nodes to process resource reservation messages or store any information associated with flows. Third, it does not assume or require any specific scheduling mechanism in the network and that multiple queueing disciplines can co-exist. Fourth, route pinning, a key ingredient for deterministic service, is not fundamentally required. Fifth, egress routers can perform admission control on traffic aggregates and do not need to store or monitor per-flow traffic conditions.

While the approach is novel and elegant, the scheme is vulnerable to sudden traffic-pattern changes. Since the technique used to make admission decisions is based on statistical inference through measurements, the scheme will work best in an environment where the network is stable, the pattern of traffic is relatively unchanging, the amount of traffic added or subtracted at each flow admission or termination is much smaller than the overall traffic being carried, and the size of the network is large. On the other hand, if this scheme is applied to a network composed of few nodes with

hap-hazard traffic patterns, it can result in an unpredictable and unacceptable outcome. Since the accuracy of this scheme is closely tied to the network condition, it would be difficult to establish contractual agreements between the user and the service provider. Furthermore, the scheme will not work on the very first flow on any given pair of edge nodes because it does not have past history to construct envelopes for admission tests. It will not hold up well when there are sudden changes in the traffic flow such as node and link failures. A lengthy convergence period may be observed after significant changes in the state of the network occur.

Since the scheme does not explicitly de-allocate the resources at flow termination, it is difficult for the network to distinguish whether a flow has been terminated or the source of a flow is being silent temporarily. Once a source becomes silent or sends traffic below the declared sustained rate for a period of time, it may need to re-initiate a flow request or send some type of control packet to restore its state. In order to do this, the source must maintain a timer and the timer must be set with some understanding of the behavior of the network. This could add further complexity not only on the network nodes, but also on the end systems. The scheme does not provide any graceful or intelligent way to drop packets when the load exceeds the anticipated limit. No provisioning for correcting the initial assessment of traffic in an explicit manner is given either.

It also implicitly assumes that the traffic sources always generate some packets for the duration of the reservation. If a flow is admitted at a certain peak rate but is silent for a long time, the scheme will admit other flows during the silent period, resulting in overbooking, and packet drops could be observed when the silent source restarts the traffic generation.

## E. Admission Control at End-User Stations

There are several versions of end-to-end measurement-based schemes proposed thus far [15]–[18]. In this section, a system proposed by Karlsson and Ronngren [18] is reviewed.

The goal of this end-to-end measurement-admission scheme is to bound the loss probability of packets in high-priority flows. A host wishing to establish a low packet-loss flow probes the network prior to sending data. Information gathered through probing is used to make an admission decision at the source host. Probing is performed as follows: a source host transmits blocks of packets for a period of time at the peak rate of the flow it wishes to establish. Each packet contains information regarding the probing, such as probe

duration and transmission rate. Upon expiration of the probe duration, the destination host returns a packet, which contains a measurement report such as the number of probing packets received. Based on the measurement report, the source host makes the admission decision.

The proposed service architecture employs simple queueing and scheduling mechanisms at each node. Data and probing packets belong to the controlled-load service and are allocated a certain portion of the link capacity. Within the controlled-load service, there are two partitions: high-priority queue and low-priority queue. Data packets are queued at the high-priority queue and always serviced prior to the low-priority queue packets. Probing packets are queued at the low-priority queue. All remaining packets belong to the best-effort traffic and are queued at the best-effort queue. This queue is serviced only when there are no packets in the controlled-load service.

The end-to-end measurement-based approach is by far the simplest of all the admission-control schemes surveyed in this study. The processing required by end system for the probing is light. The queueing and scheduling mechanisms necessary at each node are straightforward, and no flow state needs to be maintained in the network.

Due to its simplicity, the scheme is unable to provide sophisticated services. The proposed scheme can only give a statistical bound on the packet loss; delay is not considered by the admission control as it offers no guarantee since the source makes no requests to the network and the network makes no reservations for the probed flow. Bandwidth blocking could result in a highly contentious environment, where probing packets are generated at a high bandwidth rate compared to the remaining bandwidth of controlled-load service. Suppose there are multiple hosts wishing to establish sessions. Some hosts may request flows at a higher rate than the remaining bandwidth of controlled-load service, while others may wish to establish flows at a lower rate. Obviously, the attempts to establish flows at higher rates than the available bandwidth will not succeed. The slower rate flows should be accepted, so long as enough bandwidth remains in the controlled-load service. Under this type of condition, even the slower rate probing packets can be affected due to congestions in the controlled-load service and may not be able to receive the requested service.

In terms of bandwidth-use efficiency, it is desirable to keep the probing period as short as possible. However, a short probing period may not capture the average state of the network and may result in overbooking or under utilization. There is also an uncertainty in the probability of packet loss if this scheme were applied on a network without a route

pinning, yet there was no mention of it in the literature reviewed.

## Conclusion

There has been a sustained interest and effort in designing mechanisms to offer guaranteed services on IP networks. Admission control is one of the essential tools in supporting QoS. MPLS has received much attention as a promising transport architecture that could offer service differentiations in large-scale networks. The development of effective and scalable admission-control schemes and accompanying scheduling algorithms suitable for MPLS networks has become an important topic of research.

In this paper, the author introduced a location-based classification of admission-control schemes, a new taxonomy for admission-control schemes that complements the traditional parameter-based and measurement-based admission-control categorization. In this new classification system, parameter-based and measurement-based admission-control schemes are further categorized into 1) edges-based, 2) centrally-controlled, 3) ingress-based, 4) egress-based, and 5) end-to-end-based. The author also surveyed various admission-control schemes in light of location-based classification systems in order to better understand their suitability for MPLS networks. The analysis summary is given in Table 1.

**Table 1. Summary of analysis of admission-control schemes based on location classifications**

Location	Admission	Scheduling	Pro / Con
<b>Edges</b>	Parameter	Stateful	Guarantee / Limited in scope
<b>Central</b>	Hybrid	Stateful, Stateless, Core-Stateless	Flexible scheduling / Single point of failure
<b>Ingress</b>	Hybrid	Core-Stateless	Guarantee / May not scale
<b>Egress</b>	Hybrid	Any	Mathematically modeled / Not proven to work
<b>End-to-End</b>	Measurement	Any	Simple / No guarantee

Each scheme asserts some level of scalability. Indeed, there are some novel ideas proposed and elegant approaches presented. Yet, every one of them has at least one significant shortcoming that prevents it from being deployed over the Internet.

Admission controls that are hybrid, whose control mechanisms are placed at an ingress node or central node, have characteristics that are more promising for future development than others. In subsequent studies, the author plans to design an admission-control scheme that builds upon those foundations, yet exceeds in its scalability when compared with those evaluated in this study.

## References

- [1] R. Braden, D. Clark, and S. Shenker, “RFC 1633: Integrated services in the Internet architecture: an overview,” Jun. 1994.
- [2] R. Braden, Ed., L. Zhang, S. Berson, S. Herzog, and S. Jamin, “RFC 2205: Resource ReSerVation Protocol (RSVP) — version 1 functional specification,” Sep. 1997.
- [3] S. Blake, D. Black, M. Carlson, E. Davies, Z. Wang, and W. Weiss, “RFC 2475: An architecture for differentiated services,” Dec. 1998.
- [4] I. Stoica and H. Zhang, “Providing guaranteed services without per flow management,” in *SIGCOMM*, 1999, pp. 81–94.
- [5] E. Rosen, A. Viswanathan, and R. Callon, “Multiprotocol Label Switching Architecture,” RFC 3031 (Proposed Standard), Internet Engineering Task Force, Jan. 2001.
- [6] J. Milbrandt, M. Menth, and J. Junker, “Improving experience-based admission control through traffic type awareness,” *Journal of Networks*, vol. 2, no. 2, pp. 11–22, April 2007.
- [7] A. K. Parekh and R. G. Gallager, “A generalized processor sharing approach to flow control in integrated services networks: The single-node case,” *IEEE/ACM Transactions on Networking*, vol. 1, no. 3, pp. 344–357, June 1993.
- [8] A. Demers, S. Keshav, and S. Shenker, “Analysis and simulation of a fair queueing algorithm,” in *Proc. of ACM SIGCOMM '89*, 1989, pp. 3–12.
- [9] L. Zhang, “Virtual clock: A new traffic control algorithm for packet switching networks,” in *Proc. of SIGCOMM '90*, 1990, pp. 19–29.
- [10] I. Stoica, S. Shenker, and H. Zhang, “Core-stateless fair queueing: Achieving approximately fair bandwidth allocations in high speed networks,” in *SIGCOMM*, 1998, pp. 118–130.
- [11] Z. Zhang, Z. Duan, and Y. Hou, “Virtual time reference system: A unifying scheduling framework for scalable support of guaranteed services,” 2000.
- [12] Z.-L. Zhang, “Decoupling qos control from core routers: A novel bandwidth broker architecture for scalable support of guaranteed services,” in *SIGCOMM*, 2000, pp. 71–83.
- [13] F. Baker, C. Iturralte, F. L. Faucheur, and B. Davie, “RFC 3175: Aggregation of rsvp for ipv4 and ipv6 reservations,” Dec. 2001.
- [14] C. Cetinkaya, V. Kanodia, and E. Knightly, “Scalable services via egress admission control,” *IEEE Transaction on Multimedia*, vol. 3, no. 1, March 2001.
- [15] W. Almesberger, T. Ferrari, and J. Y, “Srp: a scalable resource reservation protocol for the internet,” 1998.
- [16] F. Kelly, P. Key, and S. Zachary, “Distributed admission control,” December 2000.
- [17] G. Bianchi, F. Borgonovo, A. Capone, L. Fratta, and C. Petrioli, “Pcp-dv: An end-to-end admission control mechanism for ip telephony,” in *Tyrrhenian IWDC 2001 Evolutionary Trends of the Internet*, Taormina, Italy, September 2001.
- [18] V. Elek, G. Karlsson, and R. Ronngren, “Admission control based on end-to-end measurements,” in *INFOCOM (2)*, 2000, pp. 623–630.
- [19] R. L. Cruz, “Quality of service guarantees in virtual circuit switched networks,” *IEEE Journal on Selected Areas in Communications*, vol. 13, no. 6, pp. 1048–1056, 1995.
- [20] H. Zhang and D. Ferrari, “Rate-controlled service disciplines,” 1994.
- [21] R. Sivakumar, T. eun Kim, N. Venkitaraman, J.-R. Li, and V. Bharghavan, “Achieving per-flow weighted rate fairness in a core stateless network,” in *International Conference on Distributed Computing Systems*, 2000, pp. 188–196.
- [22] E. Castillo, *Extreme Value Theory in Engineering*. New York: Academic, 1988.
- [23] D. L. Mills, “RFC 1305: Network time protocol (version 3) specification, implementation,” Mar. 1992.
- [24] J. Schlembach, A. Skoe, P. Yuan, and E. W. Knightly, “Design and implementation of scalable admission control,” in *QoS-IP*, 2001, pp. 1–16.

## Biography

**MASARU OKUDA** received the B.S. degree in Information System and Computer Science from Brigham Young University - Hawaii, Laie, HI, in 1989, and the M.S. degree in Telecommunications and the Ph.D. degree in Information Sciences from the University of Pittsburgh, Pittsburgh, PA, in 1996 and 2006 respectively. Currently, he is an assistant professor of Telecommunications Systems Management at Murray State University, Murray, KY. His teaching and research areas include computer and network security, US telecom policies, network protocol analysis, network architecture design, QoS enabled networks, peer-to-peer networks, and video distribution networks. Dr. Okuda may be reached at masaru.okuda@murraystate.edu.

# INSTRUCTIONS FOR AUTHORS

## MANUSCRIPT REQUIREMENT

The INTERNATIONAL JOURNAL OF MODERN ENGINEERING is an online/print publication, designed for Engineering, Engineering Technology, and Industrial Technology professionals. All submissions to this journal, submission of manuscripts, peer-reviews of submitted documents, requested editing changes, notification of acceptance or rejection, and final publication of accepted manuscripts will be handled electronically.

All manuscripts must be submitted electronically. Manuscripts submitted to the International Journal of Modern Engineering must be prepared in Microsoft Word 98 or higher (.doc) with all pictures, jpg's, gif's and pdf's included in the body of the paper. All communications must be conducted via e-mail to the manuscript editor at [philipw@bgsu.edu](mailto:philipw@bgsu.edu) with a copy to the editor at [editor@ijme.us](mailto:editor@ijme.us)

The editorial staff of the International Journal of Modern Engineering reserves the right to format and edit any submitted word document in order to meet publication standards of the journal.

1. Word Document Page Setup: Top = 1", Bottom = 1", Left = 1.25", and Right = 1.25". This is the default setting for Microsoft Word. Do Not Use Headers or Footers.
2. Text Justification: Submit all text as "LEFT JUSTIFIED" with No paragraph indentation.
3. Page Breaks: No page breaks are to be inserted in your document.
4. Font Style: Use 11-point Times New Roman throughout the paper except where indicated otherwise.
5. Image Resolution: Images should be 96 dpi, and not larger than 460 X 345 Pixels.
6. Images: All images should be included in the body of the paper (.jpg or .gif format preferred).
7. Paper Title: Center at the top with 18-point Times New Roman (Bold).
8. Author and Affiliation: Use 12-point Times New Roman. Leave one blank line between the Title and the "Author and Affiliation" section. List on consecutive lines: the Author's name and the Author's Affiliation. If there are two authors follow the above guidelines by adding one space below the first listed author and repeat the process. If there are more than two authors, add one line below the last listed author and repeat the same procedure. Do not create a table or text box and place the "Author and Affiliation" information horizontally.
9. Body of the Paper: Use 11-point Times New Roman. Leave one blank line between the "Author's Affiliation" section and the body of the paper. Use a one-column format with left justification. Please do not use spaces between paragraphs and use 0.5" indentation as a break between paragraphs.
10. Abstracts: Abstracts are required. Use 11-point Times New Roman Italic. Limit abstracts to 250 words or less.
11. Headings: Headings are not required but can be included. Use 11-point Times New Roman (ALL CAPS AND BOLD). Leave one blank line between the heading and body of the paper.
12. Page Numbering: The pages should not be numbered.
13. Bibliographical Information: Leave one blank line between the body of the paper and the bibliographical information. The referencing preference is to list and number each reference when referring to them in the text (e.g. [2]), type the corresponding reference number inside of bracket [1]. Consider each citation as a separate paragraph, using a standard paragraph break between each citation. Do not use the End-Page Reference utility in Microsoft Word. You must manually place references in the body of the text. Use font size 11 Times New Roman.
14. Tables and Figures: Center all tables with the caption placed one space above the table and centered. Center all figures with the caption placed one space below the figure and centered.
15. Page limit: Submitted article should not be more than 15 pages.

# College of Engineering, Technology, and Architecture

University of Hartford



For more information please visit us at  
[www.hartford.edu/ceta](http://www.hartford.edu/ceta)

For more information on undergraduate programs please contact Kelly Cofiell at  
[cetainfo@hartford.edu](mailto:cetainfo@hartford.edu).

For more information on Graduate programs please contact Laurie Grandstrand at [grandstran@hartford.edu](mailto:grandstran@hartford.edu).

Toll Free: 1-800-766-4024  
Fax: 1-800-768-5073



## DEGREES OFFERED :

### ENGINEERING UNDERGRADUATE

Acoustical Engineering and Music (B.S.E)  
Biomedical Engineering (B.S.E)  
Civil Engineering (B.S.C.E)  
-Environmental Engineering Concentration  
Environment Engineering (B.S.E)  
Computer Engineering (B.S.Comp.E.)  
Electrical Engineering (B.S.E.E.)  
Mechanical Engineering (B.S.M.E.)  
- Concentrations in Acoustics and  
- Concentrations in Manufacturing

### TECHNOLOGY UNDERGRADUATE

Architectural Engineering Technology (B.S.)  
Audio Engineering Technology (B.S.)  
Computer Engineering Technology (B.S.)  
Electronic Engineering Technology (B.S.)  
-Concentrations in Networking/  
Communications and Mechatronics  
Mechanical Engineering Technology (B.S.)

### GRADUATE

Master of Architecture (M.Arch)  
Master of Engineering (M.Eng)  
• Civil Engineering  
• Electrical Engineering  
• Environmental Engineering  
• Mechanical Engineering  
– Manufacturing Engineering  
– Turbomachinery  
3+2 Program (Bachelor of Science and  
Master of Engineering Degrees)  
E<sup>2</sup>M Program (Master of Engineering and  
Master of Business Administration)



College of Engineering,  
Technology, and Architecture  
**UNIVERSITY  
OF HARTFORD**

# IJME CELEBRATES TEN YEARS OF SERVICE

IJME IS THE OFFICIAL AND FLAGSHIP JOURNAL OF THE  
INTERNATIONAL ASSOCIATION OF JOURNALS AND CONFERENCE (IAJC)  
[www.iajc.org](http://www.iajc.org)



The International Journal of Modern Engineering (IJME) is a highly-selective, peer-reviewed journal covering topics that appeal to a broad readership of various branches of engineering and related technologies. IJME is steered by the IAJC distinguished board of directors and is supported by an international review board consisting of prominent individuals representing many well-known universities, colleges, and corporations in the United States and abroad.

## IJME Contact Information

General questions or inquiries about sponsorship of the journal should be directed to:

**Mark Rajai, Ph.D.**

Editor-in-Chief

Office: (818) 677-2167

Email: [editor@ijme.us](mailto:editor@ijme.us)

Department of Manufacturing Systems Engineering & Management  
California State University-Northridge  
18111 Nordhoff St.  
Northridge, CA 91330